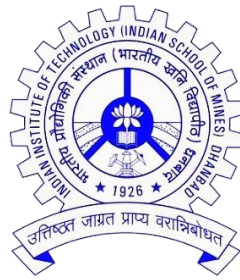# Improvement in machinability of Ti-6Al-4V alloy in EDM and high speed milling

by

SHASHANK SHUKLA
(17DR000496)

THESIS

SUBMITTED TO

INDIAN INSTITUTE OF TECHNOLOGY (INDIAN SCHOOL OF MINES) DHANBAD

For the award of the degree of

DOCTOR OF PHILOSOPHY

December 2022

INDIAN INSTITUTE OF TECHNOLOGY (INDIAN SCHOOL OF MINES) DHANBAD

CERTIFICATE FROM THE SUPERVISOR(S)
(To be submitted at the time of Thesis Submission)

This is to certify that the thesis entitled "**Improvement in machinability of Ti-6Al-4V alloy in EDM and high speed milling**" being submitted to the Indian Institute of Technology (Indian School of Mines), Dhanbad by Mr **Shashank Shukla**, Admission No **17DR000496**, for the award of Doctor of Philosophy (Ph.D.) Degree is a bonafide work carried out by hi, in the Department of **Mechanical Engineering**, IIT (ISM), Dhanbad, under my supervision and guidance. The thesis has fulfilled all the requirements as per the regulations of this Institute and, in my opinion, has reached the standard needed for submission. The results embodied in this thesis have not been submitted to any other university or institute for the award of any degree or diploma.

Signature of Supervisor (s)

Name: Prof. Vivek Bajpai

Date:

INDIAN INSTITUTE OF TECHNOLOGY (INDIAN SCHOOL OF MINES) DHANBAD

CERTIFICATE REGARDING ENGLISH CHECKING
(To be submitted at the time of Thesis Submission)

This is to certify that the thesis entitled "**Improvement in machinability of Ti-6Al-4V alloy in EDM and high speed milling**" being submitted to the Indian Institute of Technology (Indian School of Mines), Dhanbad by Mr **Shashank Shukla**, Admission No **17DR000496** , for the award of Doctor of Philosophy (Ph.D.) Degree has been thoroughly checked for quality of English and logical sequencing of topics.

It is hereby certified that the standard of English is good and that grammar and typos have been thoroughly checked.

It is now worthy for evaluation by the panel of examiners.

Signature of Supervisor (s)   Signature of Scholar

Name: Prof. Vivek Bajpai   Name: Shashank Shukla

Date: 22/06/22   Date: 22/06/22

INDIAN INSTITUTE OF TECHNOLOGY (INDIAN SCHOOL OF MINES) DHANBAD

CERTIFICATE FOR CLASSIFIED DATA
(To be submitted at the time of Thesis Submission)

This is to certify that the thesis entitled "**Improvement in machinability of Ti-6Al-4V alloy in EDM and high speed milling**" being submitted to the Indian Institute of Technology (Indian School of Mines), Dhanbad by Mr **Shashank Shukla** for award of Doctor of Philosophy (Ph.D) Degree in **Mechanical Engineering** does not contains any classified information. This work is original and yet not been submitted to any institution or university for the award of any degree.

Signature of Supervisor (s)

Signature of Scholar

INDIAN INSTITUTE OF TECHNOLOGY (INDIAN SCHOOL OF MINES) DHANBAD

COPYRIGHT AND CONSENT FORM
(To be submitted at the time of Thesis Submission)

To ensure uniformity of treatment among all contributors, other forms may not be substituted for this form, nor may any wording of the form be changed. This form is intended for original material submitted to the IIT (ISM), Dhanbad and must accompany any such material in order to be published by the ISM. Please read the form carefully and keep a copy for your files.

TITLE OF THESIS: **Improvement in machinability of Ti-6Al-4V alloy in EDM and high speed milling**.

AUTHOR'S NAME & ADDRESS: Shashank Shukla & Near shiv durga mandir, Navrang park colony, Satna, Madhya Pradesh, Pin code- 485005

COPYRIGHT TRANSFER

1. The undersigned hereby assigns to Indian Institute of Technology (Indian School of Mines), Dhanbad all rights under copyright that may exist in and to: (a) the above Work, including any revised or expanded derivative works submitted to the ISM by the undersigned based on the work; and (b) any associated written or multimedia components or other enhancements accompanying the work.
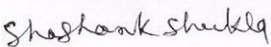
CONSENT AND RELEASE

2. In the event the undersigned makes a presentation based upon the work at a conference hosted or sponsored in whole or in part by the IIT (ISM) Dhanbad, the undersigned, in consideration for his/her participation in the conference, hereby grants the ISM the unlimited, worldwide, irrevocable permission to use, distribute, publish, license, exhibit, record, digitize, broadcast, reproduce and archive; in any format or medium, whether now known or hereafter developed: (a) his/her presentation and comments at the conference; (b) any written materials or multimedia files used in connection with his/her presentation; and (c) any recorded interviews of him/her (collectively, the "Presentation"). The permission granted includes the transcription and reproduction of the Presentation for inclusion in products sold or distributed by IIT(ISM) Dhanbad and live or recorded broadcast of the Presentation during or after the conference.

3. In connection with the permission granted in Section 2, the undersigned hereby grants IIT (ISM) Dhanbad the unlimited, worldwide, irrevocable right to use his/her name, picture, likeness, voice and biographical information as part of the advertisement, distribution and sale of products incorporating the Work or Presentation, and releases IIT (ISM) Dhanbad from any claim based on right of privacy or publicity.

4. The undersigned hereby warrants that the Work and Presentation (collectively, the "Materials") are original and that he/she is the author of the Materials. To the extent the Materials incorporate text passages, figures, data or other material from the works of others, the undersigned has obtained any

necessary permissions. Where necessary, the undersigned has obtained all third party permissions and consents to grant the license above and has provided copies of such permissions and consents to IIT (ISM) Dhanbad.

GENERAL TERMS

* The undersigned represents that he/she has the power and authority to make and execute this assignment.
* The undersigned agrees to indemnify and hold harmless the IIT (ISM) Dhanbad from any damage or expense that may arise in the event of a breach of any of the warranties set forth above.
* In the event the above work is not accepted and published by the IIT (ISM) Dhanbad or is withdrawn by the author(s) before acceptance by the IIT(ISM) Dhanbad, the foregoing copyright transfer shall become null and void and all materials embodying the Work submitted to the IIT(ISM) Dhanbad will be destroyed.
* For jointly authored Works, all joint authors should sign, or one of the authors should sign as authorized agent for the others.

Shashank shukla

Signature of the Author

Acknowledgments

I am very grateful to GOD ALMIGHTY without whose grace and blessings this study would not have been possible.

I extend my immeasurable appreciation and gratitude for the help and support I received from all the people who somehow contributed to making this study possible.

Foremost, I would like to express my sincere gratitude to my supervisor **Dr. Vivek Bajpai**, Associate professor, Department of Mechanical Engineering, for his valuable guidance, encouragement, immense support, and freedom throughout my Ph.D. His constant energy and immense enthusiasm for research always motivated me. Further, I would be thankful to him for providing excellent research facilities and resources throughout my work and for his willingness to spare time for clarifying my doubts and research discussion.

I wish to express my sincere thanks to **Dr. P.K. Singh** Chairperson of the Doctoral Scrutiny Committee (DSC), Department of Mechanical Engineering, IIT (ISM), Dhanbad for his intimate inspiration and suggestions. I also wish to express my sincere thanks to **Dr.**

Amit Rai Dixit, DSC Member, Associate Professor, Department of Mechanical Engineering, and Dr. Sukanta Das, Associate Professor, Department of Electrical Engineering, IIT (ISM) Dhanbad for their constant inspiration and thought-provoking suggestions. I also thank Prof. Rajiv Shekhar, Director, IIT (ISM) Dhanbad for providing all the necessary infrastructure and facilities for the research work during the period of study.

I also thank all faculties and staff members in the Department of Mechanical Engineering, Central Workshop and Central Research Facility, IIT (ISM) who associated with me during this study, directly and indirectly, to support me during my Ph.D. work.

I individually thank all of my lab mates **Dr. Mohan Kumar, Rachit Ranjan, Ankit Jain, Deepak Kumar, Ravi Shankar Rai, Arnab Das**, and **Rajesh Sahoo** for their continuous help and support during my research period.

I individually thank my dearest friends and seniors **Dr. Manish, Dr. Piyush, Chitransh, Mukul, Suryank, Ratnesh, Anubhav, Vishal**, and **Biplab** who shared their knowledge with me on various aspects.
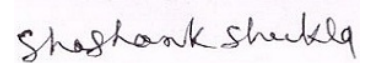
The dissertation would have been impossible without the support of my family. I express my deepest gratitude to my family- father **Mr. Ram Prasad Shukla**, mother **Mrs. Laxmi Shukla**, brother **Prashant Shukla**, sister in law **Jyoti Shukla** and sister **Parul didi** for their love and support throughout my life. Special thanks to my lovely Wife **Ashmita Shukla** for her patient during this journey. Without their love, support, respect, and care, it is not possible to complete this journey.

Shashank shukla

Place: IIT ISM Dhanbad   Shashank Shukla

Date: December 15, 2022   (17DR000496)

Abstract

Ti-6Al-4V alloy have excellent mechanical, thermal and chemical properties, hence they are widely applicable on various fields. However, machining of Ti-6Al-4V alloy is challenging task due to its higher hardness and low thermal conductivity. The machinability of Ti-6Al-4V alloy is limited by low tool life and poor surface roughness cost during traditional machining and by low mateial removal rate (MRR) and low specific energy during non-traditional machining. Thus, a exclusive approach required to be devised which can enhance the machinability of Ti-6Al-4V alloy during traditional and non traditional machining processes. It is noted from the literature that modification in microstructure can enhance machinability during high speed milling and modification in servo mechanism of gap control can enhance machinability during electrical discharge machine (EDM) system. It is estimated that this study will reduce the production cost of machining Ti-6Al-4V alloy with good surface finish and high MRR.

A maglev EDM system is introduced with modified servo mechanism to control inter electrode gap with high duty cycle. The detailed experimental study is carried out for its feasibility analysis and comparative analysis with conventional EDM system. It has been detected that maglev EDM reduced the specific energy consumption and surface roughness than conventional EDM systems. In addition, cryogenic quenching has been explored

which has enhanced the the α phases and reduced the α-β grain boundaries in Ti-6Al-4V alloy. The high-speed up-milling has been performed on cryogenic quenched and untreated Ti-6Al-4V alloy. It has been detected that cryogenic quenched samples enhanced the plastic deformability of Ti-6Al-4V alloy. Tool wear, chip thickness and surface roughness has showed better results for cryogenic quenched samples. Evaluation of maglev EDM and high speed milling has shown that maglev EDM can be opted for small size batch production and high speed milling is necessary for large size production since MRR during maglev EDM is lower than milling.

Nomenclature

List of Abbreviations

MRR: Material Removal Rate

EDM: Electrical Discharge Machining

MQL: Minimum Quantity Lubrication

EPT: Electropulsing Treatment

HCP: Hexagonal Close-Packed

BCC: Body-Centered Cubic

EBSD: Electron Backscatter Diffraction

XRD: X-Ray Diffraction

CA: Annealed+ cryogenic quenched +tempered Ti-6Al-4V alloy

CST: Solution heat treated+ cryogenic quenched +tempered Ti-6Al-4V alloy

WA: Annealed+ water quenched +tempered Ti-6Al-4V alloy

WST: Solution heat treated+ water quenched +tempered Ti-6Al-4V alloy

AA: Annealed+ air quenched +tempered Ti-6Al-4V alloy

AST: Solution heat treated+ air quenched +tempered Ti-6Al-4V alloy

UT: Untreated Ti-6Al-4V alloy

DCT: Deep cryogenic treatment

BUE: Build-up edge

HSM: High speed milling

List of Symbols

α: alpha

β: beta

μm: micrometer

μg: microgram

α′: Primary alpha

α″: Secondary alpha

Contents

List of Figures

List of Tables

1

Introduction

This chapter provides a brief introduction about the basics of issues in machinability of titanium alloy; need and scope for improvement of it; aim and organization of the thesis.

1.1 Background

Methods by which titanium is transformed from mineral ore to usable parts has a great interest in fabricating new stronger products as well as to optimize available manufacturing processes. These methods develop microstructure of titanium components in three phases viz. alpha (α), alpha + beta ($\alpha + \beta$) and beta(β). Microstructure plays a significant role in

developing higher strength to weight ratio, thermal stability and other essential mechanical properties required on different industries. Ti-6Al-4V alloys are broadly used in different forms such as sheet, billet, wire, strip and plate. Ti-6Al-4V alloys are used in aerospace, medical, marine and automobile industries since it has excellent properties such as high temperature stability, lightweight, high strength, high wear resistance, biocompatible and anticorrosive [1, 2]. Figure 1.2 shows the comparison of different structural material for
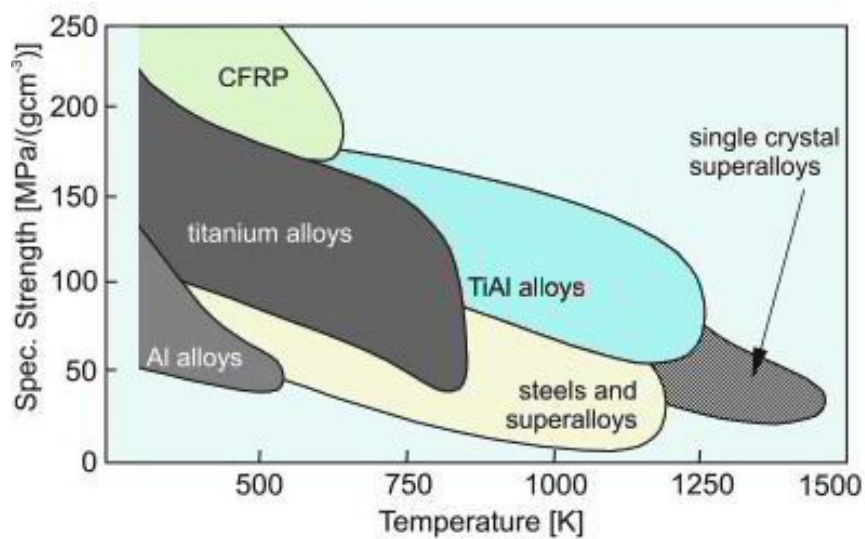
Figure 1.1: Specific strength vs higher temperature of different structural materials [3]

specific strength at higher temperature [3]. The higher specific strength at higher temperature of Ti-6Al-4V alloy is preferable mechanical property due to which this alloy has vast application in different fields. From this specific strength illustration it can be observed that only carbon fiber reinforced plastics have higher strength than titanium alloys at 300^0C, while at higher temperatures titanium alloys have high specific strength than any other material. Hence, titanium alloys mainly Ti-6Al-4V is applied for various temperature range with good specific strength. To produce different shapes turning, drilling and milling are commonly used machining technology. During machining of a Ti-6Al-4V alloy machinability is key factor to develop final product. Since machining quality with

low production cost is dependent upon machining capability. Machinability of a material is termed as an ability of a material to be machined easily at low cost with good surface finish and high MRR [4]. Therefore, it is essential to improve machinability of Ti-6Al-4V alloy to produce final product of alloy with less production cost and higher surface finish. By improving machining efficiency, it is possible to enhance the machinability of Ti-6Al-4V alloy. There are various machining processes such as conventional and non-traditional machining method. In conventional machining methods tool and workpiece are in direct contact with each other, while in non traditional machining method tool and workpiece don′t have direct contact with each other.

In conventional machining processes, a harder tool than the workpiece material is employed to remove the material through higher cutting forces. For example; milling, turning, shaping, boring, slotting, broaching etc. are such type of processes. In these processes higher cutting forces reduces the tool life and accuracy of machined part. Subsequently, to improve the machinability of Ti-6Al-4V alloy in conventional machining methods, it is essential to increase the tool life with good surface finish on workpiece. To improve the machinability during conventional machining process different techniques shown on Fig. 1.2 can be applied. These methods are further explained in detail in chapter 2. The development and machining cost of conventional machines are high which ultimately decreases the machinability of Ti-6Al-4V alloy. In current study high speed milling is applied as conventional machining method. Therefore, it is essential to introduce a method to improve the machinability of Ti-6Al-4V alloy during high speed milling without increasing the development and machining cost of it.

The primary principle of non-traditional machining methods are the application of less sharp and soft tool to remove the material by mechanical, thermal, chemical and electrical process. Mostly during unconventional machining method, tool and workpiece do not have direct contact with each other, therefore tool life is higher during such type of machining

processes. There are several type of unconventional machining methods applied for machining; such as Ultrasonic machining (USM), Abrasive Jet machining (AJM), Electric discharge Machining (EDM), Electron Beam Machining (EBM), Laser Beam Machining (LBM), and Plasma Arc Machining (PAM), etc. Among the various available unconventional methods the EDM is highly adopted machining method to cut the hard materials, since it can remove any electrical conductive material irrespective of their hardness with high accuracy and better productivity. This process has limitation of low energy efficiency and low material removal rate with high initial machine establishment cost; therefore, machinability of Ti-6Al-4V alloy can be improved during EDM process by reduction in these drawbacks of EDM process.

1.2   Brief history of machinability improvement of Ti-6Al-4V alloy

In the past years researchers applied different methods to improve the machinability of titanium alloys. Ezugwu and Wang [5] studied the machinability during cutting of Ti-6Al-4V alloy and discussed excellent machining capability of tungsten carbide tool. In their study some advanced machining method such as rotary cutting and ledge tools were discussed. In previous studies high cutting temperature, high cutting pressure and chatter discussed as the key factors which decreased the machinability of Ti-6Al-4V alloy. It was observed that special machining technique by modified ledge tool and rotary tool has increased productivity and tool life significantly. Although, both tools have limited application since it was difficult to make complex shape by both modified tools. It was proposed by their study that chemical reactive cutting fluid should be applied to reduce the thermal and mechanical loads during machining. They concluded that more special technique with non-traditional machining method should be developed to improve the machinability of ti-

tanium alloys. Veiga et al. [6] reviewed the machinability of titanium alloys on the basis of process output parameters; build up edge formation, chip morphology, cutting techniques and cutting temperature. They observed that high chemical reactivity and low thermal conductivity influenced the machinability maximum during conventional machining process. They studied about various techniques applied to improve the machinability such as dry electrostatic cooling, flood cooling, minimum quantity lubrication (MQL), water vapour, high pressure coolant, cryogenic cooling, cold air, solid lubricant, hot machining, rotary tooling, chip breaker and ramping. It detected that majority of researchers had attempted to apply the cutting fluid between tool-chip interface to reduce the cutting temperature and friction, by which tool life and surface integrity could be enhanced [7, 8]. Although it is impossible to penetrate the tool-chip interface, studies for tool wear reduction can be explored using high pressure lubrication and cryogenic cooling. Cryogenic cooling is being used by various researchers to extend tool life by lowering cutting temperatures. Cryogenic cooling was found to significantly reduce cutting temperature at medium cutting speeds of 60-90 m/min, while it had little effect on tool life at speeds greater than 90 m/min. [9, 10]. Improper cryogenic penetration in the chip-tool interface was identified as the cause of low tool life during cryogenic cooling. As a result, research into cryogenic cooling is needed to determine the true effect of cryogenic cooling at high cutting speeds. Dandekar et al. [11] applied Laser-assisted machining (LAM) and hybrid machining to improve the machinability of Ti-6Al-4V alloy. In their research work, the CO_2 laser placed on the CNC turret lathe and cutting tool was cooled by liquid nitrogen. They reduced specific energy consumption by 20% and surface roughness by 30% . It was observed that hybrid machining had improved the MRR, tool life and effectively saved cost. Muthukrishnan and Davim [12] studied the machinability of Ti-6Al-4V alloy using coolant and reported higher tool flank wear during wet machining than dry machining. Hence, it can be concluded that wet machining is not good option to improve the machinability of Ti-6Al-4V alloy. Armendia

et al. [13] studied the influence of heat treatment on machinability of titanium alloys. In their research work, three type of annealing process (mill annealed, β annealed and duplex annealed) with air cooling was applied on Ti-6Al-4V, Ti54M and Ti6246 alloy. It was observed that β annealed method modified the microstructure higher than other method while it had increased the flank tool wear and decreased the machinability. Hence, it can be concluded that annealing with air cooling is not good option to enhance the machinability of titanium alloys. Rathod et al. [14] evaluated novel surface textured tool to enhance the machinability of Ti-6Al-4V alloy. They had developed three different shapes on rake face of cemented carbide tool and then these tools were coated with Zr/WS_2 solid lubricant. It was detected from the study that square texture has more significance than circular and linear texture in the reduction of friction between tool-chip interface and cutting forces. Subsequently, improvement in machinability of Ti-6Al-4V alloy was observed with the drawback of higher tool cost since texturing and coating has increased the cost. Lou and Wu [15] applied the electropulsing treatment (EPT) in ultra precision machining to improve the machinability of Ti-6Al-4V alloy.In this method, conventional thermal treatment was replaced by EPT to modify the microstructure of the material and enhance the mechanical properties of it. The EPT process was conducted for 15 min in each sample and with 600^0C temperature. This method has enhanced the plasticity, lowered the yield stress and lowered the hardness of Ti-6Al-4V alloy, Subsequently; EPT has decreased the cutting forces and surface roughness compared to the untreated sample. By this method, it can be concluded that heat treatment at lower temperatures could increase the plastic deformability of Ti-6Al-4V alloy. Recently, Pimenov et al. [16] studied the effect of cooling lubrication technique on machinability of titanium alloys. They have found that dry machining with coated tool was essential for sustainable machining with good machinability since now a days sustainability is big criteria to be included during machining. MQL systems have shown good results in term of machinability, although the economic criteria should be studied to see

whether these systems are cost effective or not.

1.3 Need and scope of work

In recent years demand of titanium and its alloys as a workpiece material is increased in various industries such as aviation, marine, bio application, automobile etc. Excellent mechanical, chemical and thermal properties have promoted the applicability of these alloys. Titanium alloys have diversified range of properties since their microstructure consist of various range of phases such as α, $\alpha+\beta$ and β. The α phase is consist of HCP crystal structure while β phase consist of BCC crystal structure. By varying the % of these phases creep resistance, hardness, specific density, plastic deformability, age hardnability, modulus of elasticity, melting point temperature, yield strength, toughness, ductility, heat resistance, high temperature strength and machinability of Ti-6Al-4V alloys can be modified as per the requirement. Because titanium alloys have a greater machining cost, the product cost of a titanium alloy component is also higher, making industrial applications difficult to implement.

1.4 Problem definition

Ti-6Al-4V alloys are difficult to machine since they have high strength, high hardness, chatter, high melting point temperature and low thermal conductivity. Therefore, various researchers have conducted studies to achieve improvement in machinability of titanium alloys[17, 18]. To improve its machinability various methods have been applied and analyzed. The improvement in machinability of titanium alloy can be achieved by decreasing tool wear, cutting force, surface roughness, production cost, maintenance cost, machining energy; and by increasing material removal rate. Variation in chip thickness, high heat stress, high pressure load, springback, and residual stresses are the main mechanisms that

cause problems while machining of titanium alloys. During machining, this mechanism causes excessive tool wear and a poor surface finish. For machining titanium alloys carbide, binderless CBN, natural diamond and sintered diamond cutting tools have been proven to be appropriate. Application of high pressure coolant and cryogenic cooling are in trend, although these methods are not improving machinability impressively[19] . Therefore, it is necessary to attain improvement in machinability by modifying and developing different techniques such as heat treatment processes [20], cryogenic machining [21], hybrid machining process [22], additive manufacturing [23] and novel manufacturing processes [24]. The Fig. 1.2 shows the schematic representation of methods which can be applied to improve the machinability of titanium alloy.
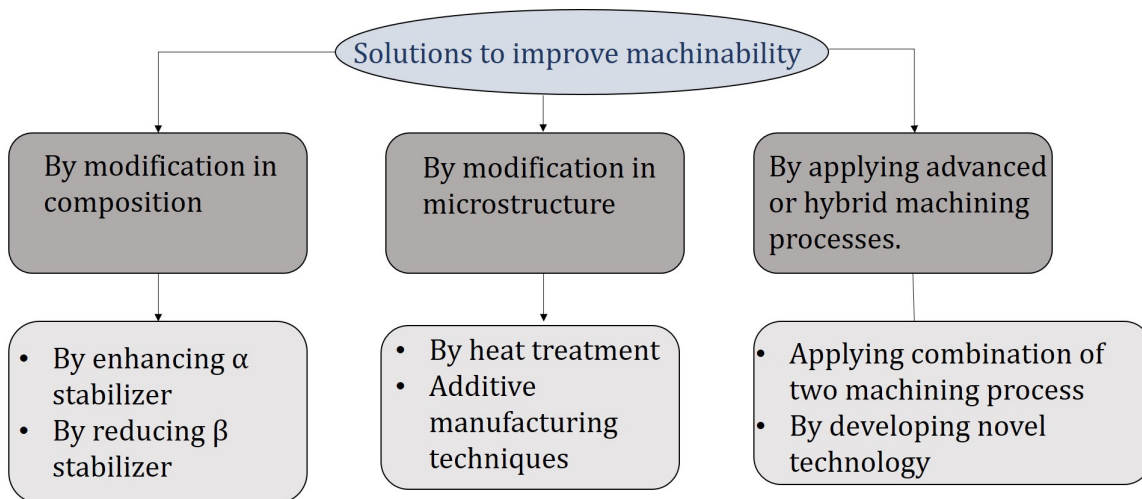
Figure 1.2: Schematic representation of methods to achieve improvement in machinability of titanium alloys

1.5   Aim and novelty of present work

Aim of the present work is to develop a method to modify microstructure or to develop a machining process to improve machinability of Ti-6Al-4V alloy. This can be achieved by

following objectives:

- Develop a novel EDM process since machining capacity would not affected by high hardness and yield strength of material.

- Conduct evaluation of novel EDM process by conventional EDM process.

- Modification of microstructure by furnace heat treatment and different quenching medium.

- Experimental study by high speed milling of modified microstructure.

- Characterization of experimental values on the basis of output parameters such as chip thickness, burr formation, tool wear and surface roughness.

- Evaluation of EDM and high speed milling processes to identify the better machining process for high machinability of Ti-6Al-4V alloy.

To complete the above mentioned objectives, task required to be done are shown below in Fig. 1.3

Task 1

Microstructure control by heat treatment process
  1. Air Quenching
  2. Water Quenching
  3. Cryogenic Quenching

Task 4

Development of novel technology to improve machinability
  1. Propose a Novel Technology
  2. Experimental characterization of it.
  3. Assessment of it with conventional machining method.

Task 2

Characterization of microstructure
  1. Modified grain boundaries and microstructure
  2. Microhardness
  3. EBSD analysis
  4. XRD analysis

Task 3

High speed milling of controlled micro structure
  1. Roughness
  2. Tool life
  3. Burr formation
  4. Chip formation

Figure 1.3: Flowchart of tasks

1.6   Organization of presented report

The thesis comprise of six chapters and brief description of each chapters are given below:

Chapter 1 deals with the brief introduction about the need and motivation of the present study. In this chapter problem is defined with aim of the present study. *Chapter 2* is providing literature survey of the methods applied by researchers for the effortless machining of the titanium alloys. Research gap and research methodology obtained from the previous studies are shown on it. *Chapter 3* focuses on development of maglev EDM and evaluation of it with conventional EDM by output parameters such as material removal rate, surface roughness and specific energy. *Chapter 4* focuses on the modification in microstructure of Ti-6Al-4V alloy achieved by heat treatment and quenching. It shows characterization of microstructure by optical microscope images, EBSD analysis and XRD analysis. Effect of microstructure on microhardness and % area of grain boundaries. *Chapter 5* reveals the effect of heat treated and cryogenic quenched specimen during high-speed up-milling process. Analysis of machining is achieved by characterization of output parameters tool wear,

burr formation, chip thickness and surface morphology. ***Chapter 6*** focuses on evaluation of the developed EDM and high speed milling process , to identify the better machining method. ***Chapter 7*** presents key concluding remarks about the studies conducted on Ti-6Al-4V alloy and scope of future work.

2

Literature Review

The different aspects of metallic bioimplants, limitations, desired surface properties, the need for surface modifications have been discussed in chapter 1. The present work is aimed at creating surface textures via mechanical micromachining technique i.e., micro-milling in Ti-6Al-4V alloy and their functional characterization for bio applications. The literature review presents the prior work done in the relevant areas, namely, limitations and challenges of existing surface modification techniques, mechanical micromachining techniques for the creation of controlled engineered surfaces. Furthermore, recent past work has been done in the fields of surface texturing, improvement in biocompatibility,

and surface properties. The research gap and objectives of the present work have been included in this chapter.

2.1   Introduction

In this chapter the state of art is the prediction of critical process to achieve higher machinability with good mechanical properties in the scenario of industrial application. In the following sections methods to improve machinability are briefly explained such as modification in composition, modification in microstructure and some advanced machining processes.

2.2   Effect of composition on different Titanium alloys machinability

For enhancement in machinability of titanium alloy it is essential to obtain optimum composition during the alloying of pure titanium. Since, some elements enhances α phase and other enhances β phase in titanium alloy. In titanium alloys composition, elements which enhances the β transus temperature by stabilizing the α phase at higher temperature are known as α stabilizer, while; elements which decreases the β transus temperature by stabilizing the β phase at lower temperature are known as β stabilizer. Some example of α stabilizers are aluminum (Al), oxygen (O),carbon (C) and nitrogen (N); meanwhile, β stabilizers are molybdenum (Mo),niobium (Nb),vanadium (V),copper (Cu) and silicon (Si) [5]. Generally, it is observed that both α and β phases are less resistant to crack propagation and dislocation in comparison to α-β interfaces or grain boundaries. Therefore in titanium alloys, it is recommended to create α-β interfaces for aiming at better fracture resistance and strength, although it will decrease the machinability of titanium alloy [25].

In general, pure titanium alloy contains titanium from 99.9 to 99.99 of wt. %; while C, N, O, iron (Fe) and some other elements are present as impurity. The microstructure of pure titanium is polycrystalline α phase in which by increase in contaminants such as C, N and O improvement in hardness, yield strength, ultimate strength and α to β transformation is found [26]. Ouchi et al.[27] found improvement in the proof strength by 0.2% (19 to 55 MPa) with the doping of 0.02–0.03 wt.% of O, N or C to high purity titanium. N has higher while C has a lower effect on the increment of strength among these three elements. Commercially pure (CP) titanium is found in four different grades in α phase according to their composition from 99.495 to 98.955 wt. % and variation of composition presence due to Fe, O and N elements[3]. Simbi et al.[28] found that when interstitial component O and Fe increased 0.40 and 0.2 wt. % respectively on CP then it enhances proof stress, tensile strength and hardness. Wasz et al.[29] found that interstitial O improved room temperature strength, decreased the ductility and impact resistance while hydrogen (H) had affected titanium at very low or high strain rates. Near α titanium alloys contain solutes which stabilize α phase and a small amount of β phase elements (1 to 2%). The β transus temperature of these alloys is high; therefore, they can be applied at high temperature[30]. Gollapudi et al.[31] performed an experiment on Ti-3Al-2.5V at high temperature and low-stress condition creep is managed by an increment of dislocation along slip band boundaries, while at high stress and low-temperature condition grain boundary sliding mechanism of deformation and power-law creep regimes occurred. Tan et al.[32] did high-temperature experiment with varying strain rates on Ti-5Al-2.5Sn and concluded that optimum deformation occurs at 800^0C at 0.0001/s strain rate. They concluded that high strain rates play a significant role in dynamic recrystallization while temperature affects only up to recrystallization temperature. By doing Synchrotron X-ray diffraction on Ti–6Al–2Sn–4Zr–2Mo–0.08Si (near α alloy) and Ti–6Al–4V ($\alpha+\beta$ phase alloy) Malinov et al.[33] found less amount of O content in near α alloy than $\alpha+\beta$ alloy sample, which was the adequate cause behind the

existence of small amounts of β phase in it. Ti 17 termed as β rich titanium alloy since the presence of beta stabilizer content Mo and chromium (Cr) up to 8 % of wt. with better control of forging or heat treatment process. Ti 17 could be formed as a β or $\alpha+\beta$ region by minimizing the "β flecks" which is formed by the enormous separation of β stabilizer[30]. Lee et al. [34] modified microstructure of Ti-15Mo-5Zr-3Al alloy by heat treatment process and found that Al addition in Ti-15Mo-5Zr alloy changes microstructure and yield stress drastically for the same time period. It was concluded that a small amount of Al resists twinning which plays a significant role in the deformation of β-Ti alloys. It is easier to increase the strength of β-Ti alloys by inducing metastable phases or lattice defects into the β matrix[35]. Some elements like boron (B) and carbon (C) also modifies the microstructure and mechanical properties of β-Ti alloys. Hotta et al [36] observed that in many titanium $\alpha+\beta$ alloys such as SP700; small amount of Yttrium (Y) is used as an additive due to their capability of β grain refinement and creating hindrance in grain growth. Resultantly, SP700 has better superplastic formability, mechanical properties and heat treatability than TI-6Al-4V as a result of the fine microstructure of it. They refine β grain size as well as the size of aged α and also create boride and carbide with titanium, hence hardness and tensile strength of β Ti alloy increased. However, there is reduction in ductility occurred since the presence of hard carbide and boride. Meanwhile, aging also increases the hardness and strength with some decrement in ductility of alloy, since the presence of α precipitates [37, 38]. As a result of the above detailed composition description, the following relationships can be established between pure α, near $\alpha,\alpha +\beta$, metastable β, and β phase titanium alloy; which is shown in table 2.1 :

As it can be observed from table 2.1, the machinability, creep resistance property, modulus of elasticity, ductility, heat resistance and strength at high temperature of titanium alloys are decreased as approached towards β phase alloy. While hardness, specific density, plastic deformability, age hardnenability, strength at room temperature and toughness

Table 2.1: Types of titanium alloys and change in its properties as β phase is stabilized in it

Property	From $\alpha \rightarrow$ near $\alpha \rightarrow \alpha+\beta \rightarrow$ metastable $\beta \rightarrow \beta$ phase alloy increasing or decreasing
Machinability	Decreasing
Creep resistance	Decreasing
Hardness	Increasing
Specific density	Increasing
Plastic formability	Increasing
Age hardenability	Increasing
Modulus of elasticity	Decreasing
Strength at room temperature	Increasing
Toughness at room temperature	Increasing
Ductility	Decreasing
Heat resistance	Decreasing
High-temperature strength	Decreasing

at room temperature has increased when moving toward β phase alloy from pure α phase titanium. Hence, to improve the machinability of titanium alloy by modification in composition can be achieved by compromising with some properties of titanium alloy. Therefore, it is necessary to develop or find composition in which without deteriorating required mechanical or thermal property, the machinability of titanium alloy could be increased.

2.3 Microstructure of titanium alloy and its effect on machinability

The microstructure of titanium alloys varies from α phase to β phase alloys, and machinability varies according to phase, as do the shape and size of grains. Features of titanium and its alloys are dependent on their composition and microstructure. Titanium alloys have

two crystal structure viz. hexagonal close-packed (HCP) and body-centered cubic (BCC), and these two structures are divided into phases by β transus temperature (882[0]C) of titanium. At 882[0]C; α phase from HCP metallic structure converted into β phase with BCC by allotropic transformation and this transformation can take place up to melting point temperature of titanium (1668[0]C). BCC structure has a higher plastic deformability in comparison to HCP structure since closed packing density of HCP is higher and number of slip system are less than BCC. Although, ductility of α phase alloy is higher than β phase alloy[3]. Figure 2.1 shows the difference between α and β phase of titanium alloy.
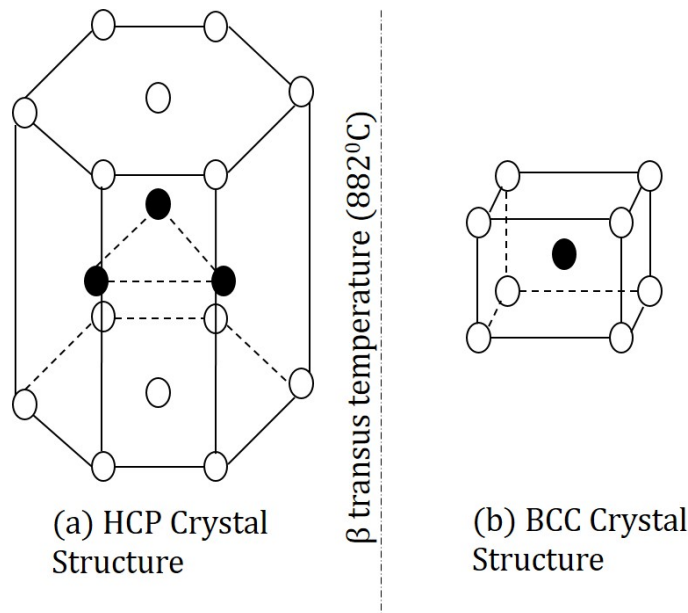
Figure 2.1: (a) α Phase with HCP crystal structure (b) β phase with BCC crystal structure [3]

Lutjering [39] obtained fully lamellar and bi-modal structure for Ti-6Al-4V; and found α colony size and β grain size is larger for fully laminar structure than bi-modal structure. Additionally, he has found relationship between mechanical properties and α colony size or β grain size. It was observed that α colony size or β grain size is in inverse relationship with yield stress, ductility, crack nucleation resistance and the resistance towards microcracks development, while in direct relationship with resistance towards macrocracks

development and fracture toughness. Poondla et al. [40] compared microhardness and macrohardness of CP grade 2 and Ti-6Al-4V. They observed that large volume of β phase enhances the microhardness higher than macrohardness on Ti-6Al-4V, while; presence of large volume of α phase enhances the macrohardness higher than microhardness. Yashwant and Harold [41] performed an experiment on Ti-6AI-2Sn-4Zr-6Mo which is $\alpha+\beta$ phase titanium alloy. They concluded that at low strain condition crack initiation takes place at α-β interfaces of equiaxed (α'), Widmanstatten + grain boundary $\alpha(W\alpha + GB\alpha)$ and in the aged β matrix. As a result of bigger β grain size; longer Wα and GBα particles grow, these longer particles give an elongated path to initialize crack growth hence longer surface cracks induced. Johnson et al.[42] compared two microstructure of Ti-6Al-4V viz. Widmanstatten and equiaxed by varying strain rates and had found that failure was higher in equiaxed microstructure than Widmanstatten microstructure. It was observed that by application of tailored bimodal microstructure; tensile strength, creep performance and fatigue resistance at 600^0C of near alpha titanium alloy IMI834 improved [43]. The minimum temperature at which dynamic transformation of CP grade 2 from α to β phase takes place is 765^0C and increase in the volume fraction of β phase takes place up to the melting point temperature of CP 2 titanium [44]. In α phase titanium alloy β phase is in a very small amount; therefore, Harper–Dorn creep has been claimed to control the creep behavior of α-Ti alloys at high temperature and low stresses condition[45]. Ti-10V-2Fe-3AI is metastable β alloy and Terlinde et al.[46] studied its microstructure. They have concluded that yield stress and microstructure had a direct impact on ductility, and if yield stress increased during static microstructure, then a decrement in ductility occurred. In this study it was observed that α film in microstructure grain boundary plays a significant role in fracture and low ductility since the plastic strain is formed in a small volume of film. Froes et al. [47] conducted an experiment on Ti-11.5Mo-6Zr-4.5Sn and concluded that if aging was done on alloy at 480^0C then athermal omega (ω) phase formed uniformly

in the matrix which was inversely proposal to the presence of O element on the β alloy. Moreover, quenched hardness was higher in the presence of small amount of O element, therefore, it can be concluded that ω phase increases quenched hardness of the material. Ti-555 alloy had a very fine nodular structure with a harder β grain size of about 1μm, therefore, machining of it became a difficult task to do [48]. Higher specific cutting force and specific feed force occurred in Ti-555 than Ti-6Al-4V since the high microhardness of Ti-555 [49].

Titanium alloys are widely used on different industries although production cost of the component from these alloys is higher since low machinability. Therefore, it is crucial to decrease production cost by increasing their machinability with improvement in desired properties according to specific industries. Machinability is dependent on tool life, the microstructure of titanium alloy and surface finish of workpiece since if the tool can do machining of workpiece easily with good surface finish then production cost will be minimum. By modification in the microstructure of titanium alloy low in cutting forces, low tool wear rate and low surface roughness can be achieved; or in other words, machinability can be increased.. Hence, here state of art is the optimization of the microstructure of titanium alloy and tool life to obtain minimum production cost.

2.3.1   Heat treatment process

Heat treatment is a cyclic heating and cooling process to modify material physical, microstructural and mechanical properties without changing the shape of the material. Through the heat treatment process, it is possible to achieve the desired microstructure, which has changed since other processes such as cold rolling, cryogenic treatment, surface modification, etc. Matsumoto et al.[50] applied cold working on β phase Ti-Nb-Sn alloys and had found Stress-induced martensite (α'') then tempered it at 250^0C to reverse it as β grains and fine α precipitation with high-density dislocations from α''. They have found an increment

in Young's modulus, tensile strength, and large elastic strain, which was reduced since the cold working of the alloy. Venkatesh et al. [20] found that water quenching with ageing increased internal hardness, yield strength, and ultimate strength, but decreased ductility compared to air cooling with ageing. Zhan et al.[51] did an heat treatment experiment on Ti-Si alloy and found that Ti-8Si and Ti-13.67Si hardness were increased with high-temperature heat treatment, while T-23Si performed exactly opposite to it. It was caused by inertial actions of pro-eutectic Ti5Si3 particles of the Ti-23Si. It was seen by Zhu et al.[52] during heat treatment of TA15 that the cooling rate after heat treatment was directly related to the final microstructure of Titanium alloy. During lower cooling rate; increment in volume fraction and size of α phase with uniformity was occurred since growth time was higher to develop α phase. Chun et al.[53] developed two types of the microstructure of commercial alloy Ti-6Al-4V viz. Ti64-1 by heating at 800^0C to 1hr then air cooling and Ti64-2 by heating at 950^0C to 1hr then air cooling. In Ti64-1 lamellar $\alpha+\beta$ is present 15% of volume and in Ti64-2 58% volume, resultantly; Ti64-2 have more hardness than Ti64-1. Near α titanium alloy TA-15 can be modified in tri-modal structure by heating at near β temperature and cooling it suddenly by water quenching to convert it into primary equiaxed α_p and secondary lamellar α_s grain with small amount of β matrix. By controlling the amount of α_p and α_s, it is possible to modify its strength since α_p helps to enhance plasticity whileα_s enhance impact toughness and high-temperature strength[54, 55]. Therefore, it is possible to control plasticity to obtain good machinability and high-temperature strength with impact toughness by tri-modal microstructure approach. Lopes et al.[56] did an experiment on β phase Ti-Nb alloy and concluded that it is possible by heat treatment to enhance the mechanical strength with the compromise of increase in elastic modulus. Therefore, by applying annealing process with higher cooling rate it is possible to enhance the ductility and machinability of titanium alloys.

2.3.2   Cryogenic treatment and cryogenic quenching

Cryogenic treatment is a process to put workpiece inside the cryogenic liquid to cool down at cryogenic temperature and put it for some time to modify the microstructure of it. In this method material is cooled to cryogenic temperature; thus desired mechanical properties such as increment in hardness, tensile strength and wear resistance property can be obtained. Cryogenic treatment transformed the β metastable phase into α phase and β phase, therefore; decreases the amount of β phase. Resultantly, enhancement in plasticity is observed while no effect on microhardness of Ti-6Al-4V alloy was occurred. It is achieved by enhancement in the density of dislocations and twins; which increased the plasticity of Ti-6Al-4V alloy[57]. Recently Gu et al. [58] studied the effect of deep cryogenic treatment (DCT) on change in the microstructure of metastable β titanium alloy Ti-15Mo-3Al-2.7 Nb-0.2Si (TB8). They merged the specimen for DCT (at -196^{0}C for 24 Hr and cooling rate of 20^{0}C/min), solution heat treatment (specimen put at 800^{0}C for 2Hr) and aging (specimen put at 580^{0}C for 8Hr with air cooling). They compared microstructure of five types of treatment viz. raw (R) untreated annealed, raw DCT (RD) treated annealed, solution and aging (SA) treated annealed, solution +DCT +aging (SDA) treated annealed and solution + aging + DCT (SAD) treated annealed Ti-alloy. They concluded that RD and SAD not influencing the microhardness and tensile properties of this alloy while SDA improved microhardness about 15% and tensile strength 5% in comparison to commonly used strengthening process SA. It happened since DCT after solution heat treatment had offered enhancement in the formation of needles like α phase with refinement and volume fraction of α phase increased from 23% to 27%. In another study it was observed that to get the desired effect on microstructure soaking time should be longer, since atoms movement at -192^{0}C is very slow. Cryogenic treatment modifies the worn surfaces flatter and reduces the amount of plastic deformation, hence increment in wear resistance and the low friction coefficient properties were found[59]. Another study conducted to see the effect of

deep and shallow cryogenic treatment on Ti-6Al-4V alloy. It was observed that [60] lower cryogenic temperature had higher impact in modification of mechanical properties than higher cryogenic temperature and detected β to α transformation during DCT process. Molinari et al.[61] studied the effect of DCT on tool wear resistance property and they achieved improved tool life by it. They had achieved improvement in tool life since DCT process had increased hardness and toughness of the tool. Lal et al.[62] did DCT process on coated and uncoated tool with two different cryogenic temperature and treatment time. They detected that cryogenic treatment not affected the coated tool pretty much since coating material and the substrate shrinked irregularly, which leaded to incipient cracks at the interface. Additionally, they had observed that soaking time influenced too much in increment of tool wear resistance property and achieved greater wear resistance for 24 Hr DCT process rather than 6 Hr DCT process. Cryogenic quenching is termed as a process of rapid cooling of workpiece material inside cryogenic liquid upto cryogenic temperature and then quickly remove from cryogenic liquid to warm up to a room temperature. Han et al. [63] studied the effect of cryogenic quenching on friction stir welded 6061-T6 aluminum joint. They achieved highest yield strength and microhardness for solution treated+ cryogenic quenched and then tempered sample than other samples. Grahol et al.[64] conducted cryogenic quenching on laser cladded sample to modify the microstructure of coating into fine grains and to enhance the hardness of coating. The cryogenic quenching sprayed in the coating and it enhanced the cooling rate of the deposited material, hence achieved required microhardness on it. Cryogenic treatment and cryogenic quenching processes are looking similar to each other but there is a difference between both processes and that difference is time of sinking the workpiece inside the cryogenic liquid. Cryogenic quenching is similar to water or air quenching process in which researcher put the specimen to do the rapid cooling and stabilizing the formed microstructure as it is in the heat treated form. Hence, by applying the cryogenic quenching the cooling rate after the heat treatment can be en-

hanced at maximum value and desired properties can be obtained by it. To enhance the machinability and ductility of titanium alloy cryogenic quenching after the annealing process can be applied, since annealing process enhances the α phase and by higher cooling rate of cryogenics those α phases could be stabilized.

2.3.3   Additive manufacturing

Additive manufacturing are rapid prototyping or 3D printing processes and these methods have huge demands now a days since its characteristics such as modified lattice structure, can build complex shape and desired mechanical properties. Now a days production of titanium alloys through additive manufacturing is in trend. The directed energy deposition (DED), selective laser melting (SLM) and electron beam melting(EBM) are common methods to produce titanium alloys. The product developed from EBM methods have strength comparable to conventionally developed product while product developed from SLM and DED methods had strength 25% more than conventionally developed product [65]. In this method requirement of post process machining and material loss is very less since 3D shapes are made directly layer by layer with computer added design data. There are different kinds of additive manufacturing processes which are shown on Fig. 2.2 [66]. These methods have high demand in various field such as electronic, bioimplant, marine, consumer, food industries etc [67, 68]. Singh et al. [69] manufactured Ti-6Al-4V alloy by metal fused filament fabrication and had observed factors affecting its properties. They had formed highly accurate and fine surface with this process. By increment of O % from 0.16 wt% to 0.30 wt%, the ultimate tensile strength of Ti-6Al-4V alloy had been increased from 500 MPa to 960 MPa. Carroll et al. [70] fabricated Ti-6Al-4V alloy by directed energy deposited additive manufacturing process. It was concluded that high ductility could be achieved by minimizing fused porosity. Therefore, by modification in any composition, desired machinability with strength could be developed by additive manufacturing process
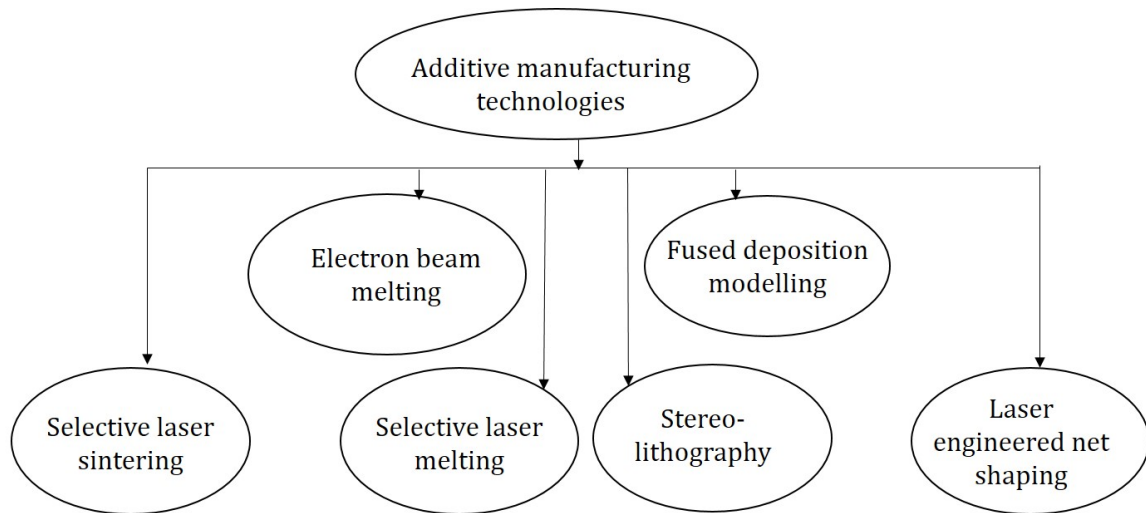
Figure 2.2: Different kind of additive manufacturing processes [66]

and less material will be waste since less post processing is required in it.

2.4   Advanced machining processes to enhance machinability of titanium alloys

There are some major issues during the machining of titanium alloys such as higher cutting pressure,higher tool wear rate, higher chatter, higher melting point temperature, higher chemical reactivity, higher machining cost and lower thermal conductivity. Therefore, it is crucial to reduce these effects by some advanced machining processes. Following are some methods to achieve this task:

2.4.1   Cryogenic machining

Cryogenic machining has dominance over other conventional machining processes and used as a sustainable manufacturing process, due to its characteristics such as minimum heat generation, eco- friendly, no chemical dissociation, low production cost, and highly productive etc. In Fig. 2.3 relationship between conventional emulsions cooling with cryogenic machining has shown in terms of production cost and productivity for AISI304 material. As compared to conventional machining, cryogenic machining yields the dual benefit of low production cost and high productivity. Therefore, cryogenic condition plays an important role for sustainable machining purposes. Consequently, cryogenic machining has been more focused in research and industrial application in the recent past[71]. Cryogenic machining can be done by three methods viz. indirect cooling, direct jet cooling and cryogenic minimum quantity lubrication (CMQL). Theses approaches have different effect during machining of titanium alloy. Therefore these methods are briefly explained in following sections:
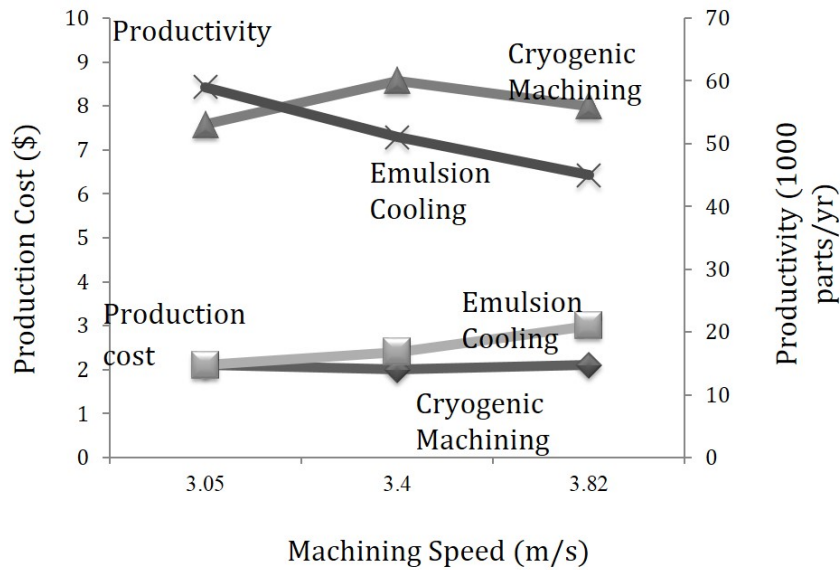
Figure 2.3: Economical evaluation between cryogenic and emulsion cooling [71]

2.4.1.1 Indirect cryogenic cooling

This cooling process is known as conductive remote cooling and cryogenic tool back cooling. In this method cutting point cooled by heat conduction of cryogenic material situated at tool holder or tool face. This approach of cryogenic cooling is impressive if contact area of cryogenic coolant with tool surface is more. Figure 2.4 illustrates the schematic of experimental system for indirect cryogenic cooling. Here, LIN (Liquid nitrogen) provided on an enclosure bounded by tool and shim to cool the tool rear part. Here, LIN is not in contact with the workpiece hence; no effective modification in properties of the sample[72]. However, this method of cooling has some limitations like low thermal conductivity of the tool material and thick section should be high and necessity of proper tool thickness for heat conduction of cryogenic coolant.
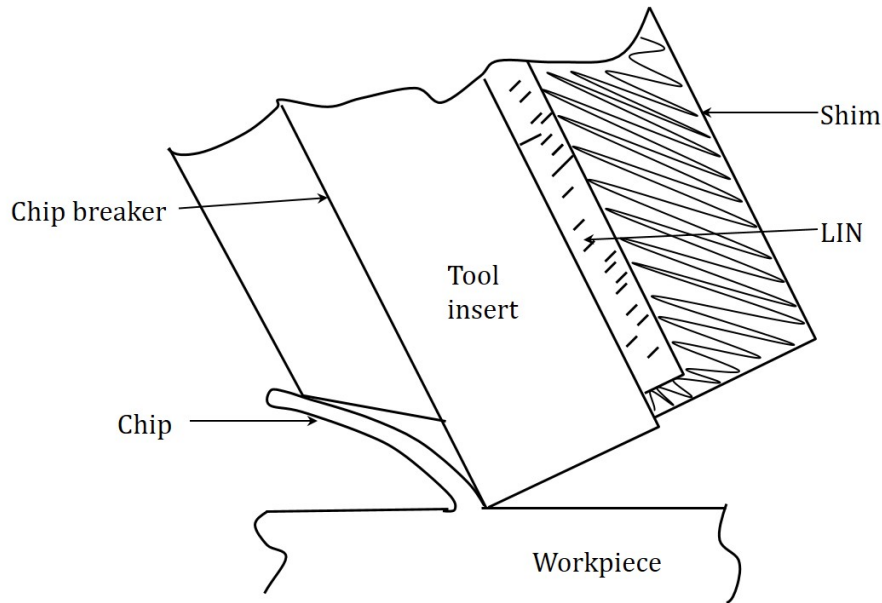
Figure 2.4: Illustration of experimental system for indirect cryogenic cooling
[72]

2.4.1.2   Cryogenic Jet machining

This machining is known as jet machining because cryogenic coolant is supplied to the tool-chip interface through micro-nozzles. In this method cryogenic coolant is provided on tool cutting tip with the help of nozzles. Hong et al.[73] applied two nozzles primary and secondary as shown in Fig. 2.5. Primary nozzle was inserted between tool surface and chip breaker; while secondary nozzle placed to freeze flank surface close to cutting tip for more decrement of flank surface wear. They had used LIN delivery nozzle system, with a chipbreaker and LIN is inserted into chipbreaker and rake surface of tool. Chips were uplifted with the help of chipbreaker, hence LIN extended upto chip- tool boundary. Hong and Broomer[71] used three nozzles in a design for spraying LIN into chip-tool boundary. LIN is focused on three directions through flank nozzle on cutting edge, through Z-direction nozzle on parallel to the spindle axis and through X- direction nozzle on perpendicular to the spindle axis. In design of Venugopal et al.[9] , nozzle placed on tool post for injecting LIN jet on flank and rake face of tool. In their analysis, tool wear at 70 m/min
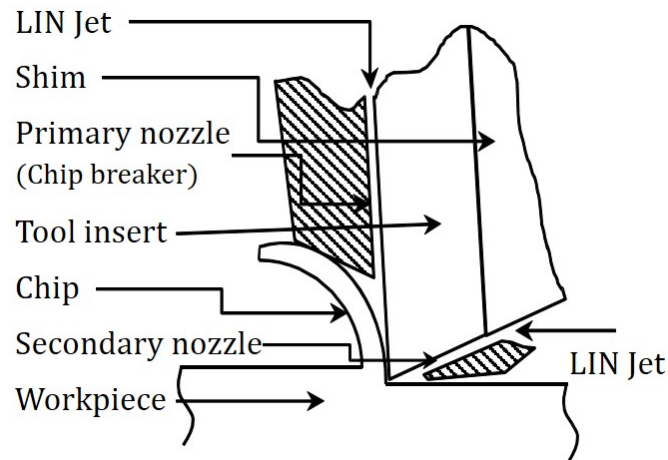
Figure 2.5: Cryogenic jet cooling with two nozzles
[73]

was decreased while no significant reduction during cutting speeds of 100 and 117 m/min was observed. This condition was discovered since the LIN had not properly invaded the tool-chip interface. In another design, Dhar et al.[74] focused LIN jet on flank and rake face, alongside to principal and secondary cutting edges. They had observed similar condition since cryogenic jet cooling had enhanced tool life during lower feed and lower cutting velocity. Additionally, cryogenic jet cooling has distinct advantage such as minimal waste due to coolant applied directly to tool location, where the object is parted off and high temperature produced. Cryogenic material injection should have to be in the region where heat developed during machining progress, therefore over cooling of workpiece sample can be avoided with efficient machining condition[73].

2.4.1.3 Cryogenic minimum quantity lubrication

In cryogenic minimum quantity lubrication is termed as a method to apply cryogenic liquid with minimum quantity lubrication system, to enhance the machining efficiency. In an experiment Zou et al.[75] approached to new method namely cryogenic minimum quantity lubrication (CMQL) and studied on ease of machining by combination of cryogenic

machining and MQL. In this experimental work they combined compressed gas, micro lubrication oil and vaporized to create a cryogenic gas liquid mixture and this mixture is supplied to cutting region with some velocity and pressure by nozzle. These minute oil droplets are penetrated inside the cutting region effectively for better cooling and lubrication. Using this experimental setup they induced cooling temperature -30^{0}C, flow rate 40 ml/h and air pressure 60 bar. Maximum temperature of diamond tool measured by infrared thermal imager and compared for effect of cooling and lubrication. CMQL has given enhanced output for machinability through diamond tool than flood oil cooling, cryogenic machining, and MQL. In other words, CMQL can be defined as direct cooling produced through cryogenic gas and minute lubrication oil which consist of indirect cooling activity and direct lubrication activity of minute lubrication oil. For cutting oil carbon nanofluid showed enhanced tool life and better surface finish than PEG (polyethylene glycol), synthetic ester oil and emulsion cooling. This method was costly and required complex arrangement to do machining, therefore, in industrial application this method required to be modified for simple application of it.

Cryogenic machining is emerging as a cost-effective, eco- friendly and advance sustainable manufacturing process for difficult to cut materials. Cryogenic materials fulfill the need of coolant as well as lubricant with enhancement in various desirable characteristics of the sample. Therefore, researchers and scientist are more focused specifically on developing method for machining superalloys used in aerospace industries, nano-crystalline surface regeneration and inducing desired properties to any material. LIN is the material used in most of the machining cases as cryogenic fluid and during machining process, it cools tool as well as workpiece. Cooling of the tool makes it harder by altering its microstructure and reduces wear. It is reported that the maximum tool life is achieved by putting cryogenic fluid through the rake face and flank face together. Workpiece cooling may not be useful at all the time because it makes the workpiece harder and therefore in-

creases the cutting forces. Most of the analysis is done on turning and orthogonal process; however, few are done in other operations like milling/micro milling. In a milling operation, the tool comes in contact with the workpiece for half of the time in its rotation and half of the time it rotates freely without contacting the workpiece. Therefore, the cryogenic fluid was provided to the back of the milling tool which reduces the workpiece precooling and showed efficient cooling to the tool. Further, research work can be focused on minimizing the force required to cut the sample. Until now cryogenic material in common cases enhances force required to cut the material therefore energy consumption increased for machining. Hence machining by CMQL process needs improvement for reducing force required and make cryogenic machining more economical from perspective of energy consumption. The major issue with the cryogenic material is its handling. A better controlled flow of cryogenic fluid can reduce the volume of the excessive liquid so that, increase in the cutting force can be controlled. It can be concluded that cryogenic cooling is a sustainable substitute of conventional wet cooling and have potential to significantly enhance the machinability of difficult-to-machine materials.

2.4.2 Ultrasonic assisted machining

Ultrasonic assisted machining is a machining approach in which conventional machining combined with ultrasonic vibration of the tool. To conduct ultrasonic assisted machining ultrasonic transducer is attached to the conventional machine and it is called as ultrasonic assisted drilling (UAD), ultrasonic assisted turning (UAT) or ultrasonic assisted milling (UAM). Figure 2.6 shows the schematic diagram of apparatus which is applied by Muhammad et al.[76] to conduct UAT by converting conventional lathe machine into UAT setup by attaching transducer, transformer, frequency generator, and sine-square oscillator. They had concluded that UAT produces shorter chips, improved surface finish and required low forces to machine in comparison of conventional turning hence machinability increased by

UAT. In an experiment of Ti-6Al-4V at UAM, it is seen that with an increase in vibration amplitude to optimum value decrement in cutting forces Fx and Fy occurred in comparison to conventional milling . Burr formation, surface defects like tool path spots and size of chips also decreased during UAM in comparison to conventional milling which helped to enhance the machinability of Ti-6Al-4V. Jamshidi and Nategh[77] conducted an experiment to compare the coefficient of friction between UAT and conventional turning. They had detected that friction of UAT is higher in comparison to conventional turning upto the cutting velocity of 33.435 m/min. Further, the friction reduced during UAT as compared to conventional turning at higher cutting velocities. Pujana et al.[78] studied UAD on Ti-6Al-4V and concluded that feed force decreased and temperature increased during UAD in comparison to conventional drilling, therefore, the optimum value of vibration amplitude needs to be taken. Hence, by applying ultrasonic assisted machining capability of con-
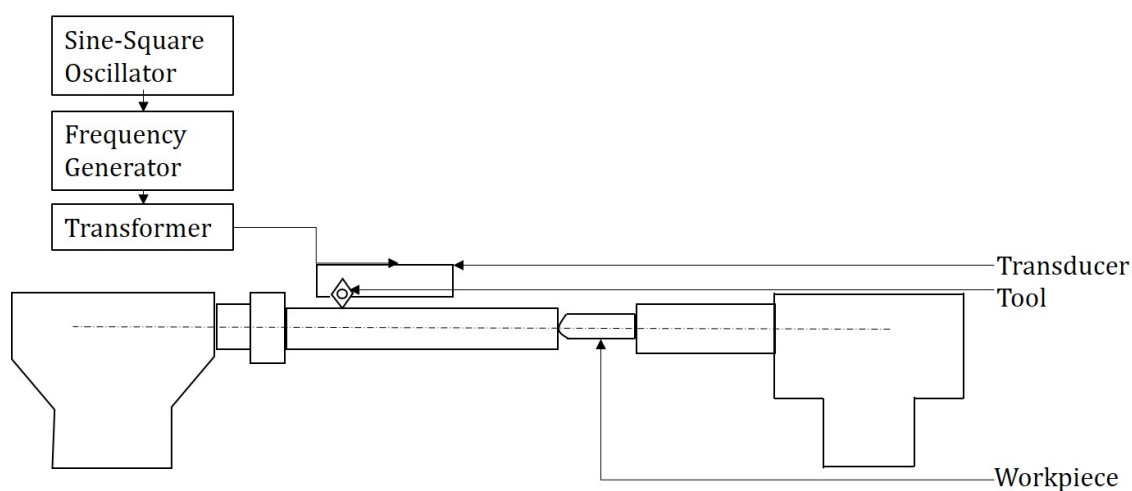
Figure 2.6: Schematic representation of UAT
[76]

ventional machines can be increased compromising with some output parameters. Hence, these methods could be recommended to enhance the machinability of titanium alloys for some specific applications.

2.4.3 Laser machining

The laser can be used in different machining applications as assistance to machining or by directly applying on the workpiece. Laser asssisted machining (LAM) is done with the help of laser power dedicated to a point which is going to be machined by the tool. By doing so workpiece material becomes low in strength and machining is done easily with less amount of force and tool wear. Rashid et al.[79] investigated about tool wear and tool life during LAM of Ti-6Cr-5Mo-5V-4Al, β titanium alloy and had found that LAM has a significant effect if it was applied in a range of laser power 1200-1600 W and cutting speed of 25-125 m/min. In this range of laser power and cutting speed LAM decreased the cutting forces. In another study comparison between conventional machining with LAM was done and found that LAM decreased the maximum cutting force by 15% in the same feed rate. They had investigated about temperature and found 1050-1250^{0}C is optimum temperature range to reduce cutting force[80]. During LAM of Ti-10V-2Fe-3Al at 56 m/min with 1600 W laser power feed force fluctuation was found which could be resulted in tool failure since high chatter, therefore researcher had concluded optimum laser power range 800-1200 W and cutting speed range 55-140 m/min during machining of β phase alloy[81]. In the Fig. 2.7 schematic diagram of LAM is shown in which a laser beam is followed by tool path and machining is performed by preheating of the workpiece with the help of laser spot. Ding et al.[82] investigated LAM during micro-milling and had achieved a reduction in tool wear rate and BUE on micro-milling during machining of Ti-6Al-4V. Ayed et al.[83] developed a heating model on the basis of its laser power and distance of the laser axis with tool face can be optimized. They had found variation in chip geometry and reduced cutting force during their experiment. Gao et al.[84] investigated nearα alloy BTi-6431S and concluded that LAM had less effect on it than Ti-6Al-4V alloy. Moreover, LAM has no significant effect on the improvement of tool life on machining BTi-6431S. In LAM key limitation is failure of tool during machining and it was occurred in studies since high temperature and notch

wear which should be minimized[85]. Surface treatment can be done by laser processing
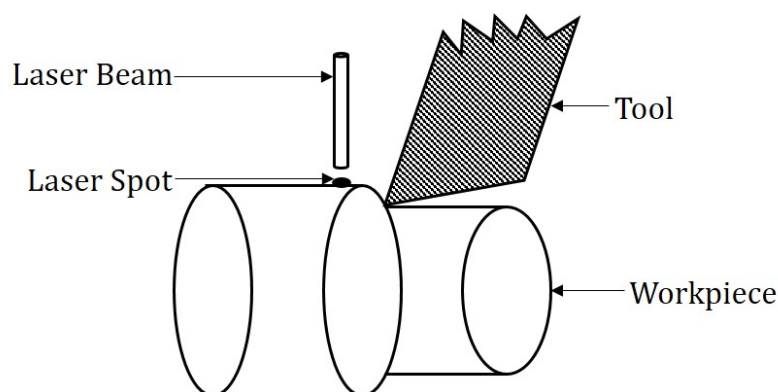
Figure 2.7: Schematic representation of LAM process

on upper surface of workpiece. To do so, firstly surface area should be cleaned by acetone then the laser beam is positioned towards the required area. During the melting of surface area, an inert gas is continuously flown on the surface to protect it from oxidation. This method was used by Badekas et al.[86] on pure titanium and they had found that the surface layer is harder than a deeper layer of pure titanium with higher anti-corrosive property than received pure titanium. This study was confirmed by Sun et al.[87] in which they had concluded that by virtue of rapid solidification, modification in microstructure takes place; as a result improvement in corrosion resistance property occurred. Therefore, to enhance anticorrosive property surface melting by laser method can be used.

2.4.4 EDM system

EDM systems work on the principle of erosion of workpiece material by electrical discharge or sparks. In this process machine consist of anode as workpiece material and cathode as tool material and electrons travels from tool to workpiece. This movement of electrons generates high energy plasma inside the dielectric medium and removed the workpiece by evaporation to form a desired shape. Various types of EDM techniques are avail-

able currently viz. die-sink EDM [88], dry EDM[89], wire EDM[90], wire electrical discharge grinding (WEDG)[91], micro EDM[92] and electrical arc machining (EAM)[93]. In wire EDM a thin wire of brass for the cathode electrode is applied to produce erosion on workpiece material and it removes the material in the required form while in die sinker EDM workpiece electrode are sink inside the insulating fluid which is called dielectric[94]. The schematic representation of die-sink EDM is shown in Fig. 2.8 which consist of pulse power supply, generator, digital oscilloscope, data recorder, EDM servo system, dielectric medium, tool electrode, workpiece electrode, filter, and the pump. Dielectric medium is continuously cleaned by the filter and supplied inside the tank by a pump. There should be a significant gap between both electrodes to maintain continuous machining of the workpiece to avoid short circuit which leads to stop the machining operation. Therefore, continuous machining process is achieved by providing a servo mechanism system which helps to maintain a significant gap to produce discharge. Pulse power supply and generator are provided to transfer electrical current to the tool and the digital oscilloscope is used to monitor the current and voltage of tool electrode. Strasky et al.[95] studied microstructure and fatigue performance after EDM of Ti-6Al-4V. They had concluded that three types of microstructure viz. coarse lamellar, bimodal and equiaxed existed in Ti-6Al-4V after EDM and EDM processed specimen showed less fatigue strength in comparison to electro polish specimen. They had attributed pre-existed surface brittleness, microcracks, and residual stress as the reason of less fatigue strength. During EDM of nickel-titanium alloy, Theisen and Schuermann[96] found cracks, precipitates and melting zone on the surface, which they had removed by polishing. In another study, high material removal rate (MRR), surface finish, debris size, and stable impulsive force is occurred by application of distilled water as a dielectric fluid in place of kerosene[97]. Moreover, it is observed that conventional EDM process reduces surface finish and fatigue strength, therefore post-processing by electro chemical polishing or bead blasting become essential to do. Since it becomes es-
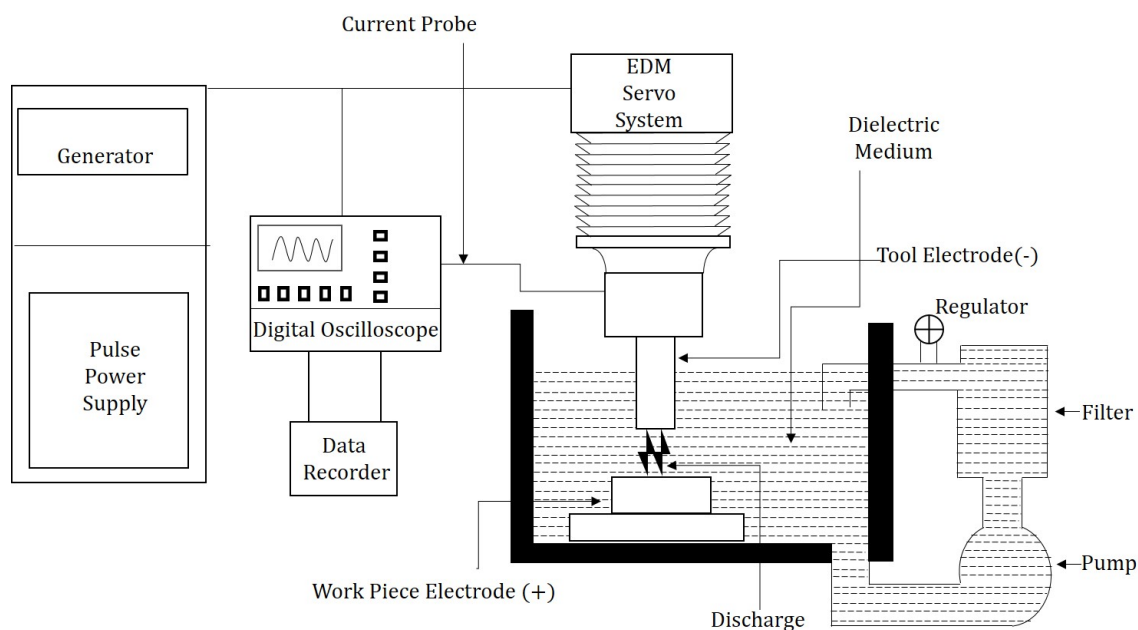
Figure 2.8: Schematic representation of Die-sink EDM machine

sential to do post-processing of material after machining thus decrements in the production rate and high machining cost is occurred by EDM [98]. EDM machine has key characteristic that it can machine any material irrespective of its strength or hardness. The limitation of EDM machine is its dependability on workpiece material should be electrically conductive to be machined. Although researchers have managed to overcome this problem by applying conductive layer on non conductive workpiece material[99]. EDM process has another limitation of low MRR, which emits EDM process to apply on industrial scale for mass production.

In EDM, sparks are produced at the interacting faces of the electrodes (workpiece and tool) by the influence of the high temperature plasma channel, while the electrode faces are submerged inside a dielectric media. Under the influence of the applied voltage, the dielectric fluid breaks down and loses its insulating property at a certain voltage, allowing the passage of discharge current by forming a conductive plasma between the electrodes. The complete operation is carried out, when the electrodes are placed by maintaining a certain

gap (discharge gap) inside the dielectric fluid. The machining gap between the electrodes is attained by the assistance of a servo-controlled motor. Material is removed from both the tool and workpiece surface through melting and vaporization. In EDM, the non-contact behavior helps in avoiding the generation of any mechanical stresses and vibrations during the operation. The discharge action in EDM occurs at a very minimal gap (micro to nanoscale) where the generation and transmission of thermal energy occurs between the electrode surfaces. The gap monitoring system is highly essential to execute the machining operation. Mostly, the servo-gap control mechanism helps in achieving the desired discharge gap in EDM for carrying out the operation. It also provides a reasonable amount of assistance to avoid arcing and short-circuiting phenomena during the machining action. Generally, the servo-control system is designed by the help of lead screw, belt-drive and gear-based arrangements which results in motion inertia, backlash and wind-up setbacks. Such concerns affect the machine productivity, stability and repeatability of product accuracy. Issues such as transmission and response delay in the servo-control system highly affect the machining efficiency.

To improve the efficiency of EDM operation several research have been reported implementing diversified approaches such as hybridized techniques, adaptive gap monitoring mechanism, improved flushing mechanism, etc. Beravala et al. [100] studied the effect of variable machining parameters in magnetic field-assisted EDM during the machining of SAE 304 steel. They reported the effects on response measures with an air assisted flushing system. The combined effect of magnetic field and air pressure helped in enhancing the MRR by 10-18%. Tong et al. [101] performed an experimental investigation on variable parametric combinations in a vibration-assisted EDM. They have studied the effect of parametric variations on micro-structure of steel plate, while non-circular impressions are generated using a tungsten electrode. The machining efficiency was enhanced by 18% and around 10μm of better dimensional accuracy was achieved. Kim et al. [102] inves-

tigated the feasibility of implementing nano-pulsed laser combined with the micro-EDM operation. They observed that pre-processing of workpiece with the laser operation and the followed by the micro-EDM operation helped in improving the machining rate in comparison to the conventional EDM. Though the reported literature established an improvement in machining rate through hybridization techniques, but it lacked any improvement regarding the gap control mechanism. Das et al.[103] had implemented a fiber Bragg grating (FBG) sensor to detect the machining gap in EDM. They investigated the deflections generated on a cantilever structure carrying the sensor and acquired the strain variations. They had observed a variation range of 1.1-18.6 μm in the machining gap using this technique. Fujiki et al.[104] demonstrated a gap control mechanism for five-axis milling EDM system along the direction of the tool orientation. They had solved the unidirectional tool retraction in the direction of machining trajectory. The implemented gap control strategy improved the MRR by 30% through discharge gap enlargement to achieve faster gap voltage. These implemented advancements had complicated the circuits to modify the gap control and monitoring through sensors, but the major issue of arcing and short-circuiting was still not introduced. Bamberg et al. [105] implemented an orbital trajectory to the tool by using a specialized machining head in micro-EDM. They had controlled the orbit radius to control the diameter of the resulting micro-hole through a 2-axis flexural machining head. The orbital motion had helped in enhancement of the flushing action and improvement of the machining efficiency. Kumar et al.[106] enhanced the EDM efficiency by implementing improvised tool for improved flushing in high-aspect ratio (AR) holes. They had eliminated the arcing and short-circuiting phenomena during EDM operation by avoiding the accumulation of debris at the machining zone. They had noticed a 300% increase in the AR of the drilled hole using the improvised tool in comparison with solid tool. Diversified approaches as discussed above have been implemented to improve the machining efficiency without addressing any improvement method to control the electrode

gap during EDM operation to avoid arcing and short-circuiting. A breakthrough research on the gap control was reported by Zhang and their co-researchers [107, 108] implemented 5-DOF controlled actuator attachment to a conventional EDM setup. They had attained gap control along the vertical and radial directions using a 2 mm positioning stroke actuator which was having a submicron and micro-radian positioning resolution. They had observed a 21.8% improvement of machining rate for obtaining 1mm diameter holes as compared to traditional EDM. Several attempts have been reported to enhance the MRR in EDM process by considering different key factors. The optimized outcomes acquired on implementing variable machining parameters show the improvement in MRR and their effect with individual attributes.

Pradhan et al.[109] investigated the effect of variable parametric combinations to achieve desired optimized responses by implementing Taguchi approach and statistical analysis in micro-EDM of Ti-6Al-4V alloy. They had considered the ANOVA and S/N ratio results to obtain the optimal machining conditions for higher MRR, lower TWR and overcut. They had detected a highest MRR of 69.5 µg/min at gap voltage (100 V), peak current (1A) and duty factor (60%). Kao et al.[110] optimized the process parameters of EDM using a combined approach of Taguchi and grey relation analysis to improve MRR, electrode wear ratio and surface roughness of Ti-6Al-4V. They had observed an increase of 12% in MRR and decrease of 19% in surface roughness at optimal settings. They had achieved a highest MRR of 3.2 mg/min at discharge current (5A), open voltage (200 V) and duty factor (70%). Mishra et al.[111] investigated the impact of different tool electrode materials on the EDM efficiency of Ti-6Al-4V. They considered both normal and cryogenic-treated tools of copper as well as tungsten material to study the impact on machining rate and surface topology. They had observed a highest MRR of 23.3 mg/min at peak current (10A), gap voltage (25 V) and duty factor (85%) for copper electrode. Kumar et al.[112] studied the effect of variable discharge current and pulse duration on the machining rate, tool erosion rate and

surface morphology of Ti-6Al-4V. The white layer thickness and the residual stress gener-
ated on the machined surface resulting in crack formation has been investigated at different
parametric combinations. The results showed a highest MRR of 12 mg/min at peak current
(10 A), gap voltage (30 V) and duty factor (85%). The above discussed literature provides
a brief idea about the variation of machining rate at variable process parameters in EDM,
thus imposing a basic relation of generated discharge energy with MRR. The set machining
conditions during the EDM operation are the limits for the desired process while the actual
discharge attributes can be observed and acquired from the real-time voltage-current wave-
forms. To generate better knowledge about the pulse variation during the EDM discharge,
the actual energy utilized during each pulse cycle can be obtained from the V-I characteris-
tics curve. The MRR of EDM process is dependent upon thermal conductivity λ, melting
point temperature θ and electrical resistivity ρ and it termed as $\lambda.\theta.\rho$ theory[113]. Ac-
cording to this theory if the workpiece material have value of multiplication of $\lambda.\theta.\rho$ is
lower than it will be easily machinable. Titanium alloy has lower thermal conductivity
which in case of EDM process make it easier to be machined. Chen et al. [90] had de-
veloped electromagnetic controlled horizontal controlled mechanism and controlled stable
precise tension in wire of EDM setup. They had observed better MRR for low thermal
conductive material. Hence, EDM process is better option to machine titanium alloy if
somehow MRR during machining of titanium alloy could be increased.

2.4.5   Hybrid Machining

In hybrid machining process combination of two or more machining processes are applied
to acquire the worthy outcome of all processes and to minimize the adverse effect of each
process. Lin et al.[97] performed EDM with ultrasonic machining and they had detected
higher MRR with an excellent surface finish during hybrid machining in comparison to
conventional EDM. In another study combination of high-speed EDM with arc machining

of Ti-6Al-4V applied, in which MRR was observed twice than conventional EDM and it's increasing with inner flushing pressure. The MRR, surface roughness and electrode wear are enhanced by an increment in every process parameter[114]. Li et al.[115] improved grindability of Ti-6Al-4V by combining ultrasonic vibration and plasma electrolytic oxidation. By this hybrid method minimum value of normal force, tangential force, workpiece surface roughness and surface hardness occurred since ultrasonic vibration had supported plasma oxidation. Madarkar et al.[116] accomplished hybrid grinding of Ti-6Al-4V by combining MQL machining with ultrasonic vibration (UMQL). During UMQL machining reduction in tangential force up to 38 % and in normal force up to 32 % in comparison to conventional MQL was achieved. While the surface finish was lower during UMQL machining since decrement in grit sharpness was observed. Therefore, UMQL is not recommended if the surface finish is an important factor to the final product. Taylor et al.[117] conducted hybrid machining on Ni-Ti alloy by combining laser machining with micro-EDM to produce a micro hole with good surface finish and higher MRR. Firstly, most of the workpiece material was removed by laser machining with high MRR then final finish is done by micro-EDM. Subsequently, the final product had a higher surface finish than laser machining and higher MRR than micro-EDM. In an analysis, hybrid machining was done by combining laser machining with a continuous supply of LIN to cool workpiece. It was detected that hybrid machining enhanced the tool life two times than conventional machining process, along with decrement in production cost and high MRR was occurred[11]. Recently, Kou et al.[22] conducted high-speed electric arc milling (H-SEAM) by breaking arc through the hydrodynamic-mechanical coupling. They had broken arc by this coupling and developed high blasting forces with the intense shock wave, hence obtained MRR about 780 mm^3/min which was five times of conventional arc breaking by mechanical or hydrodynamic method individually. Additionally, they had observed higher dimensional accuracy, higher surface finish, thinner recast layer and lesser heat affected

area than mechanical or hydrodynamic arc breaking system. Jamil et al.[118] reported the influence of hybrid cooling which consists of Al_2O_3 and multi-wire carbon nanotube fluids (MWCNT) and compared it with cryogenic CO2 cooling on machining of Ti-6Al-4V. They had detected reduction in cutting force, decrement in surface roughness and higher tool life during hybrid cooling than cryogenic cooling. In addition to these advantages, hybrid cooling has some significant disadvantages, such as greater manufacturing costs and risks to human health, subsequently; it is necessary to search for the alternative machining methods.

3

Introduction to maglev EDM experimental setup and evaluation of it through a comparative study with conventional EDM on Ti-6Al-4V alloy

This chapter introduces a revolutionary maglev EDM experimental setup that has never been used before in the EDM procedure. The discharge characteristics in EDM process

generates a distinct idea about the stability and efficiency of the operation. The current research aim to analyze the newly developed Maglev EDM operation on Ti-6Al-4V alloy with a comparative assessment with the conventional EDM. The study incorporates experimental results from both systems at variable parameters based on discharge voltage-current (V-I) characteristics, machining rate, specific energy, and surface morphology. The current study presents evidence for the eradication of major setbacks caused in conventional EDM such as frequent arcing, short-circuiting and variable ignition delay by implementing Maglev EDM. The maximum MRR achieved in Maglev EDM at discharge voltage (20V) and discharge current (0.5A) shows better energy consumption, as compared by the evaluated specific energy of conventional EDM. The surface morphology produced through 3-D surface profile defines the introduced Maglev EDM to produce work surface similar to the conventional EDM.

3.1 Introduction

In a recent survey, the growth in the demand of biomaterials has been forecasted within the year 2020-2026, as an effect of the COVID pandemic. These biomaterials include polymers, ceramics, metals and its alloys which are frequently used to develop biomedical implants. These bio-implants help in increasing the chances of survival and provides comfort living to physically impaired patients. Such medical devices can help to provide organ support, body function monitoring, and localized medication transfer tools.. Among the specified variety of materials, the clinical grade titanium and its alloys, have acted as an outstanding choice for biomedical applications due to its exceptional properties such as excellent biocompatibility, high strength-to-weight ratio, superior hardness, high thermal resistance, superior wear and corrosion resistance. Ti-6Al-4V alloy is the most widely used biomaterial for bio-implants such as artificial joints, bone covers, dental attachments

and pacemakers. To fabricate such products using conventional machining approaches is highly difficult and require harder tools which are highly expensive. The EDM process is suitable as an advanced manufacturing method to overcome such setbacks for machining electro-conductive materials. In recent years, the EDM technology has been developed to fabricate products on macro, micro and nano domains. Exploring such diversified technique for biomedical applications has opened the market for variety of complex shaped products and devices with biocompatible properties.

A recently developed Maglev EDM [119] is used in this study to determine the machinability of Ti-6Al-4V alloy at variable process parameters. A comparison with conventional EDM is presented, taking into account the specific energy, machining rate, and surface characteristics of the machined workpiece. The Maglev EDM works on the principle of magnetic levitation to control the discharge gap between the electrodes. A specific arrangement of electromagnet and permanent magnets are implemented to generate two repulsive forces for stable positioning of tool during discharge. The current system eliminates the occurrence of arcing and short-circuiting during the machining operation with better tool positioning and continuous stable discharge. To date, no study has investigated such an approach for overcoming the aforementioned setbacks during the EDM operation. The V-I curves acquired during machining in Maglev and conventional EDM is compared to determine the stability and efficiency of the novel system. Further, the specific energy of both systems are compared to understand the utilization of discharge energy for unit removal of material. The surface morphology and characteristics of machined workpiece is compared and analyzed using a 3D-surface profilometer.

3.2   Materials and Methods

In the current research work, experiments conducted using a self-developed Maglev EDM setup which is shown on Fig. 3.1. Additionally, machining was performed on commercial die-sinking EDM (Make: Sparkonix, Model: ZNC/ENC35), which is shown in Fig. 3.2. The Maglev EDM utilized the combination of an electromagnet and two permanent magnets for tool positioning and gap control between the electrodes. The working principle implemented the balance of dual repulsive forces to maintain proper discharge gap [119]. Figure 3.1 shows the Maglev EDM setup used in machining of Ti-6Al-4V alloy. Table 3.1 shows the experimental parameters and materials selected for EDM machining. For Maglev EDM, a Ti-6Al-4V plate (thickness = 2 mm) was considered as the workpiece material. A cylindrical copper rod (diameter = 3 mm) was used as the tool electrode. A pure DC power supply is used to operate the Maglev EDM. The selected set of parametric variations for the Maglev EDM was discharge voltage (30 V) and discharge current (0.25A and 0.55 A) with a duty factor of 95 %. The experiments were performed using commercial hydrocarbon oil as dielectric medium. For conventional EDM, a Ti-6Al-4V plate (thickness = 5 mm) was used as the workpiece. A rectangular cross-section copper rod (12 mm×5 mm) was selected as the tool. A complicated circuit arrangement used to generate pulsed DC for the machining process. The selected set of parametric variations for conventional EDM were discharge voltage (12 V and 50 V) and discharge current (1.2A and 2A) with a duty factor of 85%. The experiments were performed using a commercial hydrocarbon oil as dielectric medium. Therefore, workpiece, tool and dielectric medium was constant for both EDM machine, while parametric values were different due to some limitation of maglev EDM machine.

During the current study, all the experiments performed on the respective EDM setups was repeated thrice. The machining time (M_t) for each experimental run was 10 mins for both the EDM setups. The initial weight (W_1) prior to machining and the final weight (W_2)
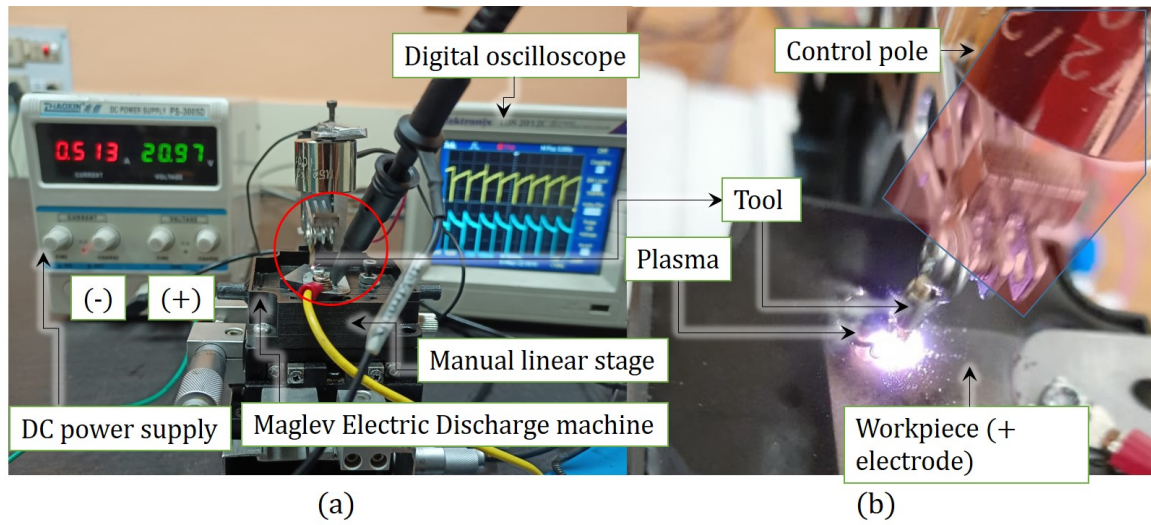
Figure 3.1: (a) Machining setup and (b) plasma formation in Maglev EDM [119]
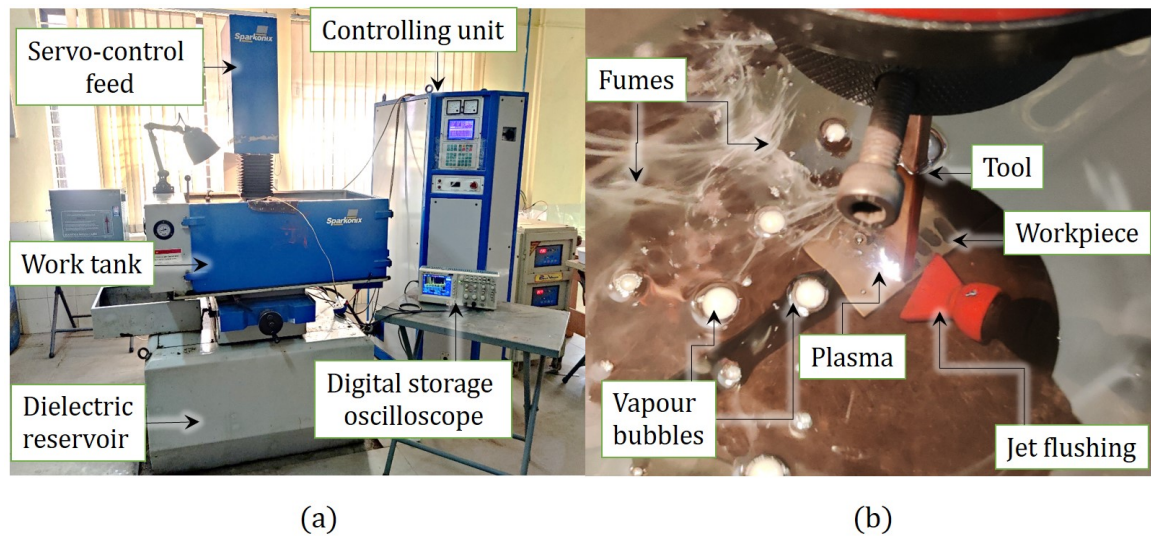
Figure 3.2: (a) Machining setup and (b) plasma formation in Conventional EDM

of the workpiece after machining was acquired using a precision balance of (Make: Mettler Toledo). The MRR (mg/min) achieved after each experimental run was evaluated by using equation (3.1).

$$MRR = (W_1 - W_2)/M_t \qquad (3.1)$$

A digital storage oscilloscope (DSO) (Make: Tektronix) was implemented on both the EDM setups for observing and acquiring the real-time discharge attributes during the machining operation. The V-I characteristic waveform was acquired at a regular interval of 2 mins during each experimental run. Later, a 3D-optical profilometer (Make: Zygo new view 9000) was used to observe the surface roughness parameters of the machined workpiece.

Table 3.1: Process parameter for EDM of Ti-6Al-4V alloy

	Maglev EDM		**Conventional EDM**	
(a) Selected materials				
Workpiece	Ti-6Al-4V plate (thickness = 2 mm)		Ti-6Al-4V plate (thickness = 5 mm)	
Tool	Copper rod (circular ϕ = 3 mm)		Copper rod (rectangular ϕ = 12 mm × 5 mm)	
Dielectric	Hydrocarbon oil		Hydrocarbon oil	
Polarity	Straight		Straight	
(b) Parametric conditions				
Peak Current (A)	1.2	2	6	6
Discharge current (A)	0.25	0.55	2	1.2
Discharge voltage (V)	30	30	12	50
Duty factor (%)	95		85	
Machining time (min)	10		10	

3.3   Results and Discussions

The current investigation is focused on providing a comparative analysis of the machining efficiency, process stability and surface integrity achieved during the machining of

Ti-6Al-4V alloy using both Maglev and conventional EDM. The achieved outcomes were compared on the basis of acquired V-I characteristic curves,specific energy, machining rate at variable parameters, and surface morphology.

3.3.1 V-I waveform analysis of conventional and Maglev EDM

Pulse discrimination for determining the real-time discharge voltage, current and pulse duration is considered to be a crucial aspect in monitoring and controlling the spark gap during EDM operation. Analyzing the pulse signals is necessary to understand the happenings at the narrow discharge gap and develop better control over machining parameters for the desired outcome. In the current investigation, the current and voltage pulse waves were observed and acquired using a differential type current (Hantek, 65A, AC/DC) and a voltage probe (TPP0201, Tektronix) in a digital storage oscilloscope (Tektronix, TDS2012C, 2-channel, 100MHz bandwidth). On observing the pulse waves, it is obvious that initially on applying suitable potential, the dielectric breaks down to form a high strength plasma channel followed by the electric discharge at the end of each pulse cycle. In conventional EDM, the presence of spark delay was quite evident and the variation in ignition delay duration was very frequent. The irregular discharges were occurred due to clustering of debris particles at the discharge gap and lack of proper control for tool positioning was very common. The accumulation of debris at the machining surface was shortened the discharge gap, leading to flow of current through a low strength plasma channel (or) causing contact of electrodes. The detection of such accumulated debris led to transmitting a signal for retraction of the tool, the transmission and reaction delay of servo-control system which further led to the arcing and short-circuiting phenomena. Figure 3.3 shows the V-I curves obtained in conventional EDM for discharge voltage (12 V) and discharge current (2 A) and figure for discharge voltage (50 V) and discharge current (1.2 A) during machining of Ti-6Al-4V. The inconsistent (or) unstable discharge duration was occurred mostly due to variable ig-

nition delay time and arcing phenomena. The pulse waveform observed during the Maglev
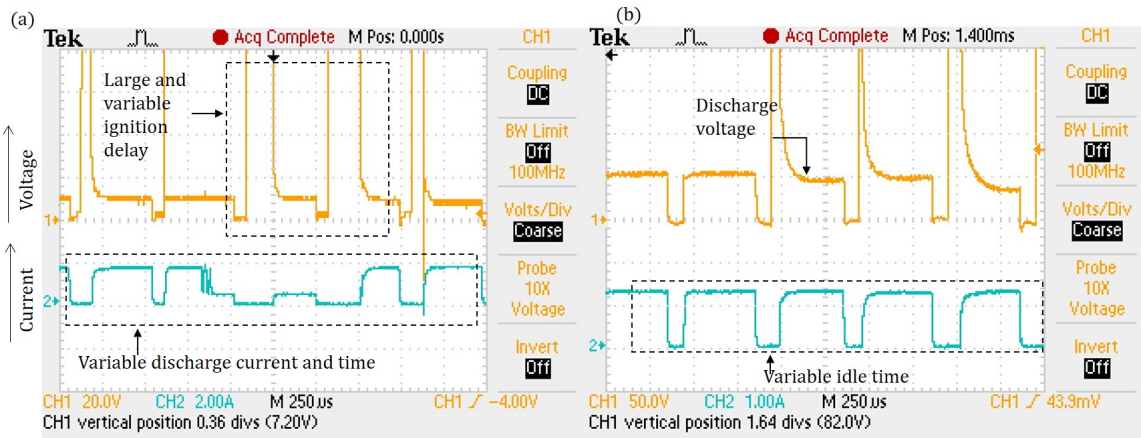
Figure 3.3: V-I characteristics pulse waves obtained at (a) discharge voltage = 12V and discharge current = 2 A and (b) discharge voltage= 50 V and discharge current = 1.2 A in conventional EDM

EDM operation depicted the absence of inconsistent and irregular pulse cycles. The pulse trains obtained throughout the operation show uniform behavior with minimal fluctuation during the electric discharge. During each pulse cycle, it was observed that the ignition delay was negligible, which allowed better utilization of discharge energy throughout the pulse duration. In comparison to conventional EDM, rhythmic and consistent discharge were produced during the Maglev EDM operation. It was observed that stable pulse cycles with better repeatability generated in the new Maglev system. It helped in attaining higher efficiency and better utilization of generated discharge energy. Figure 3.4 shows the V-I curves obtained in Maglev EDM for discharge voltage (30 V) and discharge current (0.25 A) and figure for discharge voltage (30 V) and discharge current (0.55 A) during machining of Ti-6Al-4V. It was confirmed by obtained waveform that stable and continuous discharge cycles occurred during the machining operation. The study of Maglev EDM pulse waves showed the lack of ignition delay resulting in complete utilization of pulse duration for better efficiency. The absence of frequent arcing and short-circuiting confirmed better tool positioning control in comparison to conventional EDM .
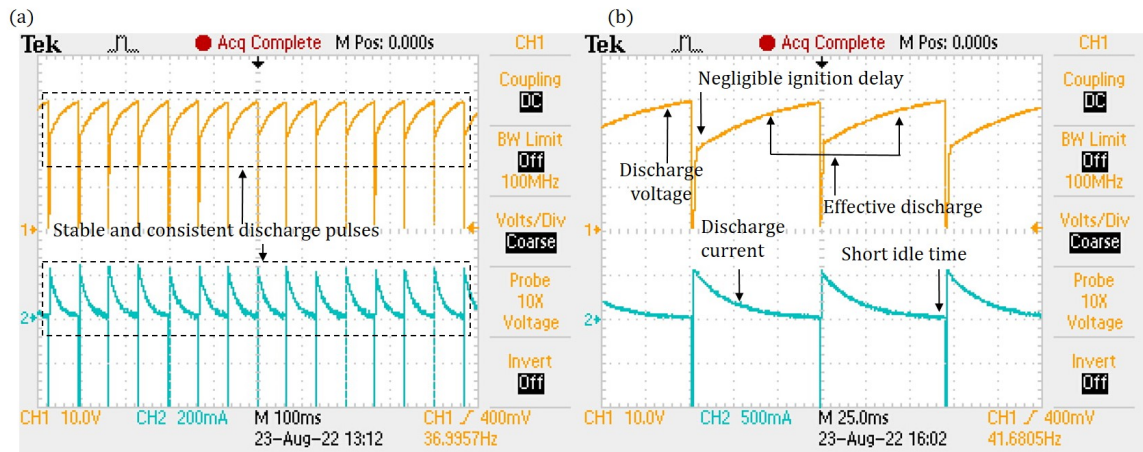
Figure 3.4: V-I characteristics pulse waves obtained at (a) discharge voltage = 30 V and discharge current = 0.25 A and (b) discharge voltage = 30 V and discharge current = 0.55 A in Maglev EDM

3.3.1.1 Real-time utilized discharge power (UDP)

The input parameters designated for each experimental run provided the limiting settings for the operation. The actual discharge attributes were extracted by using the real-time V-I pulse signals acquired by a cathode ray oscilloscope (CRO). For conventional EDM, the discharge voltage and current were generated at a sample span varying from (1μs to 4μs) for a record length of 2500 ms. For Maglev EDM, the values were acquired at a sample span varying from (0.1ms to 0.4ms) for the same record length of 2500 ms. The actual discharge current and voltage from the V-I data sheets acquired with the CRO were used to calculate the average UDP for the machining operation in both systems.

In conventional EDM, at discharge voltage (12 V) and discharge current (2 A) the achieved average UDP was approximately 7 W and at discharge voltage (50 V) and discharge current (1.2 A) the achieved average UDP was approximately 32 W. The vast difference in the input and utilized power occurs due to the large ignition delays and long idle time observed during each discharge pulse. In Maglev EDM, at discharge voltage (30 V) and discharge current (0.25 A) the attained UDP was approximately 7 W, while at the same discharge

voltage (30 V) and discharge current (0.55 A) the attained UDP was approximately 15W. It was observed that minimal variation of input and utilized power occurred in Maglev EDM, due to consistent and rhythmic discharge pulses had negligible ignition delay and small idle time with no irregular discharge pulse.

3.3.2   Variation of MRR in conventional and Maglev EDM

Figure 3.5 shows the MRR results obtained during Maglev and conventional EDM process for different discharge voltage and discharge current values. In the present research, a comparative analysis based on the machining efficiency of newly developed Maglev EDM and conventional EDM is presented using variable process parameters. The current investigation is carried out by examining the evaluated MRR of Ti-6Al-4V alloy on both the setups and observing the impact of different discharge attributes on the performance measure. For any machining operation, the MRR defines the productivity of the process for large scale industrial application. The current study for Maglev EDM implements a variation in UDP i.e., 7W and 15W to determine the machining rate. The resulting average MRR shows a significant increase from 0.2425 mg/min to 1.022 mg/min, as the discharge power was increased. The plasma channel generated at the machining gap was completely dependent on the discharge power produced. As the discharge power was increased, the strength of the plasma channel also increased and higher thermal energy produced, which led to better material removal. For conventional EDM, the variation in UDP were 7W and 32W. The acquired average MRR increases from 2.99 mg/min to 5.055 mg/min with increase in discharge power. The above discussed phenomena also occurs in case of conventional EDM. On comparing the achieved MRR with increase in discharge power for both the setups, the increase in MRR for Maglev EDM is vast in comparison to the conventional EDM. In case of Maglev EDM, the discharge energy utilization is much higher due to better gap control and lack of irregular discharges. The efficiency of the Maglev EDM is better than

the conventional EDM due to negligible ignition delay, arcing and short-circuiting.
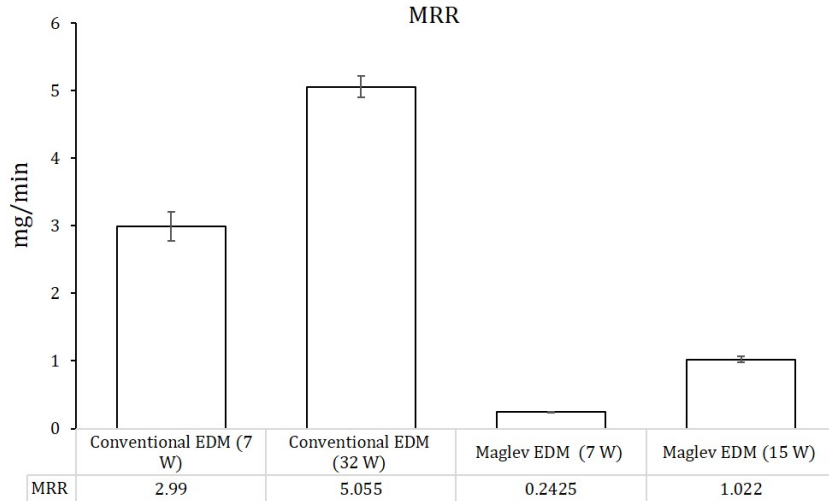
Figure 3.5: MRR for conventional and Maglev EDM during different discharge conditions

3.3.3 Comparative analysis of specific energy

The present research provides a comparative analysis of the machining efficiency of Maglev and conventional EDM based on the utilization of discharge energy. Specific energy of a machining process generates a basic idea of the operation in terms of energy and machining rate. Specific energy is termed as the amount of energy consumed to remove a unit mass/volume of material from the workpiece. In EDM, proper control over the discharge gap is very crucial for better utilization of discharge energy generated during each pulse. The present study determined the actual discharge current and voltage from the real-time V-I waveforms to evaluate the actual discharge power during each pulse for both conventional and Maglev EDM. The formula for evaluating the specific energy (SE) for unit material removal is given in equation 3.2as follows:

$$SE = UDP \times 60 \div MRR \times 1000 \qquad (3.2)$$

Where, SE is specific energy is J/μg Utilized discharge power (UDP) is in Joule/sec and MRR is in mg/min and DP can be calculated by:

$$UDP = V_d \times I_d \times DF \tag{3.3}$$

Here, V_d is the Real time discharge voltage occurred from V-I Data sheet , I_d is the real time discharge current occurred from V-I Data sheet and DF is the duty factor.

Figure 3.6 shows the specific energy in J/μg for conventional and Maglev EDM during different discharge conditions. The achieved MRR in Maglev EDM at 7 W UDP was found to vary from 0.241 to 0.244 mg/min and at 15 W UDP, it varied from 0.980 to 1.064 mg/min. The evaluated specific energy of Maglev EDM for low discharge power of 7 W varies from 1.66 to 1.6805 J/μg whereas, for high discharge power of 15 W, it varies from 0.8374 to 0.9092 J/μg. The huge fall in specific energy was observed with increase in discharge power for Maglev EDM indicated better utilization of discharge energy at higher discharge conditions. An enormous improvement in machining efficiency was observed as the discharge power increased, due to high discharge frequency, negligible ignition delay and lack of arcing/short-circuit pulses. For conventional EDM, the achieved MRR at 7 W UDP was found to vary from 2.78 to 3.2 mg/min and at 32W UDP, it varied from 4.9 to 5.21 mg/min. The evaluated specific energy of conventional EDM for low discharge power of 7W, was varied from 0.1331 to 0.1532 J/μg whereas, for high discharge power of 32 W, it varied from 0.3685 to 0.3918 J/μg. In conventional EDM, as the discharge power increased, it was observed that a modest increase in specific energy occurred. With increase in discharge power the amount of irregular pulses were increased and the conventional servo mechanism lacked in proper monitoring of spark gap. The frequency of arcing and short-circuiting was increased at higher discharge power led to higher specific energy.
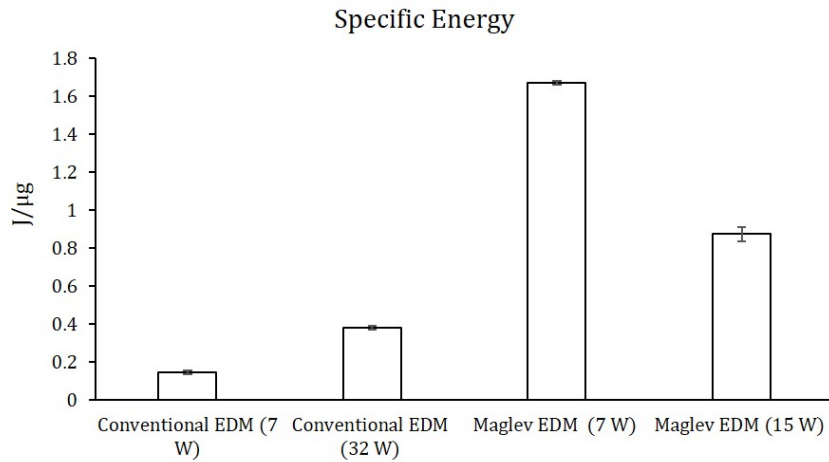
Figure 3.6: Specific energy for conventional and Maglev EDM during different discharge conditions

3.3.4 Analysis of surface topography in conventional and Maglev EDM

In EDM, rapid fluctuation in temperature and pressure due to plasma generation and termination resulted in formation of semi-circular craters and various surface anomalies. The minute cavities (or) craters were formed on the work surface at the point of spark contact due to material erosion which added the irregularities on the machined surface. The non-uniform resettling of molten matter on the machined work surface formed thick recast layer, micro-surface cracks and micro-pores. The present research analyzed the irregularities of the machined surface formed during Maglev and conventional EDM operation to determine the average surface roughness (R_a), ten-point height (R_z) and RMS (R_q) using an optical profilometer (Make: Zygo, Model: New view 9000). Each machined work surface acquired at variable process parameters from both the EDM setups were examined thrice with a sampling length of 1.5 mm for 'R_a' within a range of 2-10 μm, as per the ISO (4288-1997) standards.

Figure 3.7 shows the roughness parameter obtained from 3D optical profilometer for machined surface. During Maglev EDM operation, the average surface roughness acquired

at 7 W UDP was 4.877 μm and at 15W UDP was 5.882 μm.With increase in discharge power, the depth and width of craters formed during each spark occurrence also increased. Higher depth and wider craters were resulted in higher surface roughness. Similarly, during conventional EDM operation, the average surface roughness acquired at 7 W UDP was 6.273 μm and at 32 W UDP was 8.124 μm. These R_a values gave general description of height variation while it was not sensitive for small changes in profile, the R_q value gave standard deviation of the distribution of surface heights and the R_z value gave more sensitive results than R_a value for high peaks or deep valleys [120]. From Fig. 3.7 it was observed that machined surface from maglev EDM has more uniform surface profile than machined surface of conventional EDM system.
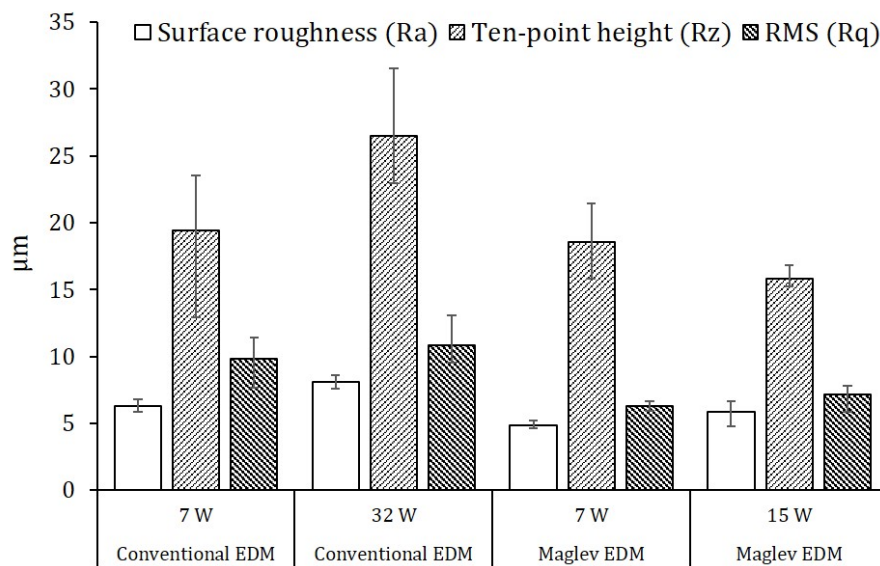
Figure 3.7: Roughness parameters obtained in conventional and Maglev EDM during different discharge conditions

3.4 Conclusion

In present work, the maglev EDM setup has been evaluated with conventional EDM setup on the basis of variation in discharge voltage, discharge current and tool electrode material during machining of Ti-6Al-4V alloy. This study can be concluded as follows:

- Better and stable discharge waveform is observed for maglev EDM than conventional EDM. Pulse off time was less during maglev EDM than conventional EDM which enhances the duty factor without short circuiting. Hence, for maglev EDM higher UDP than conventional EDM iss observed.

- Although the peak current and open circuit voltage used in maglev EDM were lesser than those used in conventional EDM, the MRR in both machining processes was comparable.

- The surface finish of the maglev EDM process was superior to that of the conventional EDM procedure. Furthermore, the ten-point height (R_z) value revealed uniform crater creation, indicating that the maglev EDM procedure had improved the surface formation.

- With increase in UDP decrease in specific energy is detected during maglev EDM while contrary effect observed in conventional EDM. Hence, it can be concluded that at higher discharge power in maglev EDM the greater gap control, reduced ignition delay, and the absence of arcing/short-circuit pulses have enhanced machining efficiency.

4

Effect of cryogenic quenching on
Ti-6Al-4V alloy

The state of the art of the current chapter is to investigate the effect of cryogenic quenching on mechanical properties of Ti-6Al-4V such as microhardness and microstructure. Cooling rate plays significant role in the reformation of grains and grains boundaries. Three type of quenching viz. water, cryogenic and air were used in combination with annealing and solution treated samples. It is found that the application of the cryogenic quenching with annealing process achieved minimum microhardness with lowest percentage area of grain

boundaries. However, the solution treated with cryogenic quenching (STC) sample showed maximum microhardness. This increment in the microhardness is due to the increased bimodal α, β grains and α-β interfaces in the STC samples. Therefore, the results of the current chapter showed that the mechanical properties of Ti-6Al-4V can be improved with the help of proper selection of heat treatment and quenching medium. Further, the analysis of microstructure is conducted by optical microscope, Electron Backscatter Diffraction (EBSD) and X-ray diffraction (XRD) results of specimens. The effect of modification is observed by change in % area of grain boundaries and microhardness of specimens.

4.1 Introduction

Titanium alloy Ti-6Al-4V is commercial material used in aerospace, biomedical and marine industries. This alloy comes in to difficult-to-machine metal due to poor thermal conductivity, higher hardness and chatter [121, 19]. Heat treatment and quenching process can alter the grain size, grain boundaries and phases; which modifies the microstructure, mechanical properties and machinability of the Ti-6Al-4V [39]. Nursyifaulkhair et al. [122] showed that optimum value of cooling rate was 4344 K/sec; which led to higher amount of fine lamellar with metastable β microstructure and enhanced mechanical properties of Ti-6Al-4V. Earlier various researcher modified the microstructure to achieve desirable mechanical property of Ti-6Al-4V alloy. Chong et al. [123] obtained desirable high tensile strength and ductility in Ti-6Al-4V alloy by β-transus process with intercritical annealing. In their study, they inter-critically annealed in $\alpha+\beta$ region and cooled at high speed to obtain the primary α lamellae and transformed β. Resultantly, bi-lamellar microstructure which enhanced tensile strength with ductility. In another study, effect of cooling rate on near α phase titanium alloy was studied by Gao et al. [124]. They observed increased α colony by decreasing cooling rate. Hence, it was observed that cooling rate signifi-

cantly influenced the formation of α phase. In present work, heat treatment was performed on Ti-6Al-4V followed by three different quenching processes to form inter-granular and inter-phase grains with grain boundaries. Their response was observed on microhardness and microstructure that will further useful in the formation of best microstructure for better machinability of Ti-6Al-4V.

4.2 Material and experimental procedure

Figure 4.1 shows heat treatment procedure followed for different quenching conditions. A total of seven samples were chosen for the experiment, three of which were heat treated at an annealing temperature of 750^0C, three at a solution treatment temperature of 920^0C, and one untreated. Three different quenching medium was performed on annealed and solution treated samples with water (WQ), air (AQ) and Liquid nitrogen (CQ) and these processes were as follows: annealing +water quenching process (AW), annealing +cryogenic quenching process (AC), annealing+air quenching process (AA), solution treatment + water quenching process (STW), solution treatment +cryogenic quenching process (STC) and solution treatment + air quenching process (STA) respectively. Heating rate for each sample was 5^0C/min and cooling rate was dependent on the quenching process. AA and STA process was done by putting the sample outside the furnace in the environment until it cooled down to room temperature, while quenching process on other sample was conducted by dipping it inside the water and liquid nitrogen. During cryogenic quenching samples were cooled down to cryogenic temperature and after 5 min they removed from it; to attain room temperature on samples. Tempering was done on each sample for 1 hr at 160^0C to stabilize and detach α phase from $\alpha' + \beta$ phase. Further all 6 samples with an untreated sample (UT) were polished to enhance material upper layer surface finish to found its microstructure. Polishing was started on the sample with 500 grit size SiC followed by

grit size 1500 and 2200 under running water. Mirror surface finish was generated with the help of diamond polishing with 3 and 0.5 mm particle size diamond paste on velvet cloth under aerosol spray. At the end etching was performed on samples by Kroll's reagent (97 ml distilled water + 2 ml HNO3 + 1 ml HF) for 15 seconds to observe the microstructure of samples. In Fig. 4.2 the generalized phase diagram of Ti-6Al-4V alloy is shown. The α' phase is acicular martensite and α'' phase is orthorhombic martensite and they are present in Ti-6Al-4V alloy on the basis of solute (% of vanadium) presence. The orthorhombic α'' phase is an intermediate stage between the formation from BCC to HCP [125, 126]. It is observed on studies that in titanium alloys martensite α' and α'' phases are softer than β phase [127].
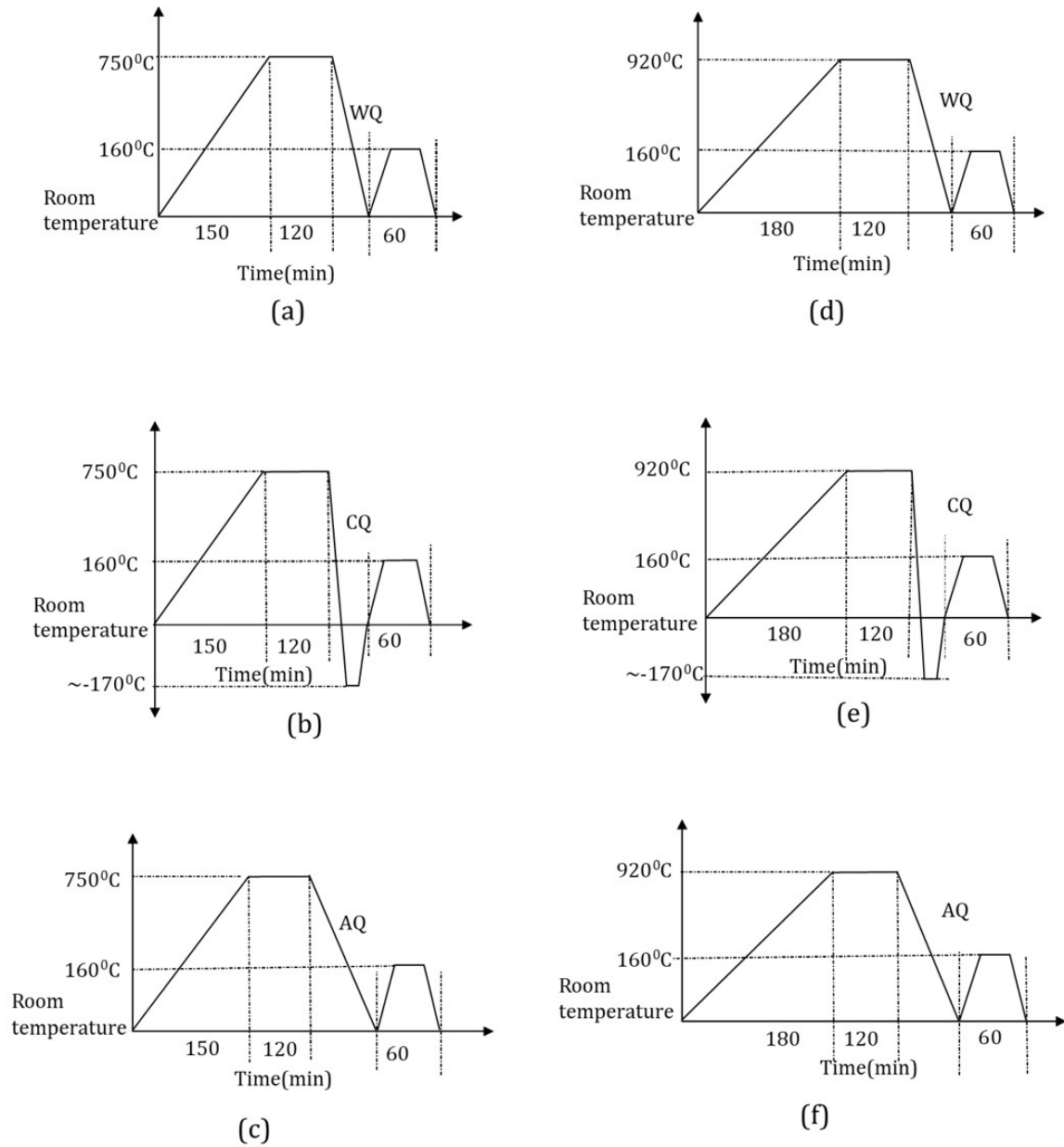
Figure 4.1: Heat treatment processes followed during (a) AW (b) AC (c) AA (d) STW (e) STC (f) STA
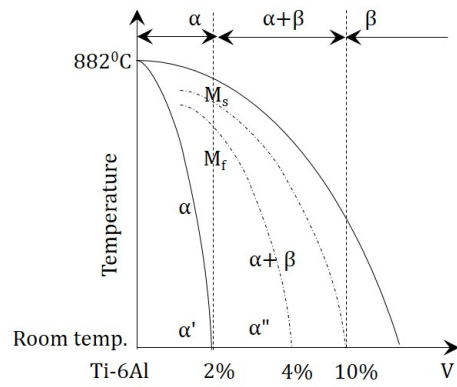
Figure 4.2: Generalised Ti-6Al-4V alloy phase diagram with effect of change in vanadium %
[125]

4.3 Result and discussion

4.3.1 Assesment of evolution of microstructure by optical microscope

Annealing process was done below the β transus temperature range, through which volume fraction of α phase particles can be increased. During annealing process shapes of α phase was relied on temperature range from lower, medium and upper $\alpha + \beta$ field [128]. Zhong et al. [129] have shown that β phases were increased at 900^0C by increasing repetition of heat treatment and generation of phases were dependent on both type of grain development process viz. nucleation and growth. Annealing was done at 750^0C to enhance α phase and solution treatment was done at 920^0C to enhance bimodal α and β phase inside the Ti-6Al-4V alloy and their influence on microstructure of samples were observed. Similar phenomenon was observed by Gornakova, et al. [130] during annealing process of Ti-6Al-4V and they have observed increment in equiaxed α in it. Figure 4.3
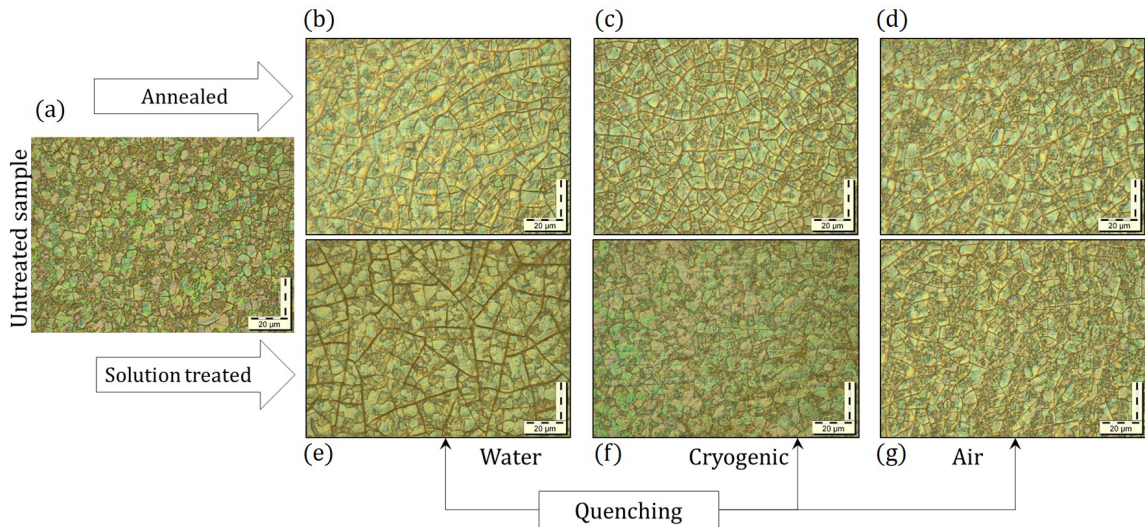
Figure 4.3: Microstructure obtained through different heat treatment and quenching processes (a) UT (b) AW (c) AC (d) AA (e) STW (f) STC (g) STA

shows the different microstructure obtained through different processes. Different sizes of microstructure with α, β and $\alpha'' + \beta$ grains were formed according to treatment and

quenching processes. These $\alpha'' + \beta$ grains were diffused into metastable β, orthorhombic α'' and $\alpha' + \beta$ grains; dependent on the cooling rate. During the quenching process control of these grains and grain boundaries were done by quenching medium. While during solution heat treatment samples were heated near the region of β transus temperature at 920 °C; therefore bimodal α, metastable β and $\alpha' + \beta$ grains were formed. By quenching process these grains were reformed and stabilized, resultantly increment in the % area of grain boundaries of Ti-6Al-4V alloy were obtained for solution heat treatment; while decrements in it for annealing process is occurred. By graphical method it was observed that during AC equally distributed fine orthorhombic α'' grains were formed in comparison of other treatments on microstructure. While unequally distributed courser bimodal α and β grains were obtained in STC process. In studies it was seen that during diffusion of grains, grain boundary 'wetting' was a key factor to form grain boundaries and promoting modification in mechanical properties [131, 132]. Figure 4.4 has showed that ′wetting′ phenomenon
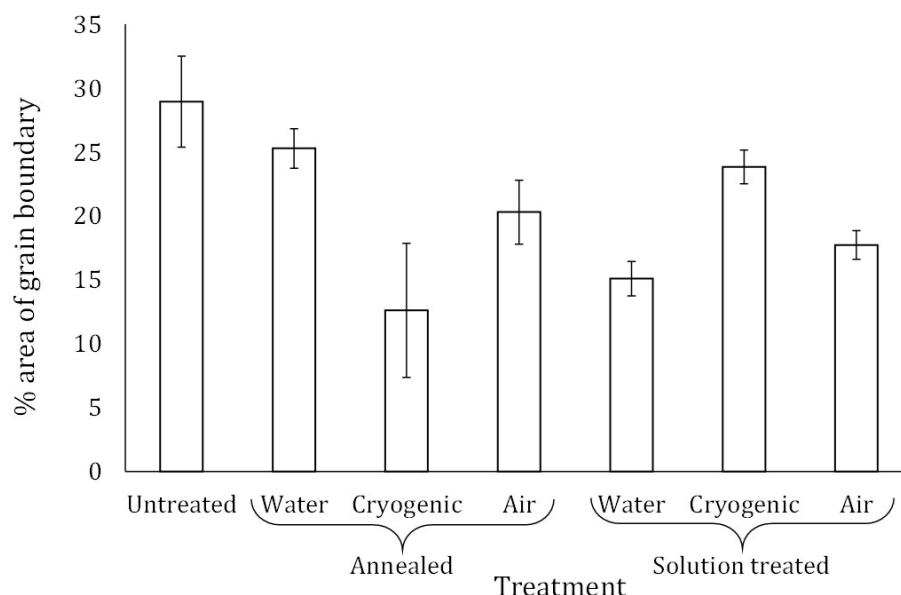
Figure 4.4: Percentage area of grain boundaries vs. Treatments

was dominant during solution treatment process than annealing process therefore % area

of grain boundary was higher in it. These grain boundaries were measured with the combi-nation of graphical and line intercept method [133]. It can be seen from graph that AC has smaller % area of grain boundaries and STC has highest % area of grain boundaries in com-parison to other treatment processes. Moreover, orthorhombic α grains are more ductile than lamellar and bimodal α grains therefore it can be found from this microstructure that AC has highest ductility than other processes. More ductility means more machinability hence through AC process highest machinability can be achieved.

4.3.2 Assesment of microstructure by EBSD and XRD analysis
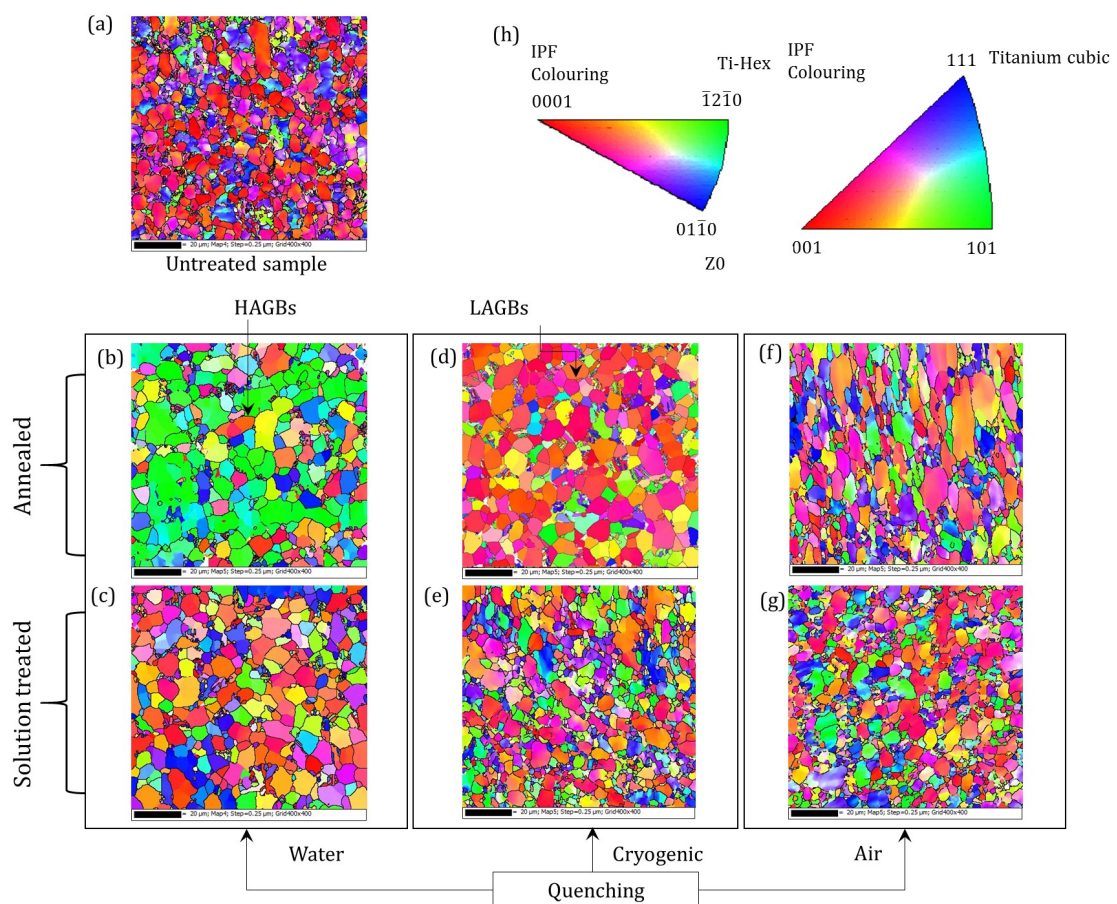
Figure 4.5: EBSD IPF maps achieved from different quenching after annealing and solution heat treatment processes (a) UT (b) AW(c) STW (d) AC (e) STC (f)AA (g)STA (h) IPF map with misorientation grain boundary

In Fig. 4.5 inverse pole figure (IPF) EBSD map concerning with the z-direction of different quenching medium after annealing and solution heat treatment processes samples are shown. The phase map of UT, AC, STC, AA, STA, AW and STW samples are analyzed and characterized using electron Backscatter diffraction (EBSD) on Zeiss supra 55 at IIT (ISM) Dhanbad. It can be observed from Fig. 4.5 that grain size was increased by annealing process and decreased by solution heat treatment process. In annealing process heating was done at 750^0C which is below the recrystallization temperature of Ti-6Al-4V alloy, hence transformation of grains from HCP to orthorhombic α crystal structure with decrement in BCC crystal structure is observed. While in solution heat treatment process Ti-6Al-4V alloy was heated above the recrystallization temperature 920^0C, hence component of β phase increased and enters between the α - α boundaries to increase the α - β grain boundaries. Quenching is the process of rapid cooling of sample to prevent the precipitation of dissolved components during heat treatment. Since cryogenic quenching has highest cooling rate as compared to water and air, microstructure of samples quenched with cryogenic stables the grains quickly on the phase which occurred by grain growth process. By observing the IPF EBSD results of UT sample it can be concluded that basal plane (0001) is shown for α phase while plane (01$\bar{1}$0) is shown for β phase. In Fig 4.5(h) misorientation angle of grain boundaries are shown, from which bold lines can be observed for high angle grain boundary (HAGB) while thin lines are observed for low angle grain boundary (LAGB). There were only orthorhombic α grains formed and there is no presence of transformed β phase observed in AC sample. The clear HAGBs with stable β phase is observed in STC sample while LAGBs with highest α is observed in AC sample. In AC sample minimum α-β grain boundaries were formed since the absence of β grains. The LAGBs had less stored energy than HAGBs, therefore plastic deformation could takes place effortlessly in AC than other samples. The XRD analysis is shown on Fig. 4.6 from which it can be observed that 7 peaks are observed. Peaks are showing the α and β phases
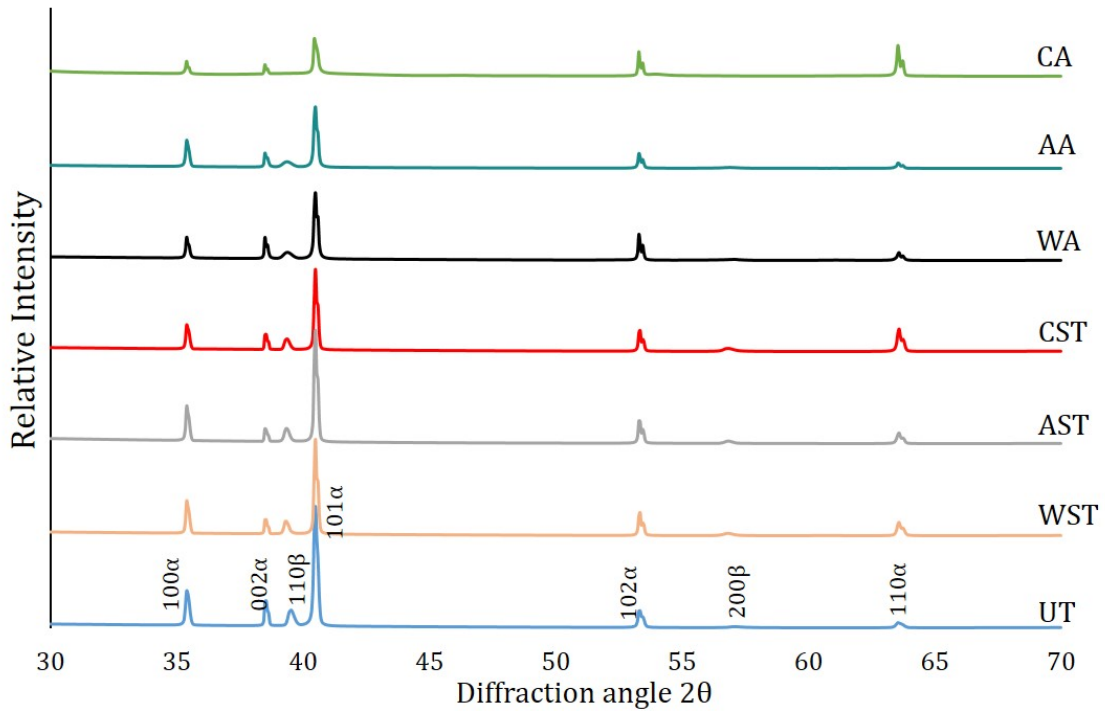
Figure 4.6: XRD analysis results obtained for different quenching after annealing and solution heat treatment processes

in XRD plots, (200) is visible in the STC, STW and STA sample while other peaks are visible in every samples. The noticeable change in peaks is observed in every plane's peak intensities. This (200) peak is indicating that the formation of the transformed β phase was taken place on it since the solution treatment is done at a higher temperature 920^0C. The (110) β phase peak is maximum in the UT sample and negligible in the AC sample which showed that percentage of β phase is minimum during the AC process. In XRD analysis it is observed that (101) lamellar α phase peak decreased and (110) orhtorhombic α phase peak increased in the AC sample than UT and STC process sample. The XRD analysis confirmed the EBSD analysis results, hence AC sample has highest plastic deformability and lowest grain boundary strength than other samples.

4.3.3   Effect of heat treatment on microhardness

Figure 4.7 shows the microhardness of Ti-6Al-4V alloy for different heat treatment and quenching processes. Microhardness test was conducted on Vickers's microhardness tester machine with 0.5 Kg load and 10 sec dwell time with 5 repetition for every sample. Results revealed maximum value for UT sample while minimum value during AC process of microhardness. These results showed correlation of % area of grain boundaries with microhardness. It is observed that annealing formed α and α'' grains while solution treatment forms bimodal α, β and $\alpha + \beta'$ grains, therefore; microhardness was increased in later process. Microhardness value during solution heat treatment method were reaching more near to UT sample than annealing, since the presence of harder lamellar α and metastable β grains. These grains increase the amount of α-β interfaces in grain boundaries which were harder than grains, hence it supported to enhance microhardness. Machinability of material depended inversely on microhardness, hence; AC has highest machinability in comparison to other processes as per the microhardness results.
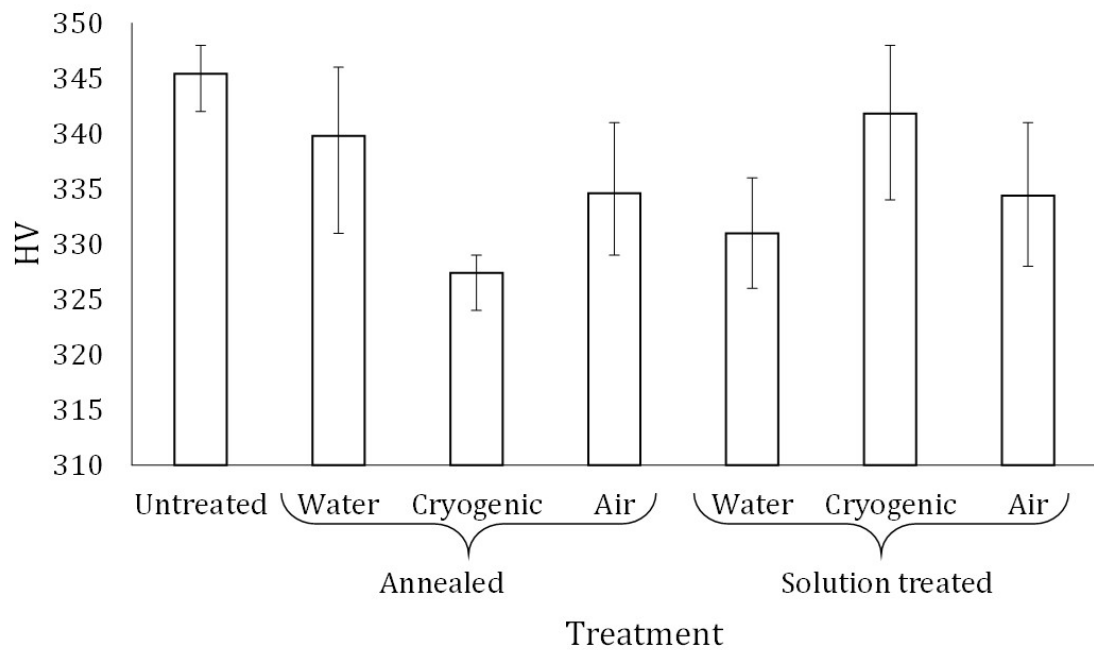
Figure 4.7: Microhardness (HV) vs. Treatment processes

4.4 Summary

By the assessment of above mentioned results, following conclusion have been obtained from the presented work :

- From EBSD and XRD results it can be concluded that AC sample has highest amount of α phase grain, minimum β phase grain and higher LAGBs, which contributed in lowest α- β grain boundaries therefore microhardness minimum in it.

- Percentage of grain boundaries and type of grain boundaries have correlation with microhardness.

- Microstructure and microhardness results show that the machinability of Ti-6Al-4V alloy is higher for annealed and cryogenic quenched sample. This is due to very high cooling rate in cryogenic quenching

5

Assessment of cryogenic quenching by tool wear, surface morphology and chip formation in high-speed up-milling of Ti-6Al-4V alloy

The purpose of this chapter is to look into the effect of cryogenic quenching after annealing and the solution heat treatment process on Ti-6Al-4V alloy. To assess the effect of

processes on Ti-6Al-4V alloy, high-speed up-milling of heat treated and untreated samples with same machining parameters are accomplished. The low microhardness and low yield strength of AC sample is observed as dominating factors during the analysis of chip formation, tool wear and burr formation. In this study low tool wear with a high surface finish is achieved in dry high-speed up-milling condition by AC process on Ti-6Al-4V alloy.

5.1 Introduction

Ti-6Al-4V alloy has vast application in the field of bio-implants, aerospace, marine, and nuclear energy plants since it has excellent mechanical properties such as high corrosion resistance, wear resistance, and strength to weight ratio. Although it has low machinability characteristics since the presence of higher cutting temperature, chatter and low thermal conductivity, which caused excessive temperature, high tool wear, and high cutting forces during machining [134]. The low machinability of Ti-6Al-4V alloy is a critical issue and to overcome this problem high- speed milling (HSM) is an exceptional substitute to conventional milling. To achieve better machining performance such as high productivity, high surface finish, micro-scale manufacturing, high dimensional accuracy, and great tool life; HSM is an excellent process to be applied[135]. High-speed cutting range to machine titanium alloys varies from 100 m/min to 1000 m/min [136]. This is seemed to be a common problem since at such a high-speed range tool wear occurred frequently; which increased the machining cost of hard-to-cut materials. During the HSM process, tungsten carbide tools (WC) are favorable cutting inserts to achieve greater tool wear resistance even at higher cutting forces and temperatures, particularly in the milling of hard-to-cut materials[137]. In a study Srinivasan et al. [138]compared diamond coated tool with uncoated WC tool during high speed milling of Ti-6Al-4V alloy. They observed better tool life and surface finish in low tool cost than polycrystalline diamond (PCD) tool. However,

the HSM process through PCD and Carbon boron nitride (CBN) tools are expensive substitutes to WC tools with superior machining properties. If the machining is achieved by PCD or CBN tools, the machining cost will be higher[139]. Hence, the WC tool played a major role to achieve an economical high production rate at reduced tool cost.

In HSM process tool wear is defined as the loss of tool material to machine the workpiece material. In the HSM operation of Ti-6Al-4V alloy with 100 m/min cutting speed and uncoated WC tool, it is observed that adhesion and abrasion are the key culprits of flank wear [140]. In another tool wear analysis of HSM, it is observed that flank wear impacts severely to the dimensional precision and surface topography of machined parts than crater wear. In an experiment maximum flank wear is established as the reference to the tool failure since the tool life has a direct relation with flank wear magnitude and it originated earlier than crater wear. During the study, they found flank wear is non-uniform and flank wear increases linearly with time. Additionally, it is witnessed that surface roughness intensifies with tool wear, and tool wear is the main cause affecting the severity of surface roughness and topography [141]. It was observed by Li et al [142] that an increment in tool wear enhances the cutting force and cutting temperature, and both of them altogether degrade the cutting condition; hence accelerating the tool wear and reducing the tool life. In another study, Liang and Liu observed [143] that surface roughness varied with deviation in tool wear from 0-0.3 mm and up to 0.2 mm surface roughness increased while beyond that it was decreased. Moreover, they concluded that with increment in tool wear, friction coefficient increased and it formed poor cutting condition. Dadgari et al. [144] observed that a low feed rate with high cutting speed improves the tool life of a 1 mm diameter tool. Additionally, they have detected that after the initial rapid tool wear, non-uniform flank wear was the leading wear mode. Wang et al. [145] measured the tool-chip interface and Ti-6Al-4V alloy temperature with variable feed rates (1, 2, and 3 μm/flute) with a 777 μm diameter tool and a constant cutting speed of 60.3 m/min. They observed that

with an increase in feed rate the temperature between tool-chip interfaces was increased, which increased the adhesive wear, build-up edge (BUE) formation, and burr formation. Amin et al. [146] performed machining by 32 mm diameter carbide end mill tool and the cutting speed range during machining was 40-160 m/min. They investigated the effect of chatter amplitude on tool wear and observed the highest tool wear during the speed of 160 m/min since the chatter amplitude was highest at that speed. Furthermore, they observed a sharp exponential curve during the cutting speed of 160 m/min than other lower cutting speeds. Lee et al. [147] analyzed cryogenic end milling with 3 mm end milling on Ti-6Al-4V alloy and observed that tool wear increased with an increase in cutting speed. Additionally, they observed that BUE formation was directly related to cutting temperature between the tool-chip interfaces. Moreover, various researchers observed high cutting temperatures (reaches up to 850^0C) between tool-chip interface during dry HSM of titanium alloys since the high friction between tool-chip interface and titanium alloys have a chemical affinity with almost every cutting tool. As a result; all of these factors propagated the burr formation, BUE, rapid tool wear, and plastic deformation of cutting tool and eventually trigger the catastrophic failure of the inserts during HSM of Ti-6Al-4V alloy [146, 148, 149, 143]. Roushan et al. [150] studied the tool wear during milling with 50 m/min cutting speed from 500 μm uncoated WC micro tool and observed that to machine the 450 mm total length of cut 25% tool diameter was reduced. Sun et al. [151] studied dry high-speed machining at 150 m/min and 220 m/min. They detected flank wear during 220 m/min was higher and more exponential than 150 m/min since the plastic deformation was higher during the dry condition. Rao et al.[152] conducted dry HSM process with uncoated carbide tool to machine 55 mm length of cut on Ti-6Al-4V alloy. It was noticed that friction enhanced the cutting temperature and flank wear during HSM process. They detected maximum wear for cutting speed of 121.9 m/min and depth of cut 0.762 mm. In another study it was observed that during high speed face milling of Ti-6Al-4V alloy the

tool cutting edge damaged. It was caused by the excessive pressure and cutting temperature between tool-chip interface[153]. Hence, by these above mentioned key findings, it can be concluded that during dry HSM cutting temperature, friction between tool-chip interface and chatter amplitude are the key factor to influence the tool wear and decide the higher cutting speed. A different approach to the traditional problem was given by shukla et al. [154], in which they reduced the microhardness and % grain boundary of Ti-6Al-4V alloy by quenching after the annealing process. Recently, Han et al. [63] applied cryogenic quenching after the solution treatment on friction stirr weld of 6061-T6 aluminum alloy. They compared STC sample with STW sample and observed that yield strength of cryogenic quenched sample were higher than water quenched sample. Such result was observed since the cryogenic quenching had a higher degree of saturated solid solution than water quenching. Singla et al. [155] applied cryogenic quenching after the solution treatment and β annealing of Ti-6Al-4V ELI alloy. They observed that β phase percentage was increased in both sample as both treatment process was done above the β transus temperature. As a result, they had observed increment in yield and ultimate tensile strength in Ti-6Al-4V ELI alloy. There were various studies have been conducted to see the effect of cryogenic cooling and cryogenic treatment on machining of Ti-6Al-4V alloy, although literature related to see the effect of cryogenic quenching on machining ability of Ti-6Al-4V alloy are limited. Therefore, The state of art in the current research work is to witness the effect of cryogenic quenching (with annealing and solution heat treatment) on tool wear and Ti-6Al-4V alloy surface quality parameters (such as surface roughness, burr formation, chip formation and BUE formation) during dry HSM process with constant cutting parameters. Dry condition applied in current work, since it is sustainable and economical manufacturing technique. Tool wear and tool life studies have the aim to conclude the machining ability of a tool material before it perishes, while workpiece surface quality parameters are showing the precision and accuracy of machined product by HSM process.

As per the studies, together these output parameters are influencing the machinability of Ti-6Al-4V alloy, which is a severe concern during its machining. There are fewer previous research using cryogenic quenching approach is reported during HSM process to measure the tool wear, chip formation, and surface morphology. This research constitutes a relatively new area which has emerged from application of cryogenic materials to modify the microstructure and improve the machinability during machining process.

5.2   Experimental materials and method

Recently, many researchers investigated the effect of cryogenic treatment on tool wear. They achieved higher hardness and wear resistant properties in cryogenic treated tools than untreated WC tools. These approaches were influential in the field of cryogenic treatment of cutting tool for increased tool life up-to some extent, while no effect on finishing of workpiece materials was shown [156, 134]. One of the major topics to be investigated in this field is effect of cryogenic quenching on machinability of workpiece material. There was no literature found related to see the effect of cryogenic quenching on tool wear and machined surface during the HSM process. In present work three type of specimen are used viz. UT, AC, and STC. Methods were based on previous experiments conducted by shukla et al. [154] to modify the microstructure of Ti-6Al-4V alloy. In Chapter 4, Fig. 4.1 heat treatment process applied to obtain two different cryogenic quenched specimens were shown. Afterward, each specimens viz. UT, AC, and STC were mirror finished by polishing and etched with Kroll's reagent to understand their microstructure. Reduction in microhardness of Ti-6Al-4V alloy was achieved by AC process, which directly influenced the plastic deformation during machining [154].

In the present work, the HSM process was done by the uncoated WC end milling tool of 3 mm diameter with tool edge radius (t_{er}) 5μm. The uncoated WC tool was used in fi-

nal experiment since the tool flank wear clearly and quickly visible on it than coated tool during the pre-experimental examination on UT sample.The machining on UT, AC, and STC specimens were repeated twice at the high-speed micro milling machine center V-60 at IIT Dhanbad. It was observed on studies that machine tool dynamic was affected by combination of cutting speed and axial depth of cut, hence chatter also varied according to them [157]. Arnab et al. [158] conducted study on V-60 machine to observe the highest amplitude peak at which chatter could occurred for constant depth of cut and spindle working frequency from 150 to 1000 Hz. They observed highest vibration amplitude at 235 Hz spindle frequency. Therefore, current HSM process is conducted at a cutting speed of 188.4 m/min (at 333.33 Hz spindle frequency) to avoid the effect of chatter (high vibration amplitude at 235 Hz). Since as per analysis beyond 235 Hz spindle frequency vibration amplitude on V-60 machine was decreased [158]. Other experimental parameters are shown below in table 5.1. The cutting speed applied during this research is higher than the recommended cutting speed by the tool supplier (40 m/min) for this uncoated WC tool. To assess the tool flank wear, the cutting tool was detached after machining fixed dimensions such as cutting lengths 20, 10, 10, and 5 mm. The selection purpose of the dry HSM process in the present research work is to examine the effectiveness of the cryogenic quenching on the evolution of tool wear and machined surface quality parameters (surface roughness, chip morphology, and burr formation).

Table 5.1: Experimental plan

Cutting speed (V_c)(m/min)	Radial depth of cut (a_r)(mm)	Axial depth of cut (a_p) (μm)	Feed rate (f) (μm/tooth/rev)
188.4	1.5	150	5

5.3 Result and discussion

5.3.1 Characterization of surface texture by EBSD and XRD

The microstructure of UT, AC, and STC samples were analyzed and characterized using electron backscatter diffraction (EBSD) on Zeiss supra 55 and high-resolution X-ray diffraction (HRXRD) on Rigaku smart lab at the central research facility, IIT (ISM) Dhanbad. The Inverse pole figure (IPF) EBSD map concerning the z-direction of the UT, AC, and STC process samples are shown in Fig. **??**. By increasing the temperature in Ti-6Al-4V alloy, the volume fraction of β phase was enhanced. During temperature increment, the concentration of vanadium (β stabilizer) was reduced, therefore the α' phase could be developed in Ti-6Al-4V alloy if the cooling rate (cryogenic quenching) was appropriate high [159]. It could be seen that in the AC process the grain size becomes larger than STC and UT process samples. As it is seen from Fig. 4.5 that in UT sample red color shown grains with the surface normal to (0001) basal plane while the blue color corresponds to grains with the surface normal $\bar{1}100$. By the AC process modification of the primary α phase to the secondary orthorhombic α'' phase was achieved, with decrements in β phase. Therefore, an increment in the formation of $\alpha|\alpha''$ grain boundaries was attained with a reduction in $\alpha|\beta$ grain boundaries. Subsequently, an increment in the formation of $\alpha|\alpha'$ grain boundaries was attained with a reduction in $\alpha|\beta$ grain boundaries. In the STC process sample, a minute enhancement in grain size than the UT sample was seen, while modification in grain texture from α to secondary α'' and modified β phase was appeared.

In Fig. 4.6 XRD pattern during three different conditions of treatment viz. UT, AC and STC are shown. Peaks are showing the α and β phases in XRD plots. The number of peaks of the α and β phases was 7 acquired from the XRD plots and among them, (200) was only visible in the STC sample while other peaks were visible in three samples. The

noticeable change in peaks is observed in every plane$'$s peak intensities. This (200) peak is indicating that the formation of the transformed β phase has taken place on it since the solution treatment was done at a higher temperature 920^0C. The (110) β phase peak was maximum in the UT sample and minimum in the AC sample which shows that percentage of β was minimum during the AC process. In XRD analysis it was observed that $(10\bar{1}1)$ α lamellar phase peak decreased and $(10\bar{1}2)$ α'' orthorhombic phase peak maximized in the AC sample than UT and STC process sample. Based on effective slip length; lamellar structure has lower ductility than orthorhombic grains, since β phase was less present in AC sample which reduced the α-β grain boundaries. The α-α grain boundaries were easily deformable than α-β. Therefore, by the results of XRD and EBSD, it can be concluded that α'' phase was increased with grain size on AC sample, while STC sample was α' phase and transformed β phase with minute change in the grain size than UT sample. Furthermore, $\alpha|\beta$ boundaries work as an active hindrance to slip transmission than $\alpha|\alpha'$ boundaries. Therefore, the present study confirmed the findings about the low microhardness of the AC processed sample than other samples [160, 161, 162].

5.3.2   Plastic deformation mechanism

In HSM process development of tool wear, chips formation and workpiece surface morphology is rely on the plastic deformation mechanism of Ti-6Al-4V alloy. Grain size and microhardness influence the deformation mechanism during machining of Ti-6Al-4V alloy since they impact the yield strength of the material. By the Hall-Petch equation yield strength of the Ti-6Al-4V alloy is indirectly proportional to the square root of grain size and microhardness ($H_v = 3 * yieldstrength$) is directly proportional to yield strength [163]. AC process sample (3188 MPa) has minimum microhardness than STC (3335 MPa) and UT sample (3385 MPa) [154]. Therefore, according to grain size and micro-hardness, AC sample has lowest yield strength than other two samples. It is important to highlight the

fact that the AC sample has the lowest yield strength and it has good plastic deformation properties than the other two samples. Plastic deformation mechanism during machining of Ti-6Al-4V alloy was dependent upon the deformation mode of microstructure and the key phenomenon of deformation mechanism in Ti-6Al-4V alloys were dislocation slips and twinning. Hence, dislocation slip is taking place in each sample and according to it plastic deformation readily occurred in the sample with a larger grain size [163, 161]. It was observed by Hua et al. [164] that lower hardness resulted in lower strength of Ti-6Al-4V alloy, higher amount of deformation without wear was occurred. From the above description, it can be concluded that AC processed sample has higher plastic deformation ability than STC and UT processed samples.

5.3.3 Mechanism of chip formation and assessment of chip thickness

The HSM process was achieved by tool passing through the engagement point, disengagement point, and center point across the tool rotation. Figure 5.1 shows the placement of tool and workpiece with tool path direction and tool rotation angle during high-speed up-milling. In this illustration first tooth path is shown with a continuous curve while the second tooth path is shown with a dashed curve and chip thickness is continuously changing with tool rotation. The HSM process was achieved by the tool passing through the engagement point, disengagement point, and center point across the tool rotation. The machining mechanisms were extremely influenced by the minimum chip thickness effect [165]. In equation (5.1) the relationship between uncut chip thickness (t_c), feed per tooth per revolution (f_r), and angle between feed direction with tooth revolution (ϕ) are shown. Maximum and minimum uncut chip thickness was occurred by tooth revolution and ploughing was dependent upon ratio of t_{er}/f_r. Therefore, during the material removal if the t_{er} was constant throughout the experiment and uncut chip thickness low then ploughing was the key cause of plastic deformation, while if uncut chip thickness is higher then shearing is the

main cause of plastic deformation [166]. In present work initially t_{er} was 3μm and uncut chip thickness is above the 3μm at ϕ among the range of 37^0 to 90^0. Therefore, upto machining time 6 sec and tool revolution 37^0 ploughing was taken place and beyond that shearing was dominant for machining. After initial machining of 6 sec tool tip was broken and t_{er} become larger which enhanced the ploughing phenomenon in current machining work. Additionally, tool-tip was broken according to hardness of sample which was least of AC sample and highest of UT sample therefore ploughing effect influencing lesser in AC sample. Initially microhardness and yield strength of AC sample was lesser therefore friction between tool-chip interface was minimum. Subsequently; least cutting temperature and chip thickness should be occurred for machining AC sample, which can be seen from Fig 5.3.

$$t_c = f_r \sin \phi \qquad (5.1)$$

Figure 5.2 is taken on a 3D optical profilometer Zygo model newview 9000 with white light scanning (non-contact) at IIT Dhanbad. It depicted the chip formed during the HSM process in AC, STC, and UT samples after the 6, 9, 12, and 13.5 seconds. During the HSM process, intense deformation was taken place on localized primary shear zone at higher strains and strain rates, and this type of deformation created an adiabatic shear band. Generally, as a result of adiabatic shear bands, the semi-continuous (segmented) chips were formed during high-speed machining of titanium alloy [167, 168]. Additionally, it was proposed in the thermoplastic model used by Komanduri and Hou [169] that adiabatic shear bands were developed within the primary shear zone since the increase in temperature. The higher temperature developed extreme softening within the shear bands which led to crack initiation in the chips. While a crack began in a specific shear band, stresses were released and extreme shear-localization led to develop crack propagation at some interval of distance as shown in segmented chips on Fig. 5.2 in UT, STC and AC samples. The
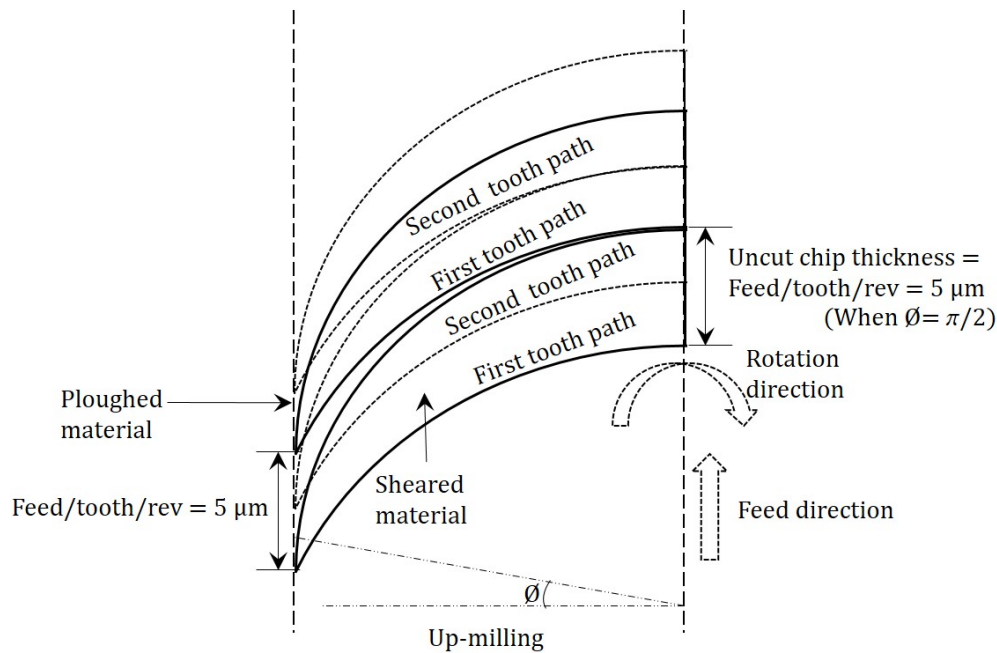
Figure 5.1: Tool path direction and rotation angle in high-speed up-milling process

primary fundamental cause of the segmented chip during the HSM process is that the crack propagates in a primary shear plane, while tool has already travelled forward due to the high cutting speed. Therefore, shear stress reached a value to initiate crack formation in an uncut chip at some distance although it was not sufficient to plastically deform the chip material. It is observed from Fig. 5.2 that segmented chips were formed in all the samples.

Chip thickness of UT, AC and STC sample was measured by 3D optical profilometer Zygo model newview 9000 with white light scanning (non-contact) and the result of chip thickness variation during the different cutting times are shown in Fig. 5.3. It is visible in the illustration that machined chip thickness was increased with AC, STC, and UT samples respectively. The microhardness of AC, STC, and UT samples were varied from low to high, which was found on chapter 4 in section 4.3.3. Lower hardness for AC sample was led to lower forces which would also led to lower cutting temperature and chip thickness
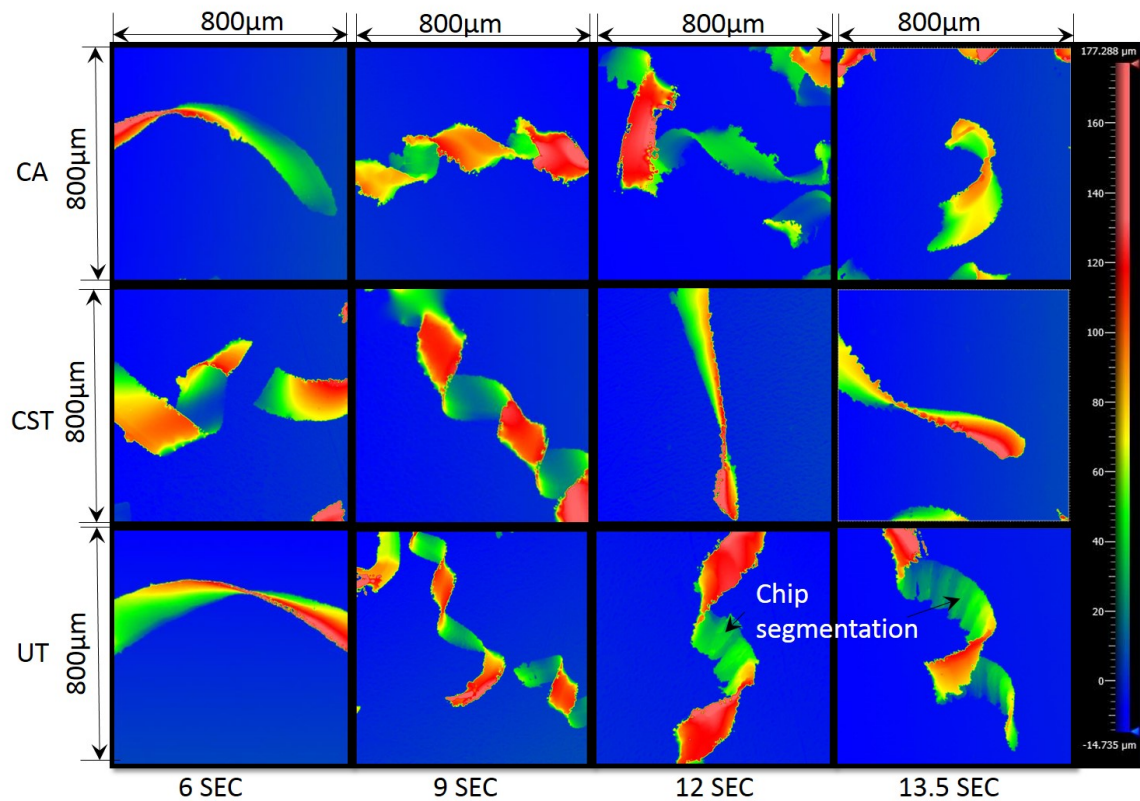
Figure 5.2: Chip formed on AC, STC and UT sample in high-speed up-milling process

during machining. As the hard asperities increased between interface, friction and cutting temperature enhanced, which ultimately increased the chip thickness more in case of STC and UT samples.

5.3.4 Assessment of Tool morphology and tool wear

In preliminary experiments it was estimated that wear on the flank face was the dominant factor during machining from the WC tool and average flank wear (VB_{avg}) of 0.3 mm was taken as criteria of flank tool wear. Additionally, it was found that after machining of UT sample with cutting parameters mentioned in table 5.1 for 13.5 seconds, the VB_{avg} traversed to its wear criteria of 0.3 mm. Therefore, WC tool flank face morphology took from optical microscope model Olympus BX 52 of the fresh tooth and worn tooth during
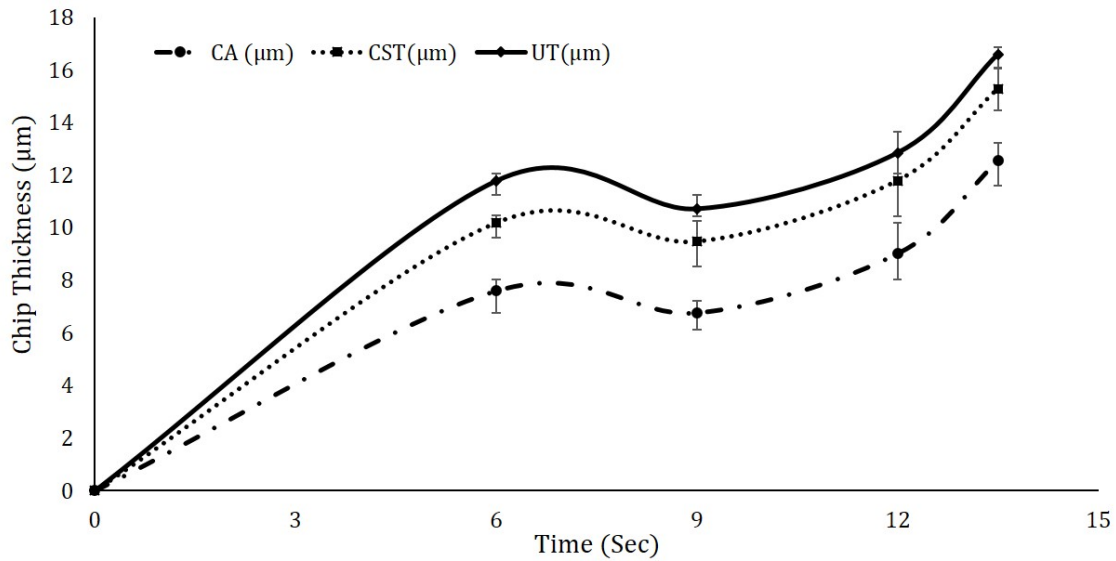
Figure 5.3: Chip thickness of AC, STC, and UT samples during different machining time

machining of AC, STC and UT sample are shown in Fig. 5.5. Initially, the physical abrasion between two moving surfaces (tool and workpiece) was taken place during the HSM process. During the abrasion process, the hard particles of Ti-6Al-4V alloy, which was harder in STC and UT than AC sample rubbed the WC tool particles. From Fig. 5.5, it can be observed that the tool tip is broken with a worn or rubbed face during machining of each sample. Since the cutting speed was higher during HSM process therefore, friction between both surfaces produced a higher temperature. Previously many researchers reported higher cutting temperature (up to 850^0C) between tool-workpiece interface during dry HSM process of Ti-6Al-4V alloy [146, 148, 143]. Hence, higher cutting temperature was contributed to the diffusion of tool and workpiece material elements into each other surface. Subsequently, arised the adhesive and diffusion wear on WC tool [140]. It can be observed from Fig. 5.5 that abrasion marks were present on the adhesive layer and not on the tool flank face. This indicated an adhesive layer that was formed on the flank face acted as a protective layer against the abrasion. In addition to this, under high machining temperature more adhesive layer was formed at the flank face. Therefore, flank wear

caused by abrasion was not as significant as adhesive wear when machining Ti-6Al-4V with a WC tool during the dry condition. The adhesive wear can be observed in the form of adhered Ti-6Al-4V alloy in the tool flank face from Fig. 5.5. In Fig. 5.5 it is illustrated that flank face worn out during machining which denoted that diffusion wear with adhesive wear dominated the tool wear during current work. The low microhardness of AC sample helped to develop more BUE formation in it which can be observed in Fig. 5.5. In AC sample BUE was visible while in STC and UT samples it was less which caused by less microhardness and high ductility of AC sample than other two samples.

In Fig. 5.4 VB_{avg} with respect to time during high-speed up-milling of AC, STC and UT
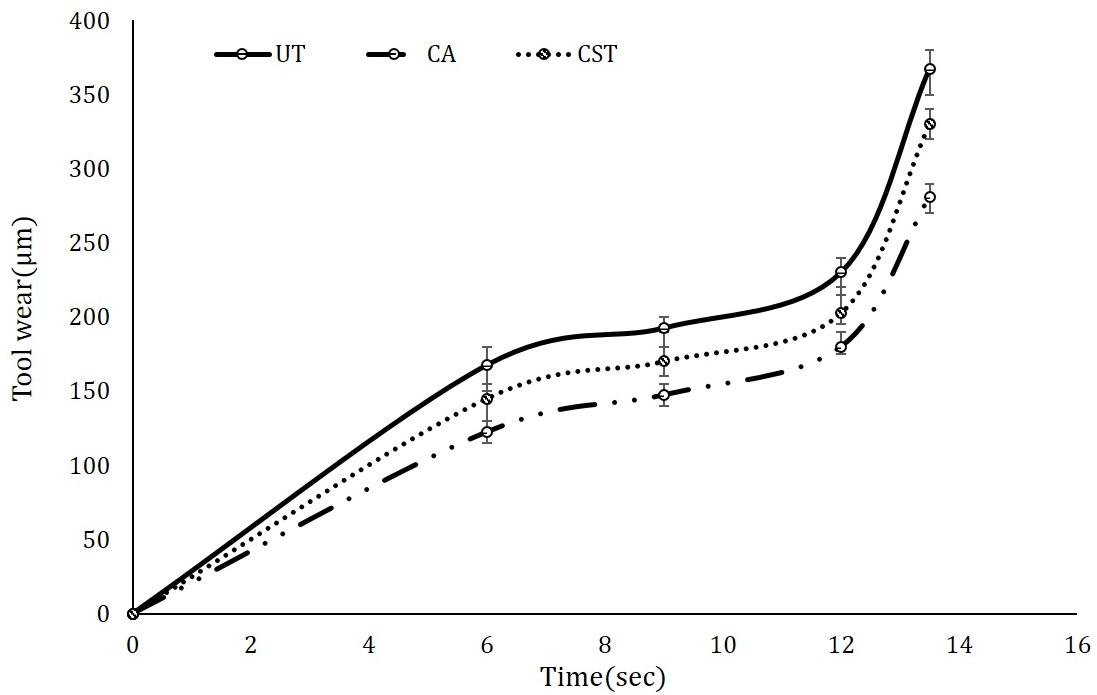

Figure 5.4: Tool wear during different machining time of AC, STC and UT sample

are shown. The results of VB_{avg} shown that cryogenic quenching after the annealing process has significantly affected the tool wear. The results shown that tool wear was taken place in three stages viz. initial wear stage, uniform wear stage and rapid wear stage and

tool wear shown exponential growth after the uniform wear stage. The higher cutting temperature during dry high-speed up-milling process caused very low machining time. Tool wear increased rapidly in machining STC and UT samples in comparison to machining of AC sample. The minimum VB_{avg} of the AC sample can be attributed to its low microhardness and low volume of β phase. Initially tool tip break according to values of yield strength, and microhardness of UT, STC and AC sample respectively and as tool tip was broken it accelerated the tool wear mechanism by increasing t_{er} and more uneven hard asperities occurred between tool-chip interface. The highest tool wear was occurred in the UT sample since hard asperities of it raised high cutting force and higher cutting temperature which resulted in quick tool tip breakage.

5.3.5   Surface characterization

Figure 5.6 shows the average surface roughness of area (S_a) and root mean square roughness of area (S_q) occurred during AC, STC and UT samples. Surface roughness was measured to see the effect of different heat treatments and quenching processes on the surface roughness of Ti-6Al-4V alloy. These values were obtained as per the ISO 4288-1997 standards by the non-contact type optical profilometer Zygo new view 9000 and. To measure the surface roughness between 0.1 to 2 μm the sampling length should be between 0.8 mm, hence area to calculate the S_a and S_q was taken 0.8×0.8 mm^2. S_a values were denoted the average entire deviation of the surface abnormalities while S_q denoted the standard deviation of distribution of surface elevations. The S_q values were more sensitive to large deviation from the mean line of surface profile, although in current work there was not much variation observed between both parameters, which represents the surface profile during high-speed up-milling has not witnessed severe spots or asperities in the machined surface. The high-speed up-milling procedure shown in Fig. 5.1 determines the surface morphology after the HSM process. During the HSM process, surface finish was depen-

dent upon the abrasion and adhesion of workpiece material [170]. It was observed that in the primary stages of machining, surface roughness decreased with an increase in machining time and after some time it started to increase with an increment in machining time. At the start t_{er} was less since the tool tip was not broken and a shearing mechanism was taking place. As machining advances the t_{er} increases since the tool tip is broken and adhesive wear increases. Aramcharoen and Mativenga [171] stated that the minimum surface roughness was observed for the (t_{er}/f_r) ratio equal to 1 beyond that ploughing mechanism was increased which ultimately increased the surface roughness of the machined surface [170]. From Fig. 5.6 it can be concluded that the AC sample has achieved a minimum S_a and S_q than the other two samples since tool wear and coefficient of friction between tool-chip interface was least during machining of the AC sample.

5.3.6 Characterization of burr formation

The burrs could occurred in eight edges of the workpiece during face milling although these burr locations are not much significant always. In current work, top burr was significant therefore it was measured and analyzed for high-speed up-milling [172]. Assessment of burr formation was achieved by calculating burr volume in AC, STC, and UT samples during different machining times. Figure 5.7 shows the burr formed by up-milling process. The burr volume was obtained from no contact profilometer Zygo newview 9000 and analyzed by Zygo′s Mx™ software, which is shown in Fig. 5.8.To obtain the burr volume from a non-contact optical profilometer, the total area of machined slot was scanned by the stitching method as shown in Fig. 5.7.

Subsequently, volume up and volume down output results were added to obtain the elevated volume on the machined area, which was the top burr formed during slot up-milling in the current work as shown in Fig. 5.7. To find the top burr volume, the unmachined area was set as a reference plane by using the fit mask option on the software. Hence, the soft-

ware shown top burr volume as volume up value and volume down were shown the volume of the unmachined area as well as machined area. It can be observed from Fig. 5.8 that burr volume was achieved minimum during machining of UT sample while maximum in AC sample. This increase in burr volume was obtained since the temperature of workpiece increased during dry high-speed up-milling. Since the AC sample had more ductility due to the presence of less β phase and lamellar α phase microstructure, it formed more top burr on its surface [173]. The effect of t_{er} was observed in previous studies, according to which increment in t_{er} increased the tool roundness, as well as burr formation in workpiece material [172]. Subsequently, the increment of burr volume in AC, STC and UT samples can be attributed to the increment in t_{er} with temperature of the tool. In the studies, it was observed that to improve the surface finish of a machined material one should have to compromise with burr formation since both of them are contradictory to each other [149]. The results showed that cryogenic quenching with annealing process not decreased the burr formation.
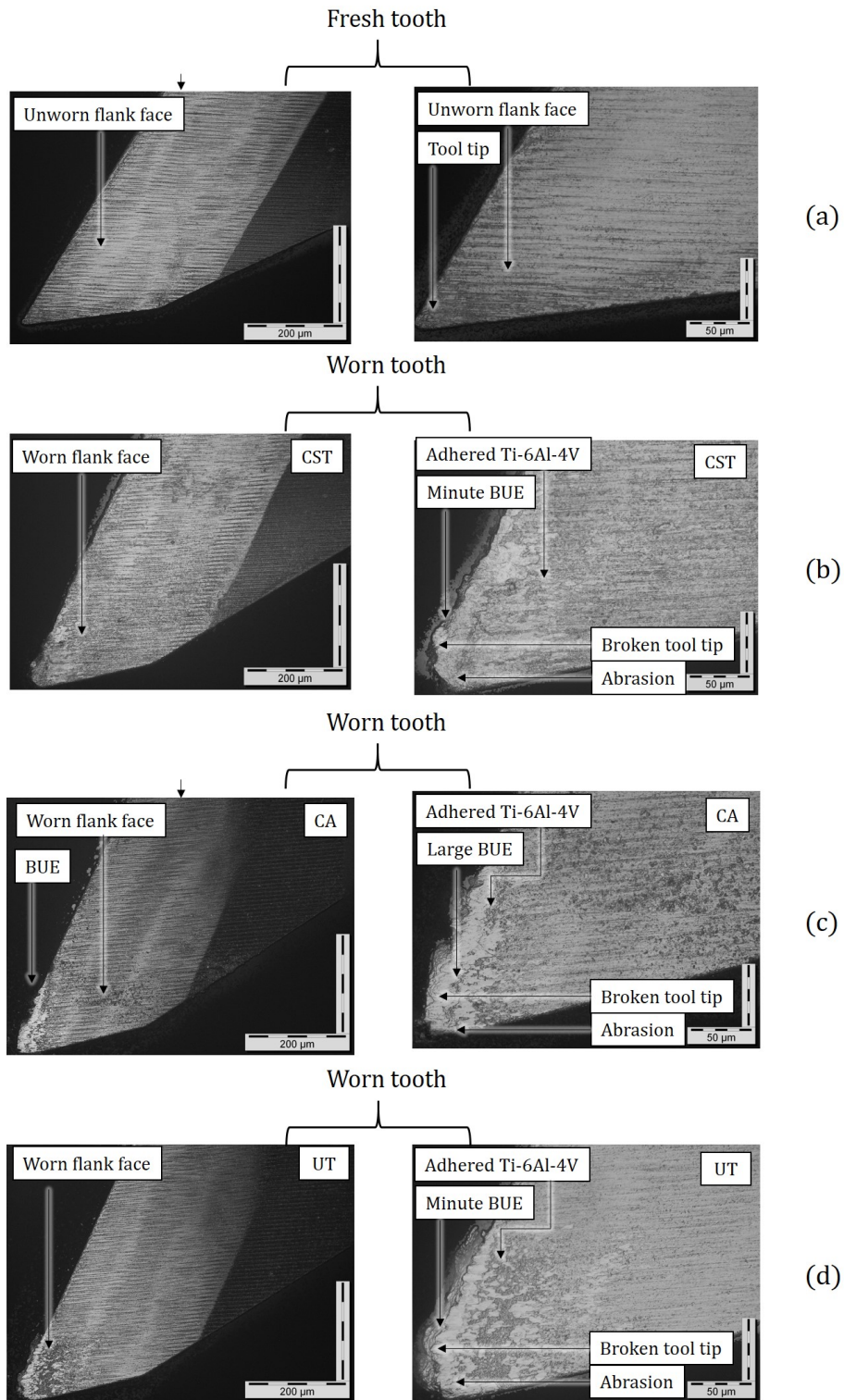
Figure 5.5: Tool morphology of fresh tooth and worn tooth after machining 13.5 sec of AC, STC and UT sample
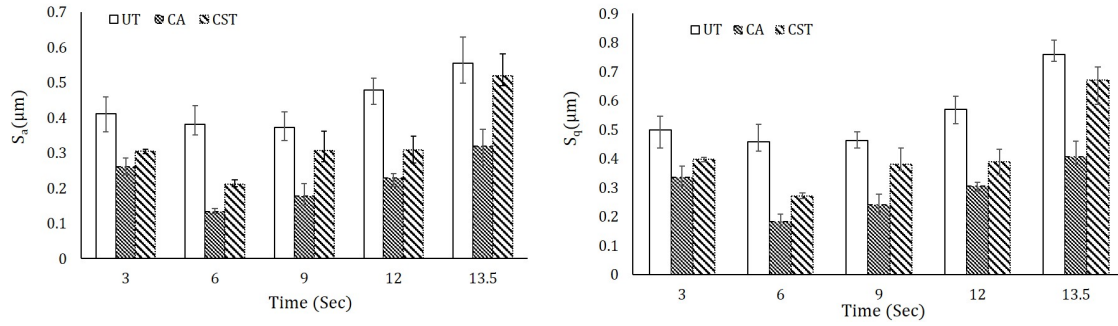
Figure 5.6: Surface roughness area (S_a) and square root mean roughness area (S_q) of AC, STC and UT samples after machining
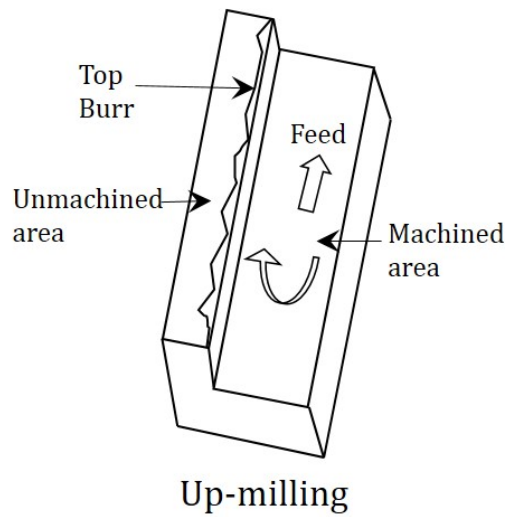
Figure 5.7: Morphology of burr formation in slot up-milling process
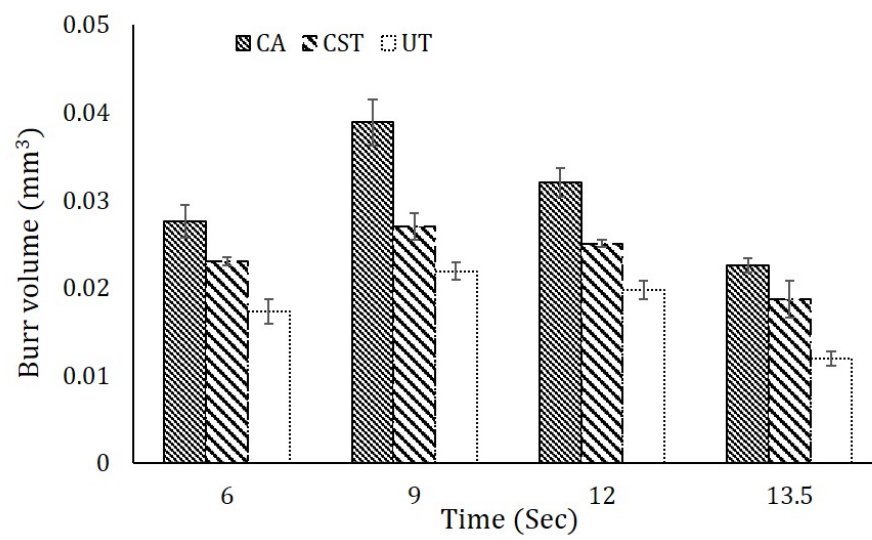
Figure 5.8: Top burr volume formed in AC, STC and UT sample

5.4   Conclusion

To our knowledge, this is the first report conducted to establish how the heat treatment with cryogenic quenching affects the machining output parameters such as chip formation, surface roughness, burr formation, and tool wear during the high-speed up-milling process of Ti6Al-4V alloy. Therefore initially, AC and STC process has conducted and compared their microstructure by EBSD and XRD result with the UT sample. The analysis of high-speed up-milling machining result leads to the following conclusions:

- The chip thickness,tool wear and surface roughness observed during high-speed up-milling of AC sample possessed the least value since it had good plastic deformability and low microhardness. Moreover, chip thickness has increased with machining time since cutting temperature enhanced due to low thermal conductivity of Ti-6Al-4V alloy.

- A low yield strength and microhardness of AC material has affected the burr formation. Subsequently, Burr formation has increased slightly during machining of AC sample than STC and UT sample.

Future research should consider the potential effects of cryogenic quenching on burr formation more carefully, to reduce it. Furthermore, an optimization technique with lubrication could be introduced in the future work to optimize the result of burr formation with surface finish and tool life. By these concluding statements it can be observed that by the AC process, the machinability of Ti-6Al-4V alloy can be increased in terms of chip formation, tool life and surface finish of Ti-6Al-4V alloy.

6

Evaluation of machinability improvement by Maglev EDM and high speed milling process

The aim of the chapter is to evaluate the both proposed method of improvement in machinability of Ti-6Al-4V alloy viz. maglev EDM and high speed milling. The maglev EDM is unconventional machining process while high speed milling is conventional machining process of material removal.

6.1   Introduction

Ti-6Al-4V is an electrically conductive material therefore it can be machined by unconventional EDM process. High speed milling on Ti-6Al-4V alloy is difficult to perform since the low thermal conductivity and high hardness enhances the cutting temperature and cutting forces. Klocke et al. [174] compared the milling, sinking-EDM, Wire-EDM and ECM during machining of Ti-6Al-4V alloy and Inconel 718. In the study comparison was conducted on the basis of material removal rate and roughing cost. They concluded that for Ti-6Al-4V alloy milling and ECM were cost effective while for Inconel 718 sinking EDM and ECM was better alternative for cost effective production. Vanderauwera et al.[175] compared the micro-milling and micro-EDM process during machining of rectangular shaped geometries. The assessment was achieved on the performance of output parameters such as energy consumption, surface roughness, machining time, dimensional and geometrical accuracy. It was observed from the study that surface finish, depth accuracy and flatness was better in micro-milling than micro-EDM while quality of cavity edges was better in case of micro-EDM. They concluded that for higher aspect ratio of length to depth micro-EDM can be applied for initial machining while micro-milling for finishing operation. Therefore, it could be concluded from the studies that EDM is better in machining sharp inside corners, deep areas of the mold, very complex geometry, rib machining and hard materials. The milling process can be applied for mirror finish, large batch production and high precision.

6.2   Technological assessment

For the two studied technology maglev EDM and high speed milling the MRR and specific energy are presented in this section to compare them. These results are based on the experimental results of previously presented chapters.

6.2.1 Material removed by a tool

Currently comparison of maglev EDM and high speed milling is achieved on the basis of MRR during machining of Ti-6Al-4V alloy. In the study high speed milling was conducted by 3 mm diameter end milling tool with 5 μm tool edge radius, 15^0 helix angle and uncoated carbide material. The process parameter selected for high speed milling were given on table 5.1. In maglev EDM 3 mm diameter and 20 mm length of copper material tool were applied, which is very soft in comparison to carbide material. During the high speed milling cavity with large hole or texture could not be achieved since depth of cut is limited by tool shank length. To calculate the MRR during high speed milling following formula is applied -

$$M_m = doc \times W \times F \times \sigma \tag{6.1}$$

Where, M_m is MRR in mg/min, doc is depth of cut in mm, W is width of cut in mm, F is feed rate in mm/min during high-speed up-milling and σ is density of Ti-6Al-4V alloy in mg/mm^3. MRR is higher by applying such kind of high feed rate and depth of cut, although; this is obtained by compensation in reduced tool life. In the presented work MRR during high- speed up-milling process was same for untreated and treated samples since the value of depth of cut, width and feed rate.

The MRR during maglev EDM was calculated by formula given on eq. (3.1). The MRR obtained by maglev EDM is very low in comparison to high-speed up-milling process since the non-traditional machining has low MRR during most of the time. While tool life during maglev EDM is very high in comparison to high-speed up-milling process since for the simple cavity shape formation only circularity should be maintained after each machining. To make the good circular cavity each time during EDM machining, tool flatness was observed and polished after each experiment with 2000 number grit size paper. Polishing of tool surface and tool wear rate (70-80μg/min) during maglev EDM has decreased the

electrode length after each experiment, hence tool life during maglev EDM is calculated by multiplying number of experiments performed with 10 min machining time. By results of MRR and tool life the material removed by single tool is measured for high-speed up-milling and maglev EDM processes by following formula-

$$M_r = MRR \times T \tag{6.2}$$

Where, M_r is total material removed in mg by single tool, MRR is in mg/min and T is tool life in min for high-speed up-milling and maglev EDM processes. By eq.(6.2) the material removed by a single tool during high-speed up-milling and maglev EDM process is obtained which is shown on Fig. 6.1. It can be observed from the Fig. 6.1 that tool efficiently used in maglev EDM process than high-speed up-milling process. The tool efficiency during maglev EDM process is 57.14% higher than high-speed up-milling process in terms of material removed by single tool.
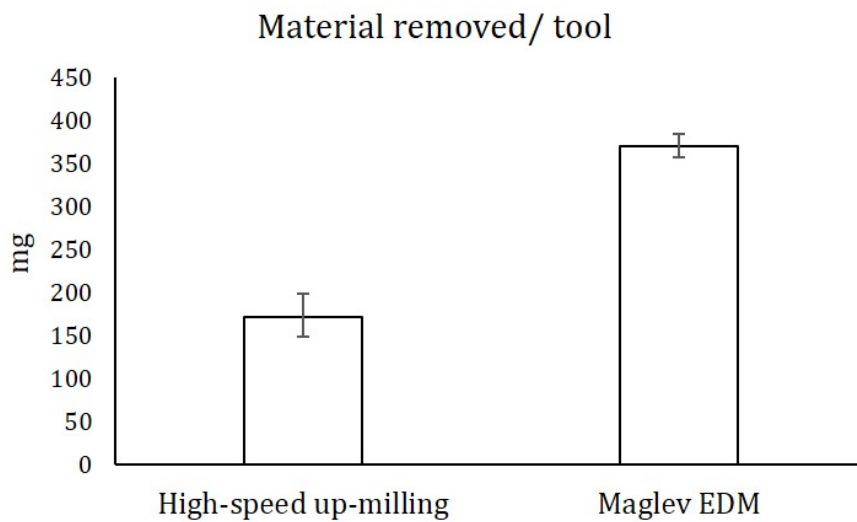
Figure 6.1: Material removed by single tool in high-speed up-milling and maglev EDM process

6.2.2   Specific energy consumption during machining process

For the comparison of high-speed up-milling and maglev EDM process the specific energy is applied. Specific energy consumed during maglev EDM system was given on section 3.3.3. The calculation and analysis of specific energy for maglev EDM was given on section 3.3.3. The maglev EDM with best specific energy consumption is taken here for the comparison purpose and it can be seen on Fig. 6.2 Specific energy consumption for high-speed up-milling process is calculated from the following formula-

$$SE_m = P \times 60 \div M_m \times 1000 \qquad (6.3)$$

Where, SE_m is specific energy of high speed milling in J/μg, P is spindle motor power in J/sec and M_m is MRR in mg/min during high-speed up-milling process. From the above mentioned eq.(6.3) the specific energy consumption to remove a unit mass of material is calculated and shown on Fig. 6.2. It is observed from the specific energy graph that high-speed up-milling is produced better result in terms of specific energy consumption. The high-speed up-milling has consumed 40 % less energy to remove a unit mass of material, which showed that it is a better method in terms of energy efficiency.
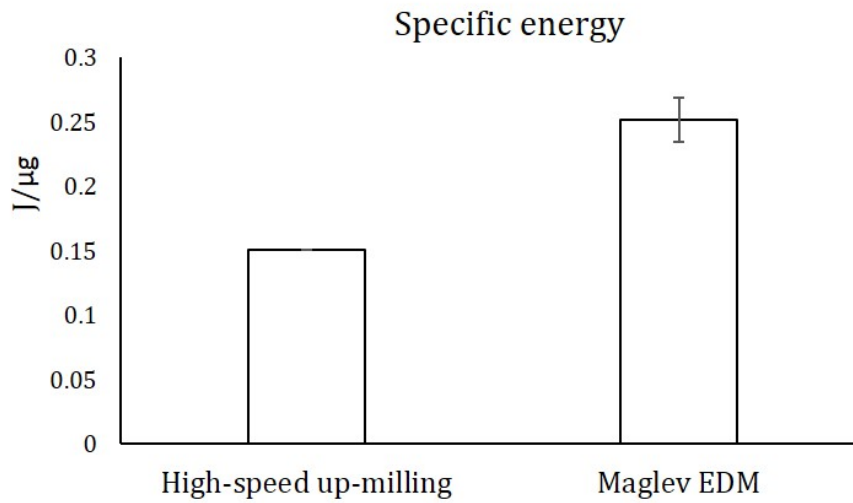
Figure 6.2: Specific energy consumption in high-speed up-milling and maglev EDM process

6.3   Economical assessment

Technological assessment has shown that both machining processes are better in one output parameter, hence it is necessary to evaluate both machining processes on the basis of economic analysis. Unattended machining capability of maglev EDM has key advantage over high speed milling in terms of wages cost, since one employee can operate more than one maglev EDM machine meanwhile one employee can operate only single high speed milling system. In the present study economical analysis is achieved by evaluation of manufacturing cost, tool cost and energy cost during high speed milling and maglev EDM system.

6.3.1   Manufacturing cost

Manufacturing cost assessment is conducted by calculating the initial machine tool development cost. In case of high speed milling the machine tool is developed by assembly of different component to reduce the manufacturing cost of it. The developed high speed

machine tool system is shown on Fig. 6.3. This experimental setup is consist of stages, spindle, granite frame, tool holder, workpiece fixture, spindle controller, stage controller etc. The overall cost of the machine tool system is addition of individual cost of each parts, resultantly, overall high speed milling machine tool cost was approximately 30 Lakh INR. The maglev EDM setup is shown on Fig. 3.1in which key component of maglev EDM system can be observed such as DC power supply, manual linear stages, digital oscilloscope, electric magnet and permanent magnets. The overall development cost of maglev EDM setup was approximate 1.5 Lakh INR. The development cost of maglev EDM is very low as compared to high speed milling system, since charges of maglev EDM key component are lower than milling components. Maintenance cost is very less in case of maglev EDM than high speed milling, since the each component of high speed milling system is costlier and it required continuous maintenance by a skilled worker.
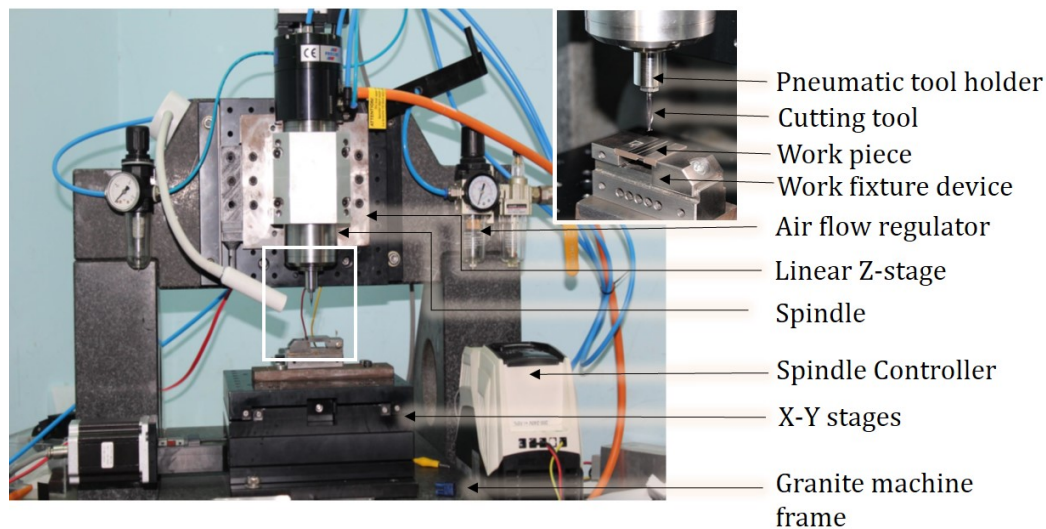
Figure 6.3: High-speed milling system

6.3.2   Tool cost

Tool cost is dependent on the material removed by single tool and the cost of single tool. The analysis of material removed by single tool is given in section 6.2.1 and according to it high speed milling removes less material than maglev EDM by single tool. In current study copper tool rod was applied as tool electrode which has very low cost approximately 10-20 INR for a single rod. Meanwhile during high speed milling uncoated carbide tool was applied, which has tool cost of approximately 1450 INR. Therefore, to remove 1 gm of
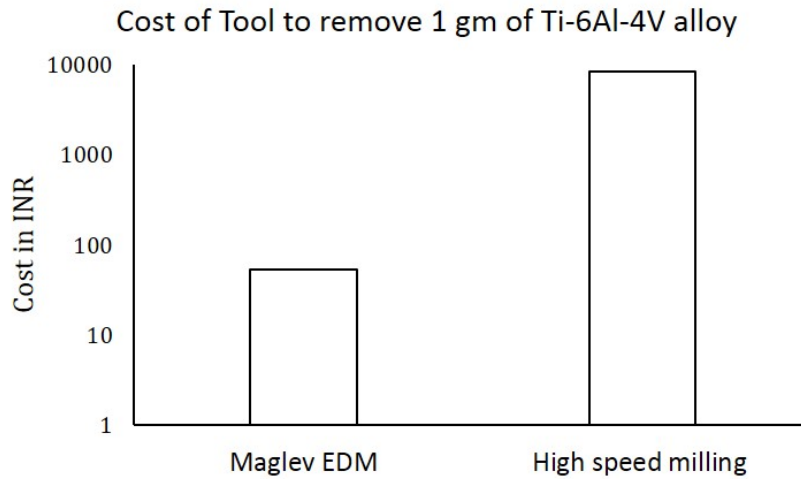
Figure 6.4: Tool cost endured to remove 1 gm of Ti-6Al-4V alloy in maglev EDM and high speed milling

material tool cost for high speed milling and maglev EDM can be calculated by following formula-

$$C_t = (1000 \div M_r) \times C_s \tag{6.4}$$

Where, C_t is Overall tool cost to remove 1 gm of Ti-6Al-4V alloy M_r is total material removed in mg by single tool, C_s is single tool cost. Figure 6.4 shows the tool cost endured to remove 1 gm of Ti-6Al-4V alloy.

The higher tool cost is occurred in high speed milling process since the single tool cost

of high speed milling tool is very high in comparison to tool cost of EDM tool. Additionally, tool life was less in high speed milling since high feed rate and cutting speed applied during it. The high feed rate is giving the higher MRR during high speed milling therefore it is not the key factor to increase the tool cost to remove the 1 gm of Ti-6Al-4V alloy.

6.4 Summary

In the present study the machinability during manufacturing technologies maglev EDM and high speed milling were compared on the basis of technological and economical analysis. In case of technological assessment two factor viz. MRR by single tool and specific energy to remove a unit mass of material is evaluated. The idea was to evaluate the machinability of Ti-6Al-4V alloy during both type of machining and to conclude which machining process is better at specific condition. The following conclusions have been made from the current study :

- In the study it was found that by a single tool MRR during maglev EDM was higher than high speed milling since the EDM tool can be applied after polishing it while in case of end milling cutter it was not possible.

- Specific energy consumed to remove a unit mass of material result showed that high speed milling process was better since it remove the material by shearing action of the tool. Meanwhile, in maglev EDM system high energy was consumed since it required to melt down and vaporize the Ti-6Al-4V alloy.

- Manufacturing cost for maglev EDM was less than high speed milling since the development cost, maintenance cost and wages cost in case of maglev EDM was very low.

- Tool cost to remove 1 gm of Ti-6Al-4V alloy was less in case of maglev EDM than

high speed milling since the single end milling cutter price is very high in comparison to EDM tool. Additionally; end milling cutter is not usable once it has wear out, while EDM tool can be applied again by maintaining and polishing the tool surface to its initial form.

- By the above mentioned points it can be summarized that maglev EDM provide excellent machinability of Ti-6Al-4V alloy in terms of cost effective manufacturing technology where small batch size production is produced, since it has very low MRR. Meanwhile high speed milling technology is better in case of large batch production required in less time since it has higher MRR.

The present study conclude that machinability of Ti-6Al-4V alloy is higher in terms of cost effectiveness during maglev EDM process, while machinability of it higher during high speed milling in terms of high MRR with high machining cost.

7

Conclusion and Future Scope

The present thesis work investigates about the machinability of Ti-6Al-4V alloy using maglev EDM and HSM system. In this regard, the development of maglev EDM system and modification of microstructure of Ti-6Al-4V alloy has been conducted. The influence of microstructure modification on machinability of Ti-6Al-4V alloy is achieved by tool wear, chip formation, burr formation and surface roughness during high-speed up-milling process.

7.1   The key conclusion of the thesis

On the basis of theoretical and experimental analysis key conclusion of the thesis are as follows:

7.1.1   Evaluation of maglev EDM for machinability of Ti-6Al-4V alloy

- Evaluation of maglev EDM system is achieved by comparing it with conventional EDM system. In this analysis stable discharge waveform enhanced the duty factor without short circuiting in maglev EDM system. Duty factor achieved in maglev EDM is 95% with stable discharge which is not obtained in conventional EDM with stability.

- Specific energy during 20 V maglev EDM process is 69.75% and 48.035% less than 50 V and 12 V conventional EDM process respectively.

- The R_z value achieved at 20 V discharge voltage in maglev EDM system indicated that crater formation was uniform in comparison to conventional EDM process since 20 V maglev EDM has 23.88% and 32.54% lesser R_z value than 12 V and 50 V conventional EDM process respectively.

- The average surface roughness in 20 V maglev EDM process was 9% and 22% lesser than 12 V and 50 V conventional EDM process respectively.

- Therefore, by development of novel technology maglev EDM system machinability of Ti-6Al-4V alloy was increased in terms of specific energy and better surface finish.

7.1.2   Assessment of modified microstructure of Ti-6Al-4V alloy

- Vicker's microhardness analysis revealed minimum hardness in case of CA samples, i.e. 7.5% less than untreated sample.

- The EBSD and XRD results of different samples revealed that CA sample possessed minimum lamellar α and β phase while UT sample possessed maximum lamellar α and β phase. By this observation it has been concluded that CA possessed the highest plastic deformability.

- LAGB's were minimum in CA sample and these boundaries easily plastic deformable therefore CA has highest plastic deformability than other samples.

7.1.3 Assessment of high-speed up-milling for machinability of Ti-6Al-4V alloy

- By high-speed up-milling process of CA sample chip thickness was observed to be less than CST and UT sample. Chip thickness during CA sample was less than CST sample about 17-32% and for UT sample 24-42%. Hence, the results confirmed that CA sample can be easily plastically deformed as compared to UT and CST samples.

- Tool wear during machining of CA sample was less than CST sample by 12-15% and than UT sample by 14-24%.

- Average area surface roughness was observed lesser in CA sample than CST and UT sample about 16-36% and 35-42% respectively.

7.1.4 Comparison of maglev EDM and high speed milling for machinability during machining of Ti-6Al-4V alloy

- According to the study, the results of the high-speed up-milling process was better in terms of specific energy consumption, MRR, and surface finish as compared to maglev EDM process. Burr formation and the challenge of creating a high cavity or depth were the limitations of high speed milling process.

- Low thermal conductivity of Ti-6Al-4V alloy had created hurdle during high speed milling while it was beneficial during maglev EDM process. Studies revealed that low thermal conductivity of Ti-6Al-4V alloy decreased heat transfer and enhanced the heat of the workpiece material, which ultimately helped to increase the MRR during it.

- Devlopment cost of maglev EDM was 93.3% less than high speed milling system, which had influenced the cost effectiveness during machining of Ti-6Al-4V alloy.

- Tool cost to remove 1 gm of Ti-6Al-4V alloy was 53.7% less in case of maglev EDM than high speed milling, which enhanced the production cost by milling process. Therefore, maglev EDM is applicable where less cost production required.

- High speed milling is applicable for large scale production while maglev EDM is applicable for small batch production.

- Therefore, it was concluded that machinability in terms of MRR, surface finish and specific energy consumption is higher in case of high speed milling process while machinability in terms of economical production was higher in case of maglev EDM process.

7.2 Contribution

The key contribution from the presented thesis work are as follows:

- Development of maglev EDM which is cost effective better substitute to conventional EDM systems.

- Development of high speed machine tool for the fabrication of 3D micro features irrespective of material hardness or toughness.

- Introduced cryogenic quenching during heat treatment process of Ti-6Al-4V alloy, which was not applied in previous studies of heat treatment processes.

7.3 Future Work

The following work can be explored for the further research on this topic:

- Measurement of cutting force during high speed milling of cryogenic quenched sample can be conducted.

- Development of modified microstructure by NEPER software can be done. Then modified microstructure can imported in ABAQUS for simulation of heat treatment with cryogenic quenching by applying subroutine UMAT, USDFILD and HETVAL.

- Simulation of high-speed up-milling process of annealed cryogenic quenched sample and untreated could be done.

- Modification of maglev EDM can be done to achieve more MRR with less surface roughness.

- Development of hybrid machining process by combination of high speed milling and maglev EDM can be done.

- Simulation of maglev EDM process could be done on ABAQUS by applying subroutine DFLUX and USDFIELD.

References

[1] M. Kulkarni, A. Mazare, E. Gongadze, Š. Perutkova, V. Kralj-Iglič, I. Milošev, P. Schmuki, A. Iglič, M. Mozetič, Titanium nanostructures for biomedical applications, Nanotechnology 26 (2015) 062002.

[2] N. Khanna, J. Davim, Design-of-experiments application in machining titanium alloys for aerospace structural components, Measurement 61 (2015) 280–290.

[3] C. Leyens, M. Peters, Titanium and titanium alloys: fundamentals and applications, John Wiley & Sons, 2003.

[4] B. Mills, Machinability of engineering materials, Springer Science & Business Media, 2012.

[5] E. Ezugwu, Z. Wang, Titanium alloys and their machinability—a review, Journal of materials processing technology 68 (1997) 262–274.

[6] C. Veiga, J. P. Davim, A. Loureiro, Review on machinability of titanium alloys: the process perspective, Rev. Adv. Mater. Sci 34 (2013) 148–164.

[7] C. S. Sharma, W. Rice, R. Salmon, Some effects of injecting cutting fluids directly into the chip-tool interface (1971).

[8] V. Naves, M. Da Silva, F. Da Silva, Evaluation of the effect of application of cutting fluid at high pressure on tool wear during turning operation of aisi 316 austenitic stainless steel, Wear 302 (2013) 1201–1208.

[9] K. Venugopal, S. Paul, A. Chattopadhyay, Growth of tool wear in turning of ti-6al-4v alloy under cryogenic cooling, Wear 262 (2007) 1071–1078.

[10] S. Trabelsi, A. Morel, G. Germain, Z. Bouaziz, Tool wear and cutting forces under cryogenic machining of titanium alloy (ti17), The International Journal of Advanced Manufacturing Technology 91 (2017) 1493–1505.

[11] C. R. Dandekar, Y. C. Shin, J. Barnes, Machinability improvement of titanium alloy (ti–6al–4v) via lam and hybrid machining, International Journal of Machine Tools and Manufacture 50 (2010) 174–182.

[12] N. Muthukrishnan, P. Davim, Influence of coolant in machinability of titanium alloy (ti-6al-4v), Journal of Surface Engineered Materials and Advanced Technology 2011 (2011).

[13] M. Armendia, P. Osborne, A. Garay, J. Belloso, S. Turner, P.-J. Arrazola, Influence of heat treatment on the machinability of titanium alloys, Materials and Manufacturing Processes 27 (2012) 457–461.

[14] P. Rathod, S. Aravindan, V. R. Paruchuri, Evaluating the effectiveness of the novel surface textured tools in enhancing the machinability of titanium alloy (ti6al4v), Journal of Advanced Mechanical Design, Systems, and Manufacturing 9 (2015) JAMDSM0035–JAMDSM0035.

[15] Y. Lou, H. Wu, Improving machinability of titanium alloy by electro-pulsing treatment in ultra-precision machining, The International Journal of Advanced Manufacturing Technology 93 (2017) 2299–2304.

[16] D. Y. Pimenov, M. Mia, M. K. Gupta, A. R. Machado, Í. V. Tomaz, M. Sarikaya, S. Wojciechowski, T. Mikolajczyk, W. Kapłonek, Improvement of machinability of ti and its alloys using cooling-lubrication techniques: A review and future prospect, Journal of materials research and technology 11 (2021) 719–753.

[17] A. Bordin, S. Bruschi, A. Ghiotti, P. Bariani, Analysis of tool wear in cryogenic machining of additive manufactured ti6al4v alloy, Wear 328 (2015) 89–99.

[18] D. He, S. Zheng, J. Pu, G. Zhang, L. Hu, Improving tribological properties of titanium alloys by combining laser surface texturing and diamond-like carbon film, Tribology international 82 (2015) 20–27.

[19] A. Pramanik, Problems and solutions in machining of titanium alloys, The International Journal of Advanced Manufacturing Technology 70 (2014) 919–928.

[20] B. Venkatesh, D. Chen, S. Bhole, Effect of heat treatment on mechanical properties of ti–6al–4v eli alloy, Materials Science and Engineering: A 506 (2009) 117–124.

[21] S. Shukla, V. Bajpai, Cryogenic machining, in: Innovations in Manufacturing for Sustainability, Springer, 2019, pp. 29–52.

[22] Z. Kou, F. Han, G. Wang, Research on machining ti6al4v by high-speed electric arc milling with breaking arcs via mechanical-hydrodynamic coupling forces, Journal of Materials Processing Technology 271 (2019) 499–509.

[23] Z. Lin, K. Song, X. Yu, A review on wire and arc additive manufacturing of titanium alloy, Journal of Manufacturing Processes 70 (2021) 24–45.

[24] F. Leijon, S. Wachter, Z. Fu, C. Körner, S. Skjervold, J. Moverare, A novel rapid alloy development method towards powder bed additive manufacturing, demonstrated for binary al-ti,-zr and-nb alloys, Materials & Design 211 (2021) 110129.

[25] J. Hirth, F. Froes, Interrelations between fracture toughness and other mechanical properties in titanium alloys, Metallurgical Transactions A 8 (1977) 1165–1176.

[26] W. L. Finlay, J. A. Snyder, Effects of three interstitial solutes (nitrogen, oxygen, and carbon) on the mechanical properties of high-purity, alpha titanium, Jom 2 (1950) 277–286.

[27] C. Ouchi, H. Iizumi, S. Mitao, Effects of ultra-high purification and addition of interstitial elements on properties of pure titanium and titanium alloy, Materials Science and Engineering: A 243 (1998) 186–195.

[28] D. Simbi, J. Scully, The effect of residual interstitial elements and iron on mechanical properties of commercially pure titanium, Materials Letters 26 (1996) 35–39.

[29] M. Wasz, F. Brotzen, R. McLellan, A. Griffin, Effect of oxygen and hydrogen on mechanical properties of commercial purity titanium, International Materials Reviews 41 (1996) 1–12.

[30] G. Welsch, R. Boyer, E. Collings, Materials properties handbook: titanium alloys, ASM international, 1993.

[31] S. Gollapudi, I. Charit, K. Murty, Creep mechanisms in ti–3al–2.5 v alloy tubing deformed under closed-end internal gas pressurization, Acta Materialia 56 (2008) 2406–2419.

[32] M. Tan, G. Chen, S. Thiruvarudchelvan, High temperature deformation in ti–5al–2.5 sn alloy, Journal of materials processing technology 192 (2007) 434–438.

[33] S. Malinov, W. Sha, Z. Guo, C. Tang, A. Long, Synchrotron x-ray diffraction study of the phase transformations in titanium alloys, Materials Characterization 48 (2002) 279–295.

[34] S.-H. Lee, K. Hagihara, T. Nakano, Microstructural and orientation dependence of the plastic deformation behavior in β-type ti-15mo-5zr-3al alloy single crystals, Metallurgical and Materials Transactions A 43 (2012) 1588–1597.

[35] T. Furuhara, T. Maki, T. Makino, Microstructure control by thermomechanical processing in β-ti–15–3 alloy, Journal of Materials Processing Technology 117 (2001) 318–323.

[36] S. Hotta, K. Yamada, T. Murakami, T. Narushima, Y. Iguchi, C. Ouchi, β grain refinement due to small amounts of yttrium addition in $\alpha+\beta$ type titanium alloy, sp-700, ISIJ international 46 (2006) 129–137.

[37] O. Kashapov, T. Pavlova, V. Kalashnikov, I. Popov, Effect of carbon additives on the mechanical properties of a titanium near-α alloy, Inorganic Materials: Applied Research 11 (2020) 1291–1298.

[38] R. Banoth, R. Sarkar, A. Bhattacharjee, T. Nandy, G. N. Rao, Effect of boron and carbon addition on microstructure and mechanical properties of metastable beta titanium alloys, Materials & Design 67 (2015) 50–63.

[39] G. Lütjering, Influence of processing on microstructure and mechanical properties of ($\alpha+\beta$) titanium alloys, Materials Science and Engineering: A 243 (1998) 32–45.

[40] N. Poondla, T. S. Srivatsan, A. Patnaik, M. Petraroli, A study of the microstructure and hardness of two titanium alloys: Commercially pure and ti–6al–4v, Journal of Alloys and Compounds 486 (2009) 162–167.

[41] Y. Mahajan, H. Margolin, Low cycle fatigue behavior of ti-6ai-2sn-4zr-6mo: Part i. the role of microstructure in low cycle crack nucleation and early crack growth, Metallurgical Transactions A 13 (1982) 257–268.

[42] A. Wagoner Johnson, C. Bull, K. Kumar, C. Briant, The influence of microstructure and strain rate on the compressive deformation behavior of ti-6al-4v, Metallurgical and Materials Transactions A 34 (2003) 295–306.

[43] M. Bache, M. Cope, H. Davies, W. Evans, G. Harrison, Dwell sensitive fatigue in a near alpha titanium alloy at ambient temperature, International journal of fatigue 19 (1997) 83–88.

[44] A. Foul, C. Aranas Jr, B. Guo, J. J. Jonas, Dynamic transformation of $\alpha \to \beta$ titanium at temperatures below the β-transus in commercially pure titanium, Materials Science and Engineering: A 722 (2018) 156–159.

[45] G. Malakondaiah, P. R. Rao, Creep of alpha-titanium at low stresses, Acta metallurgica 29 (1981) 1263–1275.

[46] G. Terlinde, T. Duerig, J. Williams, Microstructure, tensile deformation, and fracture in aged ti 10v-2fe-3al, Metallurgical Transactions A 14 (1983) 2101–2115.

[47] F. Froes, C. Yolton, J. Capenos, M. Wells, J. Williams, The relationship between microstructure and age hardening response in the metastable beta titanium alloy ti-11.5 mo-6 zr-4.5 sn (beta iii), Metallurgical and Materials Transactions A 11 (1980) 21–31.

[48] M. Nouari, H. Makich, Experimental investigation on the effect of the material microstructure on tool wear when machining hard titanium alloys: Ti–6al–4v and ti-555, International Journal of Refractory Metals and Hard Materials 41 (2013) 259–269.

[49] P.-J. Arrazola, A. Garay, L.-M. Iriarte, M. Armendia, S. Marya, F. Le Maître, Machinability of titanium alloys (ti6al4v and ti555. 3), Journal of materials processing technology 209 (2009) 2223–2230.

[50] H. Matsumoto, S. Watanabe, S. Hanada, Microstructures and mechanical properties of metastable β tinbsn alloys cold rolled and heat treated, Journal of alloys and compounds 439 (2007) 146–155.

[51] Y. Zhan, X. Zhang, J. Hu, Q. Guo, Y. Du, Evolution of the microstructure and hardness of the ti–si alloys during high temperature heat-treatment, Journal of alloys and compounds 479 (2009) 246–251.

[52] S. Zhu, H. Yang, L. Guo, X. Fan, Effect of cooling rate on microstructure evolution during α/β heat treatment of ta15 titanium alloy, Materials Characterization 70 (2012) 101–110.

[53] Y. C. Wang, T. G. Langdon, Effect of heat treatment on microstructure and micro-hardness evolution in a ti–6al–4v alloy processed by high-pressure torsion, Journal of Materials Science 48 (2013) 4646–4652.

[54] Z. Sun, X. Mao, H. Wu, H. Yang, J. Li, Tri-modal microstructure and performance of ta15 ti-alloy under near-β forging and given subsequent solution and aging treatment, Materials Science and Engineering: A 654 (2016) 113–123.

[55] P. Gao, X. Fan, H. Yang, Role of processing parameters in the development of tri-modal microstructure during isothermal local loading forming of ta15 titanium alloy, Journal of Materials Processing Technology 239 (2017) 160–171.

[56] E. Lopes, A. Cremasco, C. Afonso, R. Caram, Effects of double aging heat treatment on the microstructure, vickers hardness and elastic modulus of ti–nb alloys, Materials characterization 62 (2011) 673–680.

[57] K. Gu, H. Zhang, B. Zhao, J. Wang, Y. Zhou, Z. Li, Effect of cryogenic treatment and aging treatment on the tensile properties and microstructure of ti–6al–4v alloy, Materials Science and Engineering: A 584 (2013) 170–176.

[58] K. Gu, B. Zhao, Z. Weng, K. Wang, H. Cai, J. Wang, Microstructure evolution in metastable β titanium alloy subjected to deep cryogenic treatment, Materials Science and Engineering: A 723 (2018) 157–164.

[59] K. Gu, J. Wang, Y. Zhou, Effect of cryogenic treatment on wear resistance of ti–6al–4v alloy for biomedical applications, journal of the mechanical behavior of biomedical materials 30 (2014) 131–139.

[60] F. H. Çakir, O. N. Çelik, Influence of cryogenic treatment on microstructure and mechanical properties of ti6al4v alloy, Journal of Materials Engineering and Performance 29 (2020) 6974–6984.

[61] A. Molinari, M. Pellizzari, S. Gialanella, G. Straffelini, K. Stiasny, Effect of deep cryogenic treatment on the mechanical properties of tool steels, Journal of materials processing technology 118 (2001) 350–355.

[62] D. M. Lal, S. Renganarayanan, A. Kalanidhi, Cryogenic treatment to augment wear resistance of tool and die steels, Cryogenics 41 (2001) 149–155.

[63] G. Han, J.-R. Lee, Y. Noh, T.-S. Jun, The role of cryogenic quenching on the mechanical properties of fswed 6061-t6 aluminum alloy, Materials Science and Engineering: A 840 (2022) 142896.

[64] C. M. Grohol, Y. C. Shin, A. Frank, Laser cladding of aluminum alloys with concurrent cryogenic quenching for improved microstructure and hardness, Surface and Coatings Technology 439 (2022) 128460.

[65] H. D. Nguyen, A. Pramanik, A. Basak, Y. Dong, C. Prakash, S. Debnath, S. Shankar, I. Jawahir, S. Dixit, D. Buddhi, Additive manufacturing of ti-6al-4v alloy-a review, Journal of Materials Research and Technology (2022).

[66] S. Singh, S. Ramakrishna, R. Singh, Material issues in additive manufacturing: A review, Journal of Manufacturing Processes 25 (2017) 185–200.

[67] P. K. Gokuldoss, S. Kolla, J. Eckert, Additive manufacturing processes: Selective laser melting, electron beam melting and binder jetting—selection guidelines, materials 10 (2017) 672.

[68] H. Gong, K. Rafi, H. Gu, T. Starr, B. Stucker, Analysis of defect generation in ti–6al–4v parts made using powder bed fusion additive manufacturing processes, Additive Manufacturing 1 (2014) 87–98.

[69] P. Singh, V. K. Balla, S. V. Atre, R. M. German, K. H. Kate, Factors affecting properties of ti-6al-4v alloy additive manufactured by metal fused filament fabrication, Powder Technology 386 (2021) 9–19.

[70] B. E. Carroll, T. A. Palmer, A. M. Beese, Anisotropic tensile behavior of ti–6al–4v components fabricated with directed energy deposition additive manufacturing, Acta Materialia 87 (2015) 309–320.

[71] S. Y. Hong, M. Broomer, Economical and ecological cryogenic machining of aisi 304 austenitic stainless steel, Clean Products and Processes 2 (2000) 157–166.

[72] S. Y. Hong, Y. Ding, Cooling approaches and cutting temperatures in cryogenic machining of ti-6al-4v, International Journal of Machine Tools and Manufacture 41 (2001) 1417–1437.

[73] S. Y. Hong, I. Markus, W.-c. Jeong, New cooling approach and tool life improvement in cryogenic machining of titanium alloy ti-6al-4v, International journal of machine tools and manufacture 41 (2001) 2245–2260.

[74] N. Dhar, S. Paul, A. Chattopadhyay, Role of cryogenic cooling on cutting temperature in turning steel, J. Manuf. Sci. Eng. 124 (2002) 146–154.

[75] L. Zou, Y. Huang, M. Zhou, Y. Yang, Effect of cryogenic minimum quantity lubrication on machinability of diamond tool in ultraprecision turning of 3cr2nimo steel, Materials and Manufacturing Processes 33 (2018) 943–949.

[76] R. Muhammad, M. S. Hussain, A. Maurotto, C. Siemers, A. Roy, V. V. Silberschmidt, Analysis of a free machining $\alpha + \beta$ titanium alloy using conventional and ultrasonically assisted turning, Journal of Materials Processing Technology 214 (2014) 906–915.

[77] H. Jamshidi, M. Nategh, Theoretical and experimental investigation of the frictional behavior of the tool–chip interface in ultrasonic-vibration assisted turning, International Journal of Machine Tools and Manufacture 65 (2013) 1–7.

[78] J. Pujana, A. Rivero, A. Celaya, L. L. De Lacalle, Analysis of ultrasonic-assisted drilling of ti6al4v, International Journal of Machine Tools and Manufacture 49 (2009) 500–508.

[79] R. R. Rashid, S. Sun, G. Wang, M. Dargusch, The effect of laser power on the machinability of the ti-6cr-5mo-5v-4al beta titanium alloy during laser assisted machining, International Journal of machine tools and manufacture 63 (2012) 41–43.

[80] R. R. Rashid, S. Sun, G. Wang, M. Dargusch, An investigation of cutting forces and cutting temperatures during laser-assisted machining of the ti–6cr–5mo–5v–4al beta titanium alloy, International Journal of Machine Tools and Manufacture 63 (2012) 58–69.

[81] R. Rahman Rashid, S. Sun, S. Palanisamy, G. Wang, M. Dargusch, A study on laser assisted machining of ti10v2fe3al alloy with varying laser power, The International Journal of Advanced Manufacturing Technology 74 (2014) 219–224.

[82] H. Ding, N. Shen, Y. C. Shin, Thermal and mechanical modeling analysis of laser-assisted micro-milling of difficult-to-machine alloys, Journal of Materials Processing Technology 212 (2012) 601–613.

[83] Y. Ayed, G. Germain, W. B. Salem, H. Hamdi, Experimental and numerical study of laser-assisted machining of ti6al4v titanium alloy, Finite Elements in Analysis and Design 92 (2014) 72–79.

[84] Y. Gao, G. Wang, M. J. Bermingham, M. S. Dargusch, Cutting force, chip formation, and tool wear during the laser-assisted machining a near-alpha titanium alloy bti-6431s, The International Journal of Advanced Manufacturing Technology 79 (2015) 1949–1960.

[85] M. Bermingham, W. Sim, D. Kent, S. Gardiner, M. Dargusch, Tool life and wear mechanisms in laser assisted milling ti–6al–4v, Wear 322 (2015) 151–163.

[86] H. Badekas, C. Panagopoulos, S. Economou, Laser surface-treatment of titanium, Journal of materials processing technology 44 (1994) 54–60.

[87] Z. Sun, I. Annergren, D. Pan, T. Mai, Effect of laser surface remelting on the corrosion behavior of commercially pure titanium sheet, Materials Science and Engineering: A 345 (2003) 293–300.

[88] M. Kunieda, W. Kowaguchi, T. Takita, Reverse simulation of die-sinking edm, CIRP Annals 48 (1999) 115–118.

[89] P. Govindan, A. Gupta, S. S. Joshi, A. Malshe, K. Rajurkar, Single-spark analysis of removal phenomenon in magnetic field assisted dry edm, Journal of Materials Processing Technology 213 (2013) 1048–1058.

[90] S.-T. Chen, L.-W. Huang, J.-P. Kuo, T.-C. Pai, Development of an original electromagnetic damping-controlled horizontal cutting mechanism for microwire-edm, Journal of Materials Processing Technology 278 (2020) 116538.

[91] T. Masuzawa, M. Fujino, K. Kobayashi, T. Suzuki, N. Kinoshita, Wire electro-discharge grinding for micro-machining, CIRP Annals 34 (1985) 431–434.

[92] J. Fleischer, T. Masuzawa, J. Schmidt, M. Knoll, New applications for micro-edm, Journal of Materials Processing Technology 149 (2004) 246–249.

[93] M. Zhang, Q. Zhang, H. Wang, G. Liu, T. Guo, Research on a single pulse discharge to discriminate edm and eam based on the plasma tunnel and crater geometry, Journal of Materials Processing Technology 219 (2015) 248–256.

[94] H. Nair, A. Pramanik, A. Basak, C. Prakash, S. Debnath, S. Shankar, A. R. Dixit, Experimental investigation on material removal rate, kerf width, surface roughness and the dimensional accuracy the accuracy of hole in inconel 718 using wire electric discharge, Proceedings of the Institution of Mechanical Engineers, Part E: Journal of Process Mechanical Engineering (2022) 09544089221096025.

[95] J. Stráský, M. Janeček, P. Harcuba, M. Bukovina, L. Wagner, The effect of microstructure on fatigue performance of ti–6al–4v alloy after edm surface treatment for application in orthopaedics, Journal of the mechanical behavior of biomedical materials 4 (2011) 1955–1962.

[96] W. Theisen, A. Schuermann, Electro discharge machining of nickel–titanium shape memory alloys, Materials Science and Engineering: A 378 (2004) 200–204.

[97] Y. C. Lin, B. H. Yan, Y. S. Chang, Machining characteristics of titanium alloy (ti–6al–4v) using a combination process of edm with usm, Journal of Materials Processing Technology 104 (2000) 171–177.

[98] T. M. Mower, Degradation of titanium 6al–4v fatigue strength due to electrical discharge machining, International Journal of Fatigue 64 (2014) 84–96.

[99] G. Kucukturk, C. Cogun, A new method for machining of electrically nonconductive workpieces using electric discharge machining technique, Machining Science and Technology 14 (2010) 189–207.

[100] H. Beravala, P. M. Pandey, Experimental investigations to evaluate the effect of magnetic field on the performance of air and argon gas assisted edm processes, Journal of Manufacturing Processes 34 (2018) 356–373.

[101] H. Tong, Y. Li, Y. Wang, Experimental research on vibration assisted edm of microstructures with non-circular cross-section, Journal of materials processing technology 208 (2008) 289–298.

[102] S. Kim, B. H. Kim, H. S. Shin, C. N. Chu, et al., Hybrid micromachining using a nanosecond pulsed laser and micro edm, Journal of micromechanics and microengineering 20 (2009) 015037.

[103] A. Das, S. Ambastha, S. Halder, S. Samanta, et al., A novel methodology for spark gap monitoring in micro-edm using optical fiber bragg grating, IEEE Transactions on Instrumentation and Measurement 69 (2019) 4387–4394.

[104] M. Fujiki, G.-Y. Kim, J. Ni, A. J. Shih, Gap control for near-dry edm milling with lead angle, International Journal of Machine Tools and Manufacture 51 (2011) 77–83.

[105] E. Bamberg, S. Heamawatanachai, Orbital electrode actuation to improve efficiency of drilling micro-holes by micro-edm, Journal of materials processing technology 209 (2009) 1826–1834.

[106] R. Kumar, I. Singh, Productivity improvement of micro edm process by improvised tool, Precision Engineering 51 (2018) 529–535.

[107] X. Zhang, T. Shinshi, G. Kajiwara, A. Shimokohbe, Y. Imai, H. Miyake, T. Nakagawa, A 5-dof controlled maglev local actuator and its application to electrical discharge machining, Precision Engineering 32 (2008) 289–300.

[108] D. He, H. Morita, X. Zhang, T. Shinshi, T. Nakagawa, T. Sato, H. Miyake, Development of a novel 5-dof controlled maglev local actuator for high-speed electrical discharge machining, Precision Engineering 34 (2010) 453–460.

[109] B. Pradhan, M. Masanta, B. Sarkar, B. Bhattacharyya, Investigation of electrodischarge micro-machining of titanium super alloy, The International Journal of Advanced Manufacturing Technology 41 (2009) 1094–1106.

[110] J. Kao, C. Tsao, S. Wang, C. Hsu, Optimization of the edm parameters on machining ti–6al–4v with multiple quality characteristics, The International Journal of Advanced Manufacturing Technology 47 (2010) 395–402.

[111] D. K. Mishra, S. Datta, M. Masanta, et al., Effects of tool electrode on edm performance of ti-6al-4v, Silicon 10 (2018) 2263–2277.

[112] M. Kumar, S. Datta, R. Kumar, Electro-discharge machining performance of ti–6al–4v alloy: studies on parametric effect and phenomenon of electrode wear, Arabian Journal for Science and Engineering 44 (2019) 1553–1568.

[113] M. Mahardika, T. Tsujimoto, K. Mitsui, A new approach on the determination of ease of machining by edm processes, International Journal of Machine Tools and Manufacture 48 (2008) 746–760.

[114] F. Wang, Y. Liu, Y. Zhang, Z. Tang, R. Ji, C. Zheng, Compound machining of titanium alloy by super high speed edm milling and arc machining, Journal of Materials Processing Technology 214 (2014) 531–538.

[115] S. Li, Y. Wu, K. Yamamura, M. Nomura, T. Fujii, Improving the grindability of titanium alloy ti–6al–4v with the assistance of ultrasonic vibration and plasma electrolytic oxidation, CIRP Annals 66 (2017) 345–348.

[116] R. Madarkar, S. Agarwal, P. Attar, S. Ghosh, P. Rao, Application of ultrasonic vibration assisted mql in grinding of ti–6al–4v, Materials and Manufacturing Processes 33 (2018) 1445–1452.

[117] A. Al-Ahmari, M. S. Rasheed, M. K. Mohammed, T. Saleh, A hybrid machining process combining micro-edm and laser beam machining of nickel–titanium-based shape memory alloy, Materials and Manufacturing Processes 31 (2016) 447–455.

[118] M. Jamil, A. M. Khan, H. Hegab, L. Gong, M. Mia, M. K. Gupta, N. He, Effects of hybrid al2o3-cnt nanofluids and cryogenic cooling on machining of ti–6al–4v, The International Journal of Advanced Manufacturing Technology 102 (2019) 3895–3909.

[119] M. S. Sisodiya, S. Shukla, V. Bajpai, Feasibility analysis of novel maglev edm by comparing with conventional micro edm, Scientific Reports 12 (2022) 1–13.

[120] E. Gadelmawla, M. M. Koura, T. M. Maksoud, I. M. Elewa, H. Soliman, Roughness parameters, Journal of materials processing Technology 123 (2002) 133–145.

[121] S. Joshi, P. Pawar, A. Tewari, S. S. Joshi, Influence of β phase fraction on deformation of grains in and around shear bands in machining of titanium alloys, Materials Science and Engineering: A 618 (2014) 71–85.

[122] D. Nursyifaulkhair, N. Park, E. R. Baek, S. Kim, Influence of cooling rate on volume fraction of α massive phase in a ti-6al-4v alloy fabricated using directed energy deposition, Materials Letters 257 (2019) 126671.

[123] Y. Chong, T. Bhattacharjee, J. Yi, S. Zhao, N. Tsuji, Achieving bi-lamellar microstructure with both high tensile strength and large ductility in ti–6al–4v alloy by novel thermomechanical processing, Materialia 8 (2019) 100479.

[124] X. Gao, W. Zeng, S. Zhang, Q. Wang, A study of epitaxial growth behaviors of equiaxed alpha phase at different cooling rates in near alpha titanium alloy, Acta Materialia 122 (2017) 298–309.

[125] N. Kazantseva, P. Krakhmalev, M. Thuvander, I. Yadroitsev, N. Vinogradova, I. Ezhov, Martensitic transformations in ti-6al-4v (eli) alloy manufactured by 3d printing, Materials Characterization 146 (2018) 101–112.

[126] S. F. Jawed, C. D. Rabadia, M. A. Khan, S. J. Khan, Effect of alloying elements on the compressive mechanical properties of biomedical titanium alloys: A systematic review, ACS omega (2022).

[127] J. Yan, TRIP titanium alloy design, Ph.D. thesis, Northwestern University, 2014.

[128] Y. Lu, H. Tang, Y. Fang, D. Liu, H. Wang, Microstructure evolution of sub-critical annealed laser deposited ti–6al–4v alloy, Materials & Design 37 (2012) 56–63.

[129] H. Zhong, M. Qian, W. Hou, X. Zhang, J. Gu, The β phase evolution in ti-6al-4v additively manufactured by laser metal deposition due to cyclic phase transformations, Materials Letters 216 (2018) 50–53.

[130] A. S. Gornakova, B. B. Straumal, S. I. Prokofiev, Coarsening of (αti)+(βti) microstructure in the ti–al–v alloy at constant temperature, Advanced Engineering Materials 20 (2018) 1800510.

[131] G. López, E. Mittemeijer, B. Straumal, Grain boundary wetting by a solid phase; microstructural development in a zn–5 wt% al alloy, Acta materialia 52 (2004) 4537–4545.

[132] S. Zherebtsov, E. Kudryavtsev, G. Salishchev, B. Straumal, S. Semiatin, Microstructure evolution and mechanical behavior of ultrafine ti6al4v during low-temperature superplastic deformation, Acta Materialia 121 (2016) 152–163.

[133] F. Hu, P. Hodgson, K. Wu, Acceleration of the super bainite transformation through a coarse austenite grain size, Materials letters 122 (2014) 240–243.

[134] V. Sivalingam, J. Sun, B. Yang, K. Liu, R. Raju, Machining performance and tool wear analysis on cryogenic treated insert during end milling of ti-6al-4v alloy, Journal of Manufacturing Processes 36 (2018) 188–196.

[135] K. A. Al-Ghamdi, A. Iqbal, A sustainability comparison between conventional and high-speed machining, Journal of Cleaner Production 108 (2015) 192–206.

[136] A. Jain, V. Bajpai, Introduction to high-speed machining (hsm), in: High Speed Machining, Elsevier, 2020, pp. 1–25.

[137] S. S. Gill, J. Singh, H. Singh, R. Singh, Metallurgical and mechanical characteristics of cryogenically treated tungsten carbide (wc–co), The International Journal of Advanced Manufacturing Technology 58 (2012) 119–131.

[138] B. Srinivasan, M. R. Rao, B. C. Rao, On the development of a dual-layered diamond-coated tool for the effective machining of titanium ti-6al-4v alloy, Journal of Physics D: Applied Physics 50 (2016) 015302.

[139] Z. Wang, M. Rahman, Y. Wong, Tool wear characteristics of binderless cbn tools used in high-speed milling of titanium alloys, Wear 258 (2005) 752–758.

[140] S. Zhang, J. Li, J. Sun, F. Jiang, Tool wear and cutting forces variation in high-speed end-milling ti-6al-4v alloy, The International Journal of Advanced Manufacturing Technology 46 (2010) 69–78.

[141] S. Zhang, J.-f. Li, Tool wear criterion, tool life, and surface roughness during high-speed end milling ti-6al-4v alloy, Journal of Zhejiang University-SCIENCE A 11 (2010) 587–595.

[142] A. Li, J. Zhao, H. Luo, Z. Pei, Z. Wang, Progressive tool failure in high-speed dry milling of ti-6al-4v alloy with coated carbide tools, The International Journal of Advanced Manufacturing Technology 58 (2012) 465–478.

[143] X. Liang, Z. Liu, Tool wear behaviors and corresponding machined surface topography during high-speed machining of ti-6al-4v with fine grain tools, Tribology International 121 (2018) 321–332.

[144] A. Dadgari, D. Huo, D. Swailes, Investigation on tool wear and tool life prediction in micro-milling of ti-6al-4v, Nanotechnology and Precision Engineering 1 (2018) 218–225.

[145] Y. Wang, B. Zou, C. Huang, Tool wear mechanisms and micro-channels quality in micro-machining of ti-6al-4v alloy using the ti (c7n3)-based cermet micro-mills, Tribology International 134 (2019) 60–76.

[146] A. N. Amin, A. F. Ismail, M. N. Khairusshima, Effectiveness of uncoated wc–co and pcd inserts in end milling of titanium alloy—ti–6al–4v, Journal of materials processing technology 192 (2007) 147–158.

[147] I. Lee, V. Bajpai, S. Moon, J. Byun, Y. Lee, H. W. Park, Tool life improvement in cryogenic cooled milling of the preheated ti–6al–4v, The International Journal of Advanced Manufacturing Technology 79 (2015) 665–673.

[148] M. Jamil, N. He, X. Huang, W. Zhao, A. M. Khan, A. Iqbal, Thermophysical, tribological, and machinability characteristics of newly developed sustainable hybrid lubri-coolants for milling ti-6al-4v, Journal of Manufacturing Processes 73 (2022) 572–594.

[149] T. Özel, T. Thepsonthi, D. Ulutan, B. Kaftanoğlu, Experiments and finite element simulations on micro-milling of ti–6al–4v alloy with uncoated and cbn coated micro-tools, CIRP annals 60 (2011) 85–88.

[150] A. Roushan, U. S. Rao, K. Patra, P. Sahoo, Performance evaluation of tool coatings and nanofluid mql on the micro-machinability of ti-6al-4v, Journal of Manufacturing Processes 73 (2022) 595–610.

[151] S. Sun, M. Brandt, S. Palanisamy, M. S. Dargusch, Effect of cryogenic compressed air on the evolution of cutting force and tool wear during machining of ti–6al–4v alloy, Journal of Materials Processing Technology 221 (2015) 243–254.

[152] B. Rao, C. R. Dandekar, Y. C. Shin, An experimental and numerical study on the face milling of ti–6al–4v alloy: tool performance and surface integrity, Journal of Materials Processing Technology 211 (2011) 294–304.

[153] B. Rao, Y. C. Shin, A study on the high speed face milling of ti-6al-4v alloy, in: ASME International Mechanical Engineering Congress and Exposition, volume 3641, pp. 277–286.

[154] S. Shukla, V. Bajpai, Effect of cryogenic quenching on microstructure and microhardness of ti-6al-4v alloy, Materials Letters 267 (2020) 127532.

[155] A. K. Singla, J. Singh, V. S. Sharma, Impact of cryogenic treatment on mechanical behavior and microstructure of ti-6al-4v eli biomaterial, Journal of Materials Engineering and Performance 28 (2019) 5931–5945.

[156] N. Khanna, C. Agrawal, M. K. Gupta, Q. Song, Tool wear and hole quality evaluation in cryogenic drilling of inconel 718 superalloy, Tribology International 143 (2020) 106084.

[157] S. Smith, J. Tlusty, Efficient simulation programs for chatter in milling, CIRP annals 42 (1993) 463–466.

[158] A. Das, S. Shukla, M. Kumar, C. Singh, M. L. Chandravanshi, V. Bajpai, Development of a vibration free machine structure for high-speed micro-milling center, The International Journal of Advanced Manufacturing Technology 116 (2021) 3489–3506.

[159] T. Morita, C. Tsuda, T. Nakano, Influences of scanning speed and short-time heat treatment on fundamental properties of ti-6al-4v alloy produced by ebm method, Materials Science and Engineering: A 704 (2017) 246–251.

[160] J. Mayeur, D. McDowell, A three-dimensional crystal plasticity model for duplex ti–6al–4v, International journal of plasticity 23 (2007) 1457–1485.

[161] H. Matsumoto, H. Yoneda, K. Sato, S. Kurosu, E. Maire, D. Fabregue, T. J. Konno, A. Chiba, Room-temperature ductility of ti–6al–4v alloy with $\alpha\prime$ martensite microstructure, Materials Science and Engineering: A 528 (2011) 1512–1520.

[162] X. Zhang, R. Shivpuri, A. Srivastava, Role of phase transformation in chip segmentation during high speed machining of dual phase titanium alloys, Journal of Materials Processing Technology 214 (2014) 3048–3066.

[163] C. Wang, D. Yu, Z. Niu, W. Zhou, G. Chen, Z. Li, X. Fu, The role of pyramidal< c+ a> dislocations in the grain refinement mechanism in ti-6al-4v alloy processed by severe plastic deformation, Acta Materialia 200 (2020) 101–115.

[164] H. Li, M. Ramezani, Z. W. Chen, Dry sliding wear performance and behaviour of powder bed fusion processed ti–6al–4v alloy, Wear 440 (2019) 203103.

[165] Y. Wang, B. Zou, J. Wang, Y. Wu, C. Huang, Effect of the progressive tool wear on surface topography and chip formation in micro-milling of ti–6al–4v using ti (c7n3)-based cermet micro-mill, Tribology International 141 (2020) 105900.

[166] D. J. Waldorf, R. E. DeVor, S. G. Kapoor, A slip-line field for ploughing during orthogonal cutting, Journal of Manufacturing Science and Engineering, Transactions of the ASME (1998).

[167] K. Palaniappan, M. Sundararaman, H. Murthy, R. Jeyaraam, B. C. Rao, Influence of workpiece texture and strain hardening on chip formation during machining of ti–6al–4v alloy, International Journal of Machine Tools and Manufacture 173 (2022) 103849.

[168] M. Miguelez, X. Soldani, A. Molinari, Analysis of adiabatic shear banding in orthogonal cutting of ti alloy, International journal of mechanical sciences 75 (2013) 212–222.

[169] R. Komanduri, Z.-B. Hou, On thermoplastic shear instability in the machining of a titanium alloy (ti-6al-4v), Metallurgical and Materials Transactions A 33 (2002) 2995–3010.

[170] K. Vipindas, J. Mathew, Wear behavior of tialn coated wc tool during micro end milling of ti-6al-4v and analysis of surface roughness, Wear 424 (2019) 165–182.

[171] A. Aramcharoen, P. Mativenga, Size effect and tool geometry in micromilling of tool steel, Precision Engineering 33 (2009) 402–407.

[172] M. Hashimura, Y. Chang, D. Dornfeld, Analysis of burr formation mechanism in orthogonal cutting (1999).

[173] S. A. Niknam, V. Songmene, Modeling of burr thickness in milling of ductile materials, The International Journal of Advanced Manufacturing Technology 66 (2013) 2029–2039.

[174] F. Klocke, M. Zeis, A. Klink, D. Veselovac, Technological and economical comparison of roughing strategies via milling, sinking-edm, wire-edm and ecm for titanium- and nickel-based blisks, CIRP Journal of Manufacturing Science and Technology 6 (2013) 198–203.

[175] W. Vanderauwera, M. Garzon, T. Aerts, F. Klocke, B. Lauwers, Comparison of micro-milling and micro-edm operations, in: Proceedings of the 8th international conference on multi-material micro manufacture, Research Publishing, pp. 285–289.

List of Publications and Presentations

Patent

1. Vivek Bajpai, Arnab Das, **Shashank Shukla**, Chitransh Singh, Mohan Kumar and Madan Lal Chandravanshi, "A machine structure to reduce vibration of micro-milling machine". (Published) Application no.201931049978, Patent office journal no. 30/2020 Dated 24/07/2020

2. Vivek Bajpai, Rachit Ranjan, **Shashank Shukla** "Magnet driven servo mechanism for macro/micro electrical discharge machining (EDM)". (Published) Application no. 202031054445 A, Patent office journal no. 06/2021 Dated 05/02/2021

3. Vivek Bajpai, Arnab Das, Ravi Shankar Rai, Ankit Jain, **Shashank Shukla** "A structure of EDM head for a portable type maglev EDM". (Published) Application no. 202231044867 A, Patent office Journal no. 32/2022 Dated 12/08/2022.

Published Journals

1. **Shashank Shukla**, Vivek Bajpai, "Effect of cryogenic quenching on microstructure and microhardness of Ti-6Al-4V alloy", Materials Letters 267 (2020) 127532, 2020

(Q2) Impact factor: 3.423.

2. Arnab Das, **Shashank Shukla**, Mohan Kumar, Chitransh Singh, M.L. Chandravanshi, Vivek Bajpai, "Development of vibration free machine structure for high-speed micromilling center", International Journal of Advanced Manufacturing Technology (2021) (Q2) Impact factor: 3.226.

3. Mangal Singh, **Shashank Shukla**, Vivek Bajpai "Feasibility analysis of Novel Maglev EDM by comparing with conventional micro EDM" Scientific Reports (2022) (Q1) Impact factor : 4.379

Communicated Journals

1. **Shashank Shukla**, Mangal singh, Vivek Bajpai "Characterization and evaluation of novel maglev EDM with existing EDM" International Journal of Advanced Manufacturing Technology (2022) (Q2) Impact factor: 3.226

2. **Shashank Shukla**, Vivek Bajpai "Assessment of cryogenic quenching by tool wear, surface morphology and chip formation in high-speed up-milling of Ti-6Al-4V alloy" Tribology International (Q1) Impact factor: 4.872

Book Chapter

1. **Shashank Shukla**, Vivek Bajpai, "Cryogenic Machining", In book: Innovations in Manufacturing for Sustainability, pp.29-52, Springer International Publishing, Springer International Publishing, 2018 (Published).

2. Mohan Kumar, Ankit Jain, **Shashank Shukla**, Vivek Bajpai, "Experimental and Statistical Analysis of Process Parameters on Micro-milling of Ti–6Al–4V Alloy", In

book :Advances in Forming, Machining and Automation, DOI: 10.1007/978-981-19-3866-5 <u>23</u>, 2022 (Published)

International Conference

1. Deepak Choudhary and **Shashank Shukla**, "Comparative study of conventional and hybrid turning processes using modeling and experimental techniques", International Conference on Precision, Meso, Micro and Nano Engineering (COPEN 2019), IIT Indore